Materials Today Sustainability 30 (2025) 101119

Contents lists available at ScienceDirect

Materials Today Sustainability

journal homepage: www.journals.elsevier.com/materials-today-sustainability

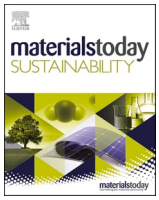

Aluminium recycling: A critical review of iron-bearing intermetallics in aluminium alloys

H.R. Kotadia [a,b,*], N. Bareker [c], M.H. Khan [b], J.I. Ahuir-Torres [a], A. Das [d]

[a] School of Engineering, Liverpool John Moores University, Liverpool, L3 3AF, UK
[b] WMG, University of Warwick, Coventry, CV4 7AL, UK
[c] Constellium University Technology Centre, Brunel University London, Uxbridge, UB8 3PH, UK
[d] Faculty of Science and Engineering, Swansea University, Bay Campus, Swansea, SA1 8EN, UK

ARTICLE INFO

Keywords:
Aluminium recycling
Iron intermetallics
Solidification
Microstructure evolution
Sustanability

ABSTRACT

This review provides a comprehensive analysis of the current understanding of Fe-bearing intermetallic compounds (IMCs) in cast and wrought aluminium (Al) alloys, also covering their significance in recycling and sustainable materials development. It explores the various types of Fe-bearing IMCs, their nucleation and growth mechanisms under diverse processing conditions, with a particular focus on chemical, physical, and thermal modification strategies aimed at mitigating their detrimental effects. The review further examines the impact of these IMCs on defect formation, mechanical performance, and corrosion resistance. While Al recycling offers substantial energy savings (up to 95 %), the accumulation of impurities, notably Fe. This work provides practical insights to guide materials scientists and engineers in optimising processing conditions for Al alloys with elevated Fe content or those derived from recycled scrap. Understanding the behaviour and control of Fe-bearing IMCs is essential for improving alloy performance and advancing the sustainable production of Al.

1. Introduction

Aluminium (Al) is the second most important structural material after steel due to its unique properties. It is known for its exceptional strength-to-weight ratio, making it ideal for applications where weight reduction is crucial, such as in the aerospace and automotive sectors [1,2]. Additionally, Al's natural corrosion resistance, originating from a protective oxide layer, makes it suitable for outdoor use and harsh environments, such as in the marine and chemical industries. Its excellent thermal and electrical conductivity further enhances its appeal, finding applications in electrical wiring, heat sinks, and cookware. Al's ductility and malleability allow for easy shaping and forming, while its recyclability makes it a sustainable material of choice.

The diverse properties of Al alloys arise from their complex microstructures, comprising primary-Al grains (called the α-Al henceforth), eutectic phases (often involving Si, Al_2Cu, and Mg_2Si), intermetallic compounds (IMCs), dispersoids (Al_6Mn, Al_3Zr, Al_7Cr), and precipitates like Al_2Cu, Al_3Sc, Mg_5Si_6, $MgZn_2$ formed through age hardening [1]. By strategically controlling alloying elements, solidification processes, and thermomechanical treatments, scientists and engineers can precisely tailor these microstructural features to achieve desired properties such as enhanced strength, ductility, and corrosion resistance. This versatility has resulted in a vast array of Al alloys, each carefully designed for specific industrial applications. Unveiling the mechanisms behind the development of these complex microstructures is crucial for both advancing research and optimising engineering applications of this vital material.

1.1. The role of aluminium recycling in sustainable growth

Al's infinite recyclability [3,4], with properties preserved throughout the process, positions it as an important player in sustainable material solutions. Secondary Al production, consuming up to 95 % less energy than primary production, offers substantial energy savings and a significantly reduced carbon footprint [4]. This is particularly crucial as the demand for Al surges, especially in the automotive industry's shift towards electric vehicles (EVs) [5]. Global Al demand is projected to surge by 40 % by 2030, requiring an additional 33.3 million metric tons – from 86.2 Mt in 2020 to 119.5 Mt in 2030 [6]. Primary Al production, with a carbon footprint of 12–16.6 tons of CO_2-equivalent per ton (contributing to roughly 3 % of global greenhouse gas emissions), is environmentally and economically unsustainable [7–9]. Therefore, Al

* Corresponding author. School of Engineering, Liverpool John Moores University, Liverpool, L3 3AF, UK.
E-mail address: h.r.kotadia@ljmu.ac.uk (H.R. Kotadia).

https://doi.org/10.1016/j.mtsust.2025.101119
Received 5 December 2024; Received in revised form 4 March 2025; Accepted 8 April 2025
Available online 11 April 2025

recycling, which dramatically reduces carbon emissions and conserves resources, is not only vital for meeting the escalating demand, particularly in the EV sector, but also crucial for ensuring a sustainable and environmentally responsible future.

The current global Al recycling rate stands at approximately 76 %, with regional variations [10]. This impressive recycling rate encompasses both closed-loop recycling, where recycled Al is reused to create the same products (e.g., recycling rate of beverage cans is approximately 70 %) [11], and downcycling, where it is repurposed into lower-grade applications such as construction materials. Despite these achievements, significant challenges persist, primarily due to the presence of diverse alloying elements in scrap Al [7,12]. This issue arises from the mixing of materials sourced from various products like beverage cans, engine blocks, and electrical components leading to impurity accumulation and reduced quality in the recycled Al. To unlock the full potential of Al recycling and facilitate more closed-loop processes, a comprehensive approach is required. This includes designing simplified and highly recyclable alloys, reducing the variety of Al alloys used in products (e.g., simplifying the alloy composition in automobiles), and implementing effective scrap segregation practices. Scrap segregation involves systematically separating different types of Al scrap and recycling them individually to preserve material quality and properties. By optimising alloy design, and efficient dismantling for recycling , the production of high-quality recycled Al can be ensured [13,14]. These measures will help reduce impurities, enhance recycling efficiency, and contribute to a more sustainable and circular Al recycling ecosystem.

Currently there is no single effective approach used for Al recycling due to the various challenges associated with using a closed-loop material system. The typical secondary Al recycling process involves collecting scrap, separating and then melting it [15]. However, for high-end Al products, primary Al is used without any scrap, while for low-end Al applications, the secondary recycling process is used with the addition of at least 50 % primary Al. On average, approximately one-third of the Al currently in use is derived from recycled scrap [4]. Data from the International Aluminium Institute indicate that the proportion of Al in use derived from recycled scrap is projected to increase to 50 % by 2050 [7, 16]. This approach is taken to ensure that the quality of the recycled Al meets the required standards for the intended application. Despite the challenges, Al recycling remains a highly energy-efficient and sustainable option for manufacturing Al products. Due to the large variety of Al alloys, additional challenges are faced with impurity contamination of Al. Eliminating these impurities is important for producing different grades of Al with the desired properties. Designing a realistic approach to recycling Al through secondary processes without losing its original properties requires the development of an ideal recycling supply chain. If such an approach is not achieved, the difficulty of Al recycling will persist, particularly when elements like Fe, Si, Cu, and Zn can damage the Al's properties and processability [12]. Thus, it is crucial to have effective methods in place to minimise the contamination of Al during the recycling process and to maintain its desired properties.

Controlling or removing impurities, particularly Fe, during Al melting is vital for optimising material performance. Techniques such as gravity separation [17,18], centrifugal and electromagnetic processing [19], electrolysis [17,20], and flux refining [21] have been proposed to address this challenge. While these methods can reduce Fe content in Al alloys, their effectiveness depends on impurity levels, alloy composition, and specific processing conditions. Further research is necessary to evaluate and improve these methods and, particularly in enhancing scrap segregation and limiting impurities. Combining techniques like alloying element addition, physical force induction, and gravity separation can promote early nucleation of Fe-bearing IMC particles allowing removal of these inclusions prior to casting. Porous ceramic filtration [22] also offers an efficient method for removing IMCs and inclusions through a continuous process with shorter holding times than gravity separation. However, its efficiency depends heavily on Al composition and adequate pre-treatment.

The economic implications of poor scrap segregation and IMC formation are significant. Mixed scraps lead to higher processing costs, as more advanced and costly refining techniques are required to remove contaminants and restore material quality. Additionally, the presence of IMCs necessitates additional alloying to mitigate their negative effects, further increasing production costs [12]. Moreover, the reduced quality of recycled Al due to contamination limits its potential for closed-loop recycling, forcing manufacturers to rely more on downcycling or even primary material. This not only increases the overall cost of recycling but also hampers the sustainability of Al recycling processes, as lower-grade products cannot be recycled back into high-quality materials. To address these challenges, innovative recycling strategies are required. These include advanced sensor-based sorting techniques for improved scrap segregation, designing alloys optimised for end-of-life recyclability, and refining metallurgical processes to better manage Fe content. Together, these approaches are essential for preserving material integrity and advancing closed-loop recycling practices in the Al industry.

1.2. Fe-bearing intermetallics in aluminium alloys

Fe impurities in Al alloys originate from initial manufacturing, contamination during fabrication, and incomplete separation during recycling [12,23]. Despite advancements in separation techniques, residual Fe remains a significant challenge in Al recycling. This is primarily due to Fe's limited solid-state solubility in Al (max. 0.05 wt%, 0.025 at.%) [24], leading to the formation of complex, hard, and brittle Fe-bearing IMCs [1,2,25,26]. These IMCs not only degrade the mechanical properties of Al alloys, reducing ductility and fatigue resistance, but also act as nucleation sites for pitting corrosion [12,26–30]. Furthermore, the presence of Fe-bearing IMCs poses processing challenges, including reduced fluidity, defect formation, and poor castability, formability and machinability.

There are a range of Fe-bearing IMCs phases, and the most common ones confirmed and identified in commercial Al alloys are; α–(Al_8Fe_2Si) or $Al_{15}(Fe,Mn)_3Si_2$ (α-IMC), β–(Al_5FeSi) (β-IMC), π–($Al_8Mg_3FeSi_6$), and δ–(Al_4FeSi_2) (δ-IMC) [12,23,25,30–38]. The formation of specific Fe-bearing IMCs is influenced by both alloy chemistry and processing methods. Understanding the nucleation, growth, and impact of each IMC on material properties is crucial, especially since Fe content in commercial alloys can increase from the standard 0.2 wt% to 0.3–0.8 wt % during recycling [39]. This level of Fe contamination promotes the formation of undesirable plate-like IMCs with acicular morphology, such as the β-IMC, which can significantly degrade the mechanical properties of Al alloys. To mitigate this, the addition of alloying elements like Mn [40–47], Co [23,48], and Cr [40,48–51] is a common industrial practice to suppress the formation of these detrimental IMCs. While other elements like P [52], Be [32,53], Mg [54,55], Sr [54,55], V [56], Ni [41,51,57], and rare earth elements (REE) [58–65] can also influence Fe IMCs, their effects are generally less pronounced than Mn. Alternatively, physically induced methods such as ultrasonic treatment [66–73], shearing [74–80], mechanical vibration [81,82], and electromagnetic fields [83,84] have been explored to suppress or modify Fe-bearing IMCs. However, these techniques require further research for effective industrial implementation. Additionally, solidification parameters like cooling rate [44,85,86], superheating [44], and thermomechanical processes like extended heat treatment [87,88] can impact the nature and morphology of Fe-bearing IMCs. Despite ongoing research, a thorough understanding of Fe-bearing IMC formation through chemical additions, external fields, and other processing conditions remains elusive and presents significant challenges.

1.3. Scope of review

This review summarises the current understanding of Fe-bearing IMCs in Al alloys focusing on their nature, formation through

nucleation and growth, influence on material performance and defect (porosity) formation, and control over their occurrence and possible modification strategies. It discusses recent advancements and identifies key gaps in the current understanding of Fe-IMCs in Al alloys and, proposes actionable strategies for optimising Al recycling processes. By emphasising the unique challenges associated with Fe-bearing phases in recycled Al alloys, this work aims to direct strategic goals to improve efficiency and sustainability of Al recycling, a critical component of the circular economy. Through a deeper understanding and better management of Fe contamination and IMC formation, this research aims to benefit sustainable Al production, aligning with Sustainable Development Goals (SDG) 12: Responsible Consumption and Production, SDG 13: Climate Action, and SDG 9: Industry, Innovation, and Infrastructure [89]. Furthermore, this review serves as a comprehensive reference for researchers and engineers, particularly those engaged in developing advanced and sustainable Al alloys for future applications in the critical aerospace, automotive, and energy sectors.

The rest of the paper is organised as follows. Section 2 discusses the types, morphology, crystal structure, nucleation and growth conditions of binary and ternary Fe-bearing IMCs. Section 3 discusses various methods employed to modify them in Al alloys, enhancing their tolerance through trace element additions, application of physical fields, and thermal processes. Section 4 then examines the role of IMCs in porosity formation. Section 5 explains their impact on the mechanical and chemical properties of Al alloys through relevant examples, and Section 6 presents a perspective on the future of Al recycling and potential strategy for impurity tolerant Al alloys. Finally, Section 7 provides a critical summary of the literature, identifies existing research gaps, and outlines future directions for increasing the utilisation of recycled Al for sustainability purposes.

2. Phase diagram and crystal structure of Fe-bearing intermetallics

2.1. Fe-bearing intermetallics phase in binary Al–Fe alloy system

During solidification of the binary Al–Fe system (<1.8 wt% Fe), α-Al dendrites initially crystallise, representing the first solid solution of Fe in Al [36]. Under conventional conditions, these dendrites grow, rejecting Fe solute atoms ahead of the solid-liquid interface [90,91]. As the liquid reaches the eutectic point, its composition transforms, leading to a eutectic reaction ($L \rightarrow \alpha - Al + Al_3Fe$) at 655 °C (Fig. 1(a)). The solubility of Fe in Al is highly limited, approximately 0.05 wt% at 655 °C [92,93]. Beyond this solubility limit, Fe tends to form stable IMCs such as Al_3Fe. These IMCs are thermodynamically favoured due to their lower Gibbs free energy (ΔG) relative to the Al–Fe liquid solution. During slow cooling, the Al deposits on α-Al crystals, while the eutectic Al_3Fe forms thin needles around the α-Al (Fig. 1(b)) [94,95]. Increased Fe content leads to thicker needles and in hypereutectic alloys (>1.8 wt% Fe), primary Al_3Fe precipitates before the eutectic reaction (Fig. 1(c)).

Although Al_3Fe is the generally accepted formula with a monoclinic lattice, other forms like Al_7Fe_2, $Al_{23}Fe_7$, $Al_{19}Fe_6$, and $Al_{13}Fe_4$ have been reported [51,96–98]. The eutectic structure is highly sensitive to solidification conditions, growth rate, and temperature gradient. Significant structural changes in binary alloys based on cooling rates have been widely documented [23,99,100]. Rapid cooling often favours the formation of metastable phases like Al_6Fe and Al_mFe (m~4.4, body-centred tetragonal [101]) over Al_3Fe [91,102]. Additionally, the Al_9Fe_2 phase has been observed in strip cast materials containing Co [103]. Fig. 2 provide a comprehensive overview of various binary AlFe IMC phases and their morphologies.

2.2. Fe-bearing intermetallic phases in cast and wrought aluminium alloys

The presence of Fe in both wrought (typically <0.3 wt%) and cast (0.3–1.3 wt%) Al alloys leads to the formation of various Fe-bearing IMCs, as listed in Table 1. Cast Al alloys generally exhibit a higher tolerance for Fe impurities compared to wrought alloys. This distinction arises due to the coarser microstructure of cast alloys and less stringent requirement for ductility, thereby being less sensitive to the negative effects of IMCs. In contrast, wrought Al alloys, which undergo deformation processes such as rolling and forming, demand stricter control of Fe content to avoid material degradation and processing challenges.

An additional consideration in casting processes, particularly in gravity die casting, is the intentional maintenance of a controlled Fe content, typically around 0.3 wt%. This controlled Fe addition is crucial for preventing the 'sticking' or 'soldering' of molten Al to steel moulds, thereby improving casting efficiency and product quality. This dual role of Fe as both a potential contaminant and a functional element highlights the importance of managing its concentration effectively in different types of Al alloys.

Expanding on this, the Al–Si–Fe phase diagram (Fig. 3(a) and (b)) further elucidates the behaviour of Fe in Al alloys. It illustrates the magnified liquidus projection near the Al corner at 540 °C, showing the maximum solubility of Fe and Si in Al [24,51,102]. Si modifies the thermodynamic landscape of the Al–Fe system, stabilising ternary IMCs like **α** and **β** over binary compounds. This is because Si reduces the ΔG of these ternary phases relative to binary phases, especially at lower Fe/Si

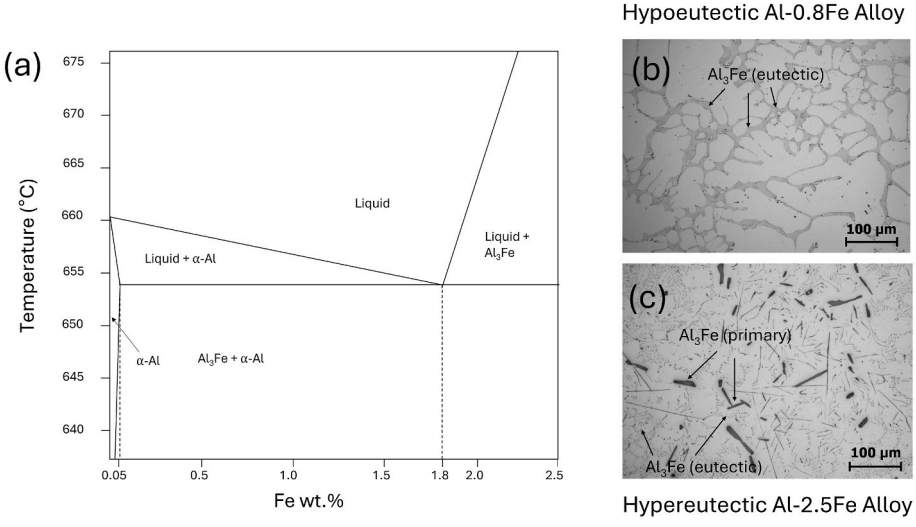

Fig. 1. (a) Al-rich side of the binary Al–Fe phase diagram; Optical micrograph of the (b) hypoeutectic Al-0.8 wt% Fe, and (c) hypereutectic Al-2.5 wt% Fe alloy.

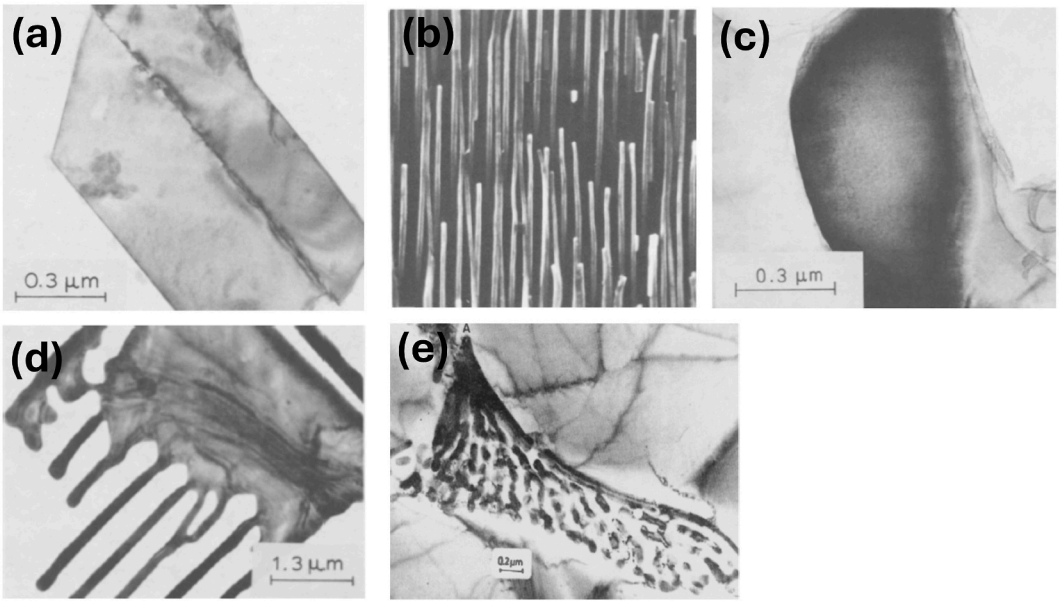

Fig. 2. Various AlFe IMCs morpholoies (a) Al_3Fe, (b) Al_6Fe (X 7100), (c) Al_xFe, (d) Al_mFe and (e) Al_9Fe, adopted from Ref. [104].

Table 1
List of common Fe-bearing IMCs found in commercial cast and wrought Al alloys.

Aluminum series	Wrought/Cast	Typical Fe-bering IMCs	Note	Reference(s)
1xxx/1xx.x (Pure Al alloys)	Wrought & Cast	Al_3Fe, Al_6Fe	Primarily binary Al–Fe phases.	[93,104, 105]
2xxx/2xx.x (Al–Cu)	Wrought & Cast	Al_mFe, Al_7Cu_2Fe, AlCuFe	Cu alters IMC formation.	[106]
3xxx/3xx.x (Al–Mn)	Wrought & Cast	$Al_6(Fe,Mn)$	Mn controls IMC effects.	[107]
4xx.x (Al–Si)	Cast (Primarily)	β-Al_5FeSi, α-$Al_{15}(Fe,Mn)_3Si_2$ (detailed listed in Table 2)	Si is a strong IMC former.	[37,93,102]
5xxx/5xx.x (Al–Mg)	Wrought & Cast	Al_3Fe, Al_3Mg_2Fe, α-$Al_{15}(Fe,Mn)_3Si_2$, $Al_8Mg_3FeSi_6$	Mg influences IMCs, especially with Si.	[108,109]
6xxx (Al–Mg–Si)	Wrought (Primarily)	β-Al_5FeSi, α-$Al_{15}(Fe,Mn)_3Si_2$, $Al_8(Fe,Mn)_2Si$, $Al_8Mg_3FeSi_6$	Similar to 5xxx with Mg influence the IMCs.	[110,111]
7xxx (Al–Zn)	Wrought (Primarily)	Al_7Cu_2Fe, $Al_5Mg_8Cu_2Zn$	Zn and Cu lead to complex IMCs.	[112,113]
8xxx/8xx.x (Other elements)	Wrought & Cast	Varies depend on the elements	IMCs highly diverse depend on alloying elements.	

Table 2
List of substrates and their planar disregistries with Fe-IMCs [133].

Substrate and Phase	Match Planes	$[uwv]_s$	$[uwv]_n$	$d_{[uwv]_s}$ (nm)	$d_{[uwv]_n}$ (nm)	∅	δ
MgO and β− Al_7Cu_2Fe	(110)s// (110)n	[001]	$[\bar{1}10]$	5 × 0.423	2 × 0.896	0	7.94
		$[\bar{1}11]$	$[\bar{1}11]$	5 × 0.733	2 × 1.736	4.19	
		$[\bar{1}10]$	[001]	5 × 0.598	2 × 1.487	0	
$MgAl_2O_4$ and β− Al_7Cu_2Fe	(110)s// (110)n	[001]	$[\bar{1}10]$	5 × 0.808	4 × 0.7859	0	5.72
		$[\bar{1}11]$	$[\bar{1}11]$	5 × 1.399	4 × 1.361	4.19	
		$[\bar{1}10]$	[001]	5 × 1.143	4 × 1.111	0	
γ − Al_2O_3 and β− Al_7Cu_2Fe	(110)s// (110)n	[001]	$[\bar{1}10]$	4 × 0.7859	3 × 0.896	0	7.18
		$[\bar{1}11]$	$[\bar{1}11]$	4 × 1.361	3 × 1.736	4.19	
		$[\bar{1}10]$	[001]	4 × 1.111	3 × 1.487	0	
α− Fe and β− Al_7Cu_2Fe	(100)s// (100)n	[001]	[001]	1.265	1.487	0	6.00
		[011]	[011]	1.789	1.616	21.62	
		[010]	[010]	1.265	1.267	0	
$Al_6(FeMnCu)$ and α− $Al_{15}(FeMn)_3(SiCu)_2$	(100)s// (100)n	[001]	[001]	3 × 0.878	2 × 1.265	0	6.46
		[011]	[011]	3 × 1.152	2 × 1.789	4.65	
		[010]	[010]	3 × 0.746	2 × 1.265	0	
Al_3Ti and α− $Al_{15}(FeMn)_3(SiCu)_2$	(100)s// (100)n	[001]	[001]	3 × 0.397	1.265	0	5.80
		[011]	[011]	3 × 0.562	1.789	0	
		[010]	[010]	3 × 0.397	1.265	0	

ratios (Fig. 3(c)). Experimental studies have confirmed the formation of Al–Si–Fe IMCs during casting [91,114]. Moreover, non-equilibrium solidification and trace element additions can influence the formation of stable ternary IMCs (e.g., α and β phases). Table 2 provides a summary of the morphologies and characteristics of these α and β IMCs, as reported in the literature [37,102]. These insights emphasise the complex relationship between Fe, Si, and processing conditions, highlighting the importance of tailored approaches to managing Fe content and

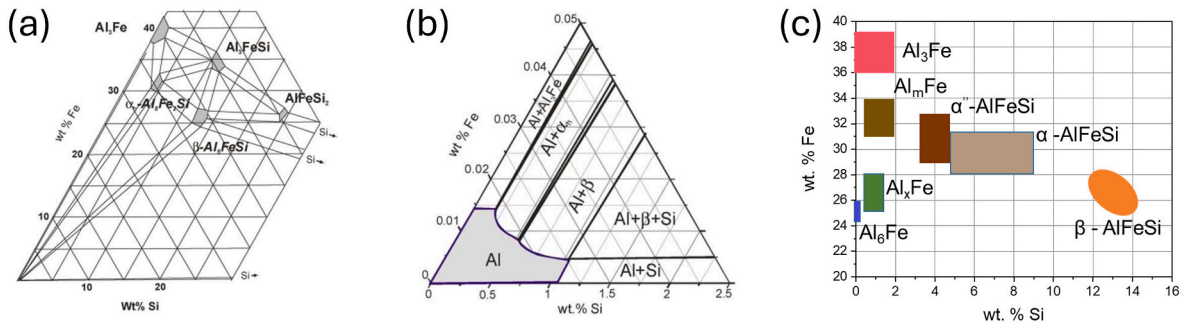

Fig. 3. (a) The Al-corner of the Al–Si-Fi phase diagram, (b) Al-rich corner of the computed Al–Fe–Si phase diagram at 540 °C, obtained using Thermo-Calc [51,115], and (c) possible IMC formation regions with respect to Si and Fe concentration, redrawn from Ref. [104].

stabilising IMC formation in both cast and wrought Al alloys. The thermodynamic stability of Fe-bearing IMCs further emphasises the critical role of controlling the Fe/Si ratio in scrap materials. An imbalance in this ratio can lead to the excessive formation of β-IMC, which is often more detrimental to material properties compared to α-IMC. Effective management of these factors is essential to optimise alloy performance and maintain the integrity of recycled materials.

2.2.1. *Fe-bearing intermetallics nucleation*

The nucleation and growth of Fe-bearing IMCs in Al alloys constitute a complex process governed by a multitude of interacting factors. These include, but are not limited to, the alloy's chemical composition, solidification parameters (such as cooling rate and thermal gradient), and the local microstructure. Fe-bearing IMCs can precipitate at various stages and locations during solidification, spanning from the pre-dendritic regions to the post-eutectic areas [116]. Understanding these nucleation mechanisms is crucial as they directly influence the size, distribution, and morphology of the IMCs, ultimately impacting the alloy's mechanical properties and overall performance.

Extensive research, employing both *ex-situ* [66,74,116–119] and *in-situ* [120–127] characterisation techniques, has been dedicated to elucidating the nucleation mechanisms and identifying potential nucleation sites for these phases. These investigations aim to establish a clear picture of the intricate interplay between the various influencing factors.

One area of focus has been the role of phosphorus (P) in Fe-bearing IMC nucleation. While some studies suggest that AlP particles, formed due to the presence of P, can act as heterogeneous nucleation sites for the β-IMC [52,85,86,128], potentially due to their structural similarity, conflicting evidence exists. Other researchers have questioned the effectiveness of AlP as a nucleant due to the significant planar disregistry between AlP and the β-IMC [31,129], suggesting that the lattice mismatch hinders effective nucleation. This highlights the complexity of the system and the need for further investigation to reconcile these contrasting observations.

Oxides have also been identified as potential nucleation sites for Fe-bearing IMCs, supported by both *ex-situ* [119] and *in-situ* observations [130]. Lattice mismatch calculations suggest that γ-Al_2O_3, α-Al_2O_3, and MgO could act as nucleation sites for the α-IMC. Khalifa et al. [34] investigated the influence of various oxides on Fe-bearing IMC nucleation (Fig. 4(a)), providing experimental evidence for their role. Que et al. [131] specifically found that $Al_{13}Fe_4$ IMCs nucleated on $MgAl_2O_4$ particles. Interestingly, the size of the oxide particles does not appear to significantly influence their nucleation potency [34,116,119], suggesting that other factors, such as surface chemistry and defect density, might be more dominant.

The influence of processing parameters, such as cooling rate and solute effects, on Fe-bearing IMC nucleation has been highlighted by Campbell et al. [119], emphasising the importance of carefully controlling these conditions. Interfacial energies associated with oxide films can also play a crucial role in Fe-bearing IMC development by providing nucleation sites. Furthermore, the addition of trace elements, like Sr and Na, can modify these interfacial energies and impact the oxide film composition at the interface, demonstrating the complex interplay between Fe-bearing IMCs, melt superheating, and these trace elements.

Intentional addition of nucleating particles (or grain refiner (GR)), such as TiB_2, TiC, and Al_3Ti, has been explored as a means to refine Fe-bearing IMCs [43,109,123,132]. Fig. 4(c) illustrates a TiB_2 particle centrally located within an Fe-bearing IMC phase, providing direct visual evidence of its role as a nucleation site. Nucleation on Al_3Ti

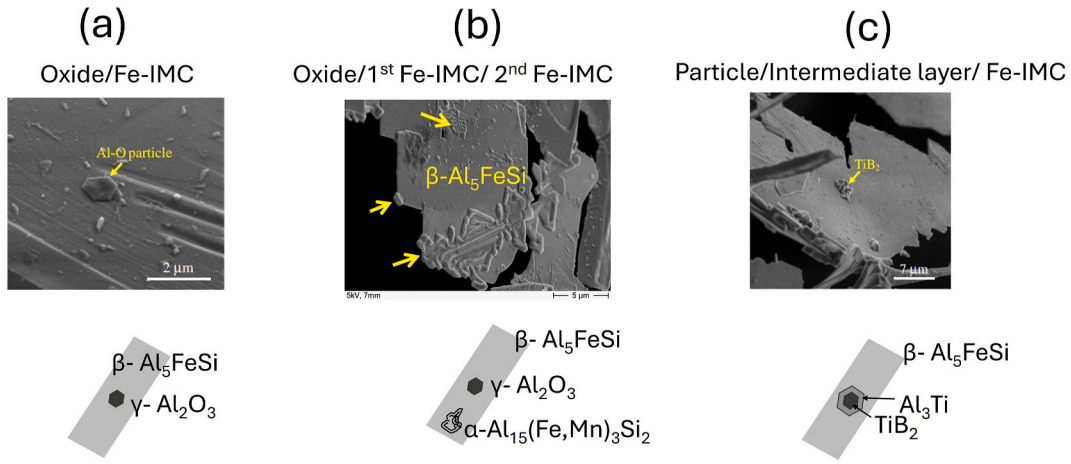

Fig. 4. Examples of various substrates acting as nucleation sites for Fe IMCs: (a) direct nucleation of an IMC on an oxide particle, (b) initial nucleation of an IMC on an oxide followed by subsequent nucleation of an α-IMC on the existing IMC, and (c) nucleation of an IMC on a TiB_2 grain refining particle [134].

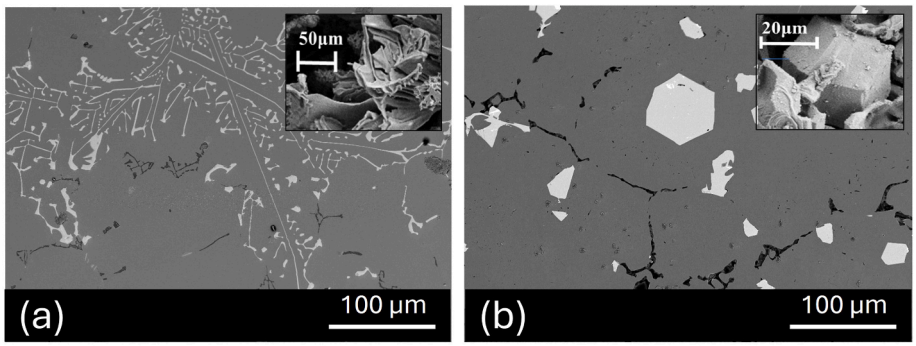

Fig. 5. Two distinct morphologies of α-IMCs: (a) Chinese script-shaped and (b) particle-shaped (from authors' work).

particles has also been observed. These inoculants, commonly used to refine α-Al grains in wrought Al alloys, can also refine Fe-bearing IMCs when present in excess. Additionally, pre-existing Fe-bearing IMCs can induce nucleation of other Fe-bearing IMCs [116], as shown in Fig. 4(b), potentially due to a peritectic reaction [133]. Table 2 presents the planar disregistry between various substrate materials and Fe-bearing IMCs, providing a quantitative measure of the lattice mismatch and thus, the potential for heterogeneous nucleation.

Feng et al. [123] demonstrated that TiB_2 and TiC inoculation increased the number density and average formation rate of primary $Al_{13}Fe_4$ IMCs under varying thermal gradients and cooling rates. They observed that $Al_{13}Fe_4$ IMCs preferentially nucleated on TiB_2 particles when present, rather than on oxide skins, highlighting the effectiveness of TiB_2 as a nucleant. Under directional solidification conditions, the IMC density was found to be primarily controlled by the thermal gradient, with a weaker dependence on the cooling rate. The research also identified various shapes of $Al_{13}Fe_4$ crystals, which were attributed to the crystal structure and twinning susceptibility [127].

2.2.2. *α-IMC phase*

The α-IMC often appears as compact or Chinese script structures (Fig. 5). In the presence of Mn, it is identified as α-$Al_{15}(Fe,Mn)_3Si_2$, a more compact and less detrimental IMC compared to the β-Al_5FeSi phase. Both faceted and non-faceted morphologies are observed in cast and wrought Al alloys. The rounded and symmetrical structure of the α-IMC is beneficial, minimising micro-shrinkage during solidification compared to the plate-like β-IMC [9]. Additionally, the α-IMC acts as a feeder, reducing shrinkage by facilitating liquid flow into interdendritic regions [135]. Among the various reported α-IMC structures (Table 3), the cubic form is most common in commercially cast products, exhibiting diverse compositions and morphologies.

In dilute Al–Si–Fe alloys undergoing non-equilibrium solidification, two monoclinic α-IMC, q1 and q2 (C-centred), can form. Reported phases such as α_T-AlFeSi and α_1-AlFeSi are likely modified structures of the common α-IMC, rather than distinct entities. Specifically, α″-AlFeSi represents an intermediate structure between Al_mFe and other α-IMCs with respect to Si content, while α_1-AlFeSi is a modified cubic form of the α-IMC. In Al–Si–Fe alloys, α-IMC formation depends on the composition

Table 3
List AlFe and AlSiFe IMC phases and their structures [37,93,102].

Name(s)	Bravais Lattice	Lattice Parameters	Effect on mechanical properties	Reference (s).
$Al_3Fe/Al_{13}Fe_4$	BCT (C 2/m)	a = 15.49 Å; b = 8.08 Å; c = 12.48 Å β = 107.75 deg	It cracks and reduces formability and fatigue resistance but improves wear resistance.	[96–98]
Al_mFe	body-centred tetragonal	a = 8.84 Å; c = 21.60 Å	When IMC is small or fibrous form (e.g. Al_6Fe), effect on fatigue properties is not very clear.	[138]
Al_9Fe_2	monoclinic	a = 8.90 Å; b = 6.35 Å; c = 6.32 Å β = 93.4 deg		[103,139]
Al_6Fe	C-centred Orthorhombic (Ccmm or Ccm20	a = 6.49 Å; b = 7.44 Å; c = 8.79 Å		[140–143] [144]
α-$Al_{15}(Fe,Mn)_3$ Si_2/ α-AlFeSi	body-centred cubic (Im3)	a = 12.5 Å	Significantly deteriorate the mechanical properties of alloy, especially reduces ductility and fatigue life.	[145]
α –AlFeSi	Primitive cubic (Pm3)	a = 12.52 Å	Overall machinability and wear properties of alloys can be improved, if it is well distributed.	[146]
α′-AlFeSi	Hexagonal (P63/mmc)	a = 12.30 Å c = 26.20 Å		[147,148]
α″-AlFeSi/q_1-AlFeSi	C-centred orthorhombic	a = 12.70 Å; b = 36.20 Å	Alloy mechanical properties can be improved after heat treatment, in comparison to cast condition.	[149,150]
α_T-AlFeSi	C-centred monoclinic	a = 27.95 Å; b = 30.62 Å; c = 20.73 Å β = 97.74 deg		[151]
q_2-AlFeSi	monoclinic	a = 12.50 Å; b = 12.30 Å; c = 19,70 Å β = 111 deg		[150]
β – Al_5FeSi	monoclinic	a = 6.12 Å; b = 6.12 Å; c = 41.50 Å α = 91.0 deg		[147,152]
β*-AlFeSi	monoclinic	a = 8.90 Å; b = 4.90 Å; c = 41.60 Å β = 92.00 deg		[149]
Al_3FeSi/γ- A1FeS	C-centred monoclinic	a = 17.80 Å; b = 10.25 Å; c = 8.90 Å β = 132 deg		[153]
Al_4FeSi_2/δ- A1FeSi	tetragonal	a = 6.14 Å; c = 9.48 Å		[147,152]

and Fe/Si ratio. Slow solidification (<1 °C/s) favours stable hexagonal Al_8Fe_2Si, with Si content varying from 7 to 9.5 wt% depending on the initial Si levels [136]. However, high cooling rates (>10 °C/s) promote metastable cubic or monoclinic α-IMC structures. Increasing melt temperature or cooling rate [117,137] can suppress primary-Fe IMC formation, with the latter minimising nucleation events [117], (detailed in Sections 3.4).

Under non-equilibrium conditions, metastable α-Al_{15}(Fe, Mn)$_3$Si can form through two solidification paths:

(i) Eutectic decomposition: α-Al_{15}(Fe, Mn)$_3$Si with a branch-like morphology precipitates directly from the melt, separating it into α and α-Al_{15}(Fe, Mn)$_3Si_2$ phases ($L \rightarrow \alpha - Al + L \rightarrow \alpha - Al + \alpha - Al_{15}(Fe, Mn)_3Si_2$).

(ii) Peritectic reaction: α-Al_{15}(Fe, Mn)$_3Si_2$ forms on the surface of Al_6Fe IMCs through a reaction between Al_6Fe and the liquid. This results in metastable α-Al_{15}(Fe, Mn)$_3Si_2$ with Chinese script morphology and higher Si content compared to the branch-like form, or it can form as particles ($L + Al_6Fe \rightarrow \alpha - Al_{15}(Fe, Mn)_3Si_2$).

2.2.2.1. Growth mechanism of α-IMC morphology. The growth mechanism of α-IMC morphology in Al alloys is influenced by composition, cooling rate, and alloying elements like Mn. The cubic crystal structure of the α-IMC phase allows for isotropic growth, leading to various shapes that depend on growth conditions and trace elements such as Cr and Mn [130,154]. Diffusion-controlled mechanisms play a critical role in these growth processes. *In-situ* X-ray imaging revealed four distinct α-IMC morphologies (Fig. 6), determined by nucleation and growth mechanisms [130]. Low cooling rates (0.5 °C/s) produced massive hopper-like crystals, while cooling at 1.0 °C/s resulted in smaller six-edged crystals. Higher cooling rates reduce diffusion distances for solute atoms, leading to increased nucleation frequency and smaller Fe-bearing IMCs [47].

The highest atomic density crystal face, like the <110> plane in BCC structures, promotes hopper or dodecahedron shapes [155]. Lower nucleation frequency accelerates crystal growth, forming smaller hopper or dodecahedron crystals [130]. Hopper crystal instability at the solid-liquid interface causes protrusions to evolve in <001> and <100> directions, followed by growth in <110> and <111> directions from pre-existing <100> arms [156]. Diffusion of rejected solute atoms around the crystal edges and corners is a critical process; these atoms preferentially migrate to areas of high curvature, where trace elements like Cr and Mn adhere, thereby limiting further growth [157]. As the crystal grows, the fast-growing faces vanish, consumed by slower-growing faces that ultimately determine the final crystal shape.

Gao et al. [158] investigated the relationship between solute concentration, supersaturation, and crystal growth initiation. Their findings, illustrated in Fig. 7, demonstrate that solute diffusion under supersaturated conditions drives growth at crystal tips, where the solute concentration is highest. This mechanism favours growth in specific regions, influencing IMC morphology. They also observed the formation of dendrite crystals (Fig. 8), a phenomenon similarly reported by Zhang et al. [137], who proposed that cooling rate influences the growth of Fe-bearing IMCs. Slower cooling rates allow more time for solute atoms to diffuse, promoting the development of coarser, dendritic structures. Xiang et al. [159], through *in-situ* studies, observed the nucleation of α-phases in two distinct ways: either from pre-existing Al_3Fe phases or directly from the liquid. Initially, the α-IMC nuclei exhibited a circular morphology. These nuclei then developed into uneven, faceted surfaces before gradually transforming into rhombic dodecahedra bounded by {110} dense planes. From the edges and vertices of these dodecahedra, skeletal growth proceeded, forming three-dimensional skeletons with α-Al residing within the hopper-like structures. This skeletal growth process repeated in three dimensions, ultimately leading to the formation of complex, convoluted Chinese-script clusters or colonies. Tachibana et al. [160] further explored this dendritic growth through the lens of the Berg effect, a layer-by-layer mechanism that begins at the corners and edges of a crystal face. Under high supersaturation, solute diffusion supports the deposition of additional layers on the outer contours of the crystal. This localised solute diffusion causes the edges to extend outward, creating a dendritic growth pattern. This behaviour is illustrated

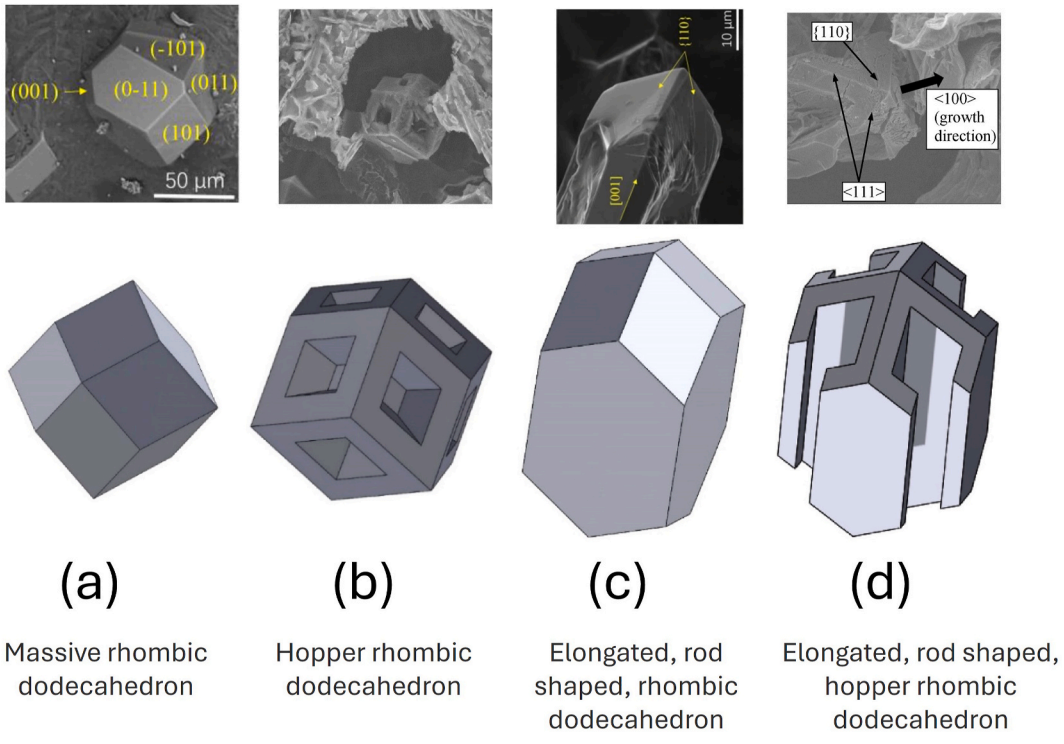

Fig. 6. Variations in the morphology of α-Al(FeMnCr)Si IMC phase. Adopted from Ref. [130].

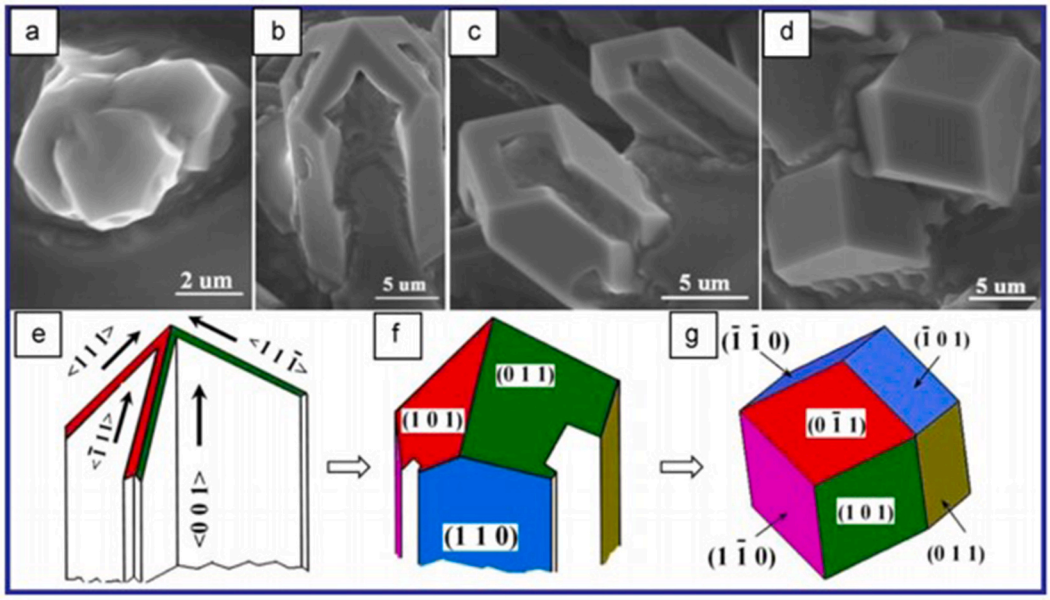

Fig. 7. Diverse morphologies of α-Al(FeMn)Si IMC (a–d), including varying growth directions for the rhombic dodecahedron morphology (e–g) [158].

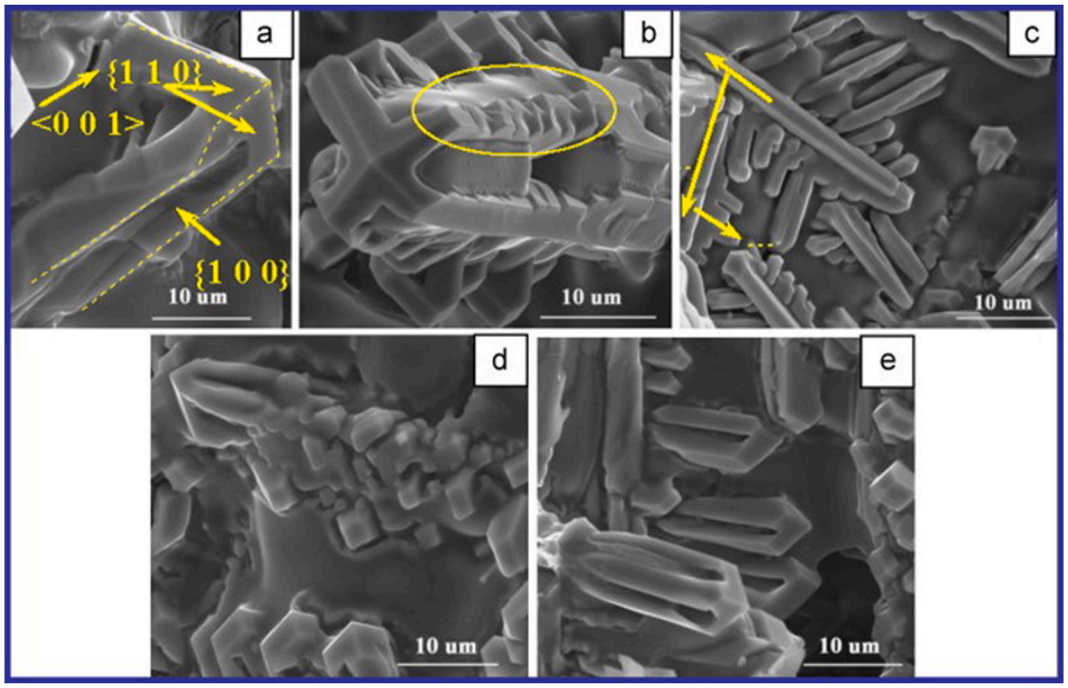

Fig. 8. Morphological variations of dendritic crystals in the α-Al(FeMn)Si IMC phase [158].

in Fig. 8(a)–(c) in the <110>, <100>, and <001> directions and is directly associated with high supersaturation conditions [160].

2.2.3. *β-IMC phase*

Within Al alloys, the β-Al_5FeSi phase, particularly in its plate-like morphology, has the most deleterious impact on mechanical properties. This is due to its highly faceted nature, resulting in poor bonding with the Al matrix. The β-IMC is characterised by unique unit cell parameters stemming from a distorted crystal structure damaged with faults and twins [161].

The faceted morphology of β-IMC acts as local stress concentrators, promoting the initiation of sharp microcracks [162–166]. Moreover, surface defects become pronounced during thermomechanical processing of wrought Al alloys, such as extrusion [167]. Due to the weak interface between the β-IMC and the Al-matrix, these particles can detach and adhere to the die surface [168]. This is problematic as the β-IMC can then scratch the Al surface, creating an undesirable "eye scratch" appearance.

Consequently, strategies to encourage the formation of alternative, less harmful IMCs like the α-IMC are employed. The α-IMC exhibits better cohesion with the Al-matrix, reducing the risk of die adhesion and enhancing the overall mechanical properties of the material [168].

In typical Al–Si–Fe cast alloys, the phase transformation sequence proceeds as follows [39]:

(i) α-Al formation: Prior to the Al–Si eutectic reaction, α-Al solidifies first, accompanied by the formation of a binary Al-β-Al_5FeSi eutectic; ($L \rightarrow \alpha - Al + \beta - Al_5FeSi$).
(ii) Ternary eutectic formation: Following the binary Al–Si eutectic reaction, a ternary eutectic reaction (Al–Si–Al_5FeSi) occurs; ($L \rightarrow (\alpha - Al + Si) + \beta - Al_5FeSi$).
(iii) Dendritic growth: The ternary eutectic forms and solidifies after the initial development of the dendritic structure; ($L \rightarrow (\alpha - Al + Si) + Al_2Cu + \beta - Al_5FeSi$).

2.2.3.1. Growth mechanism for β-IMC platelets. In contrast to the α-IMC's diverse morphology, the β-IMC exhibits a distinct plate-like structure, occasionally appearing as acicular or needle-like forms. Three main subgroups of plate-like β-IMC, with orthorhombic, tetragonal, and monoclinic crystal structures, have been reported [169,170]. The crystallographic details of these phases are summarised in Table 3, and their morphology is represented in Fig. 9.

Kral et al. [171] observed that in Al alloys with high Si content (~11 wt%), the dominant plate-like structure was typically a blade-shaped tetragonal phase, Al_3FeSi_2 (sometimes referred to as δ-Al_3FeSi_2), not to be confused with other β-IMCs. They reported an approximate 1:1 Fe:Si ratio for the β-IMC and a 1:2 Fe:Si ratio for the δ-IMC.

The growth mechanism of the β-IMC is significantly governed by its crystal system and preferred growth direction, likely along the <001> axis [172,173]. This directional growth is influenced by the rate at which solute elements diffuse and incorporate into the advancing steps of the crystal. Cooling rates strongly affect these dynamics; slower cooling allows for more solute diffusion and larger plate structures, while faster cooling results in finer, less developed plates. Additionally, imperfections such as twins and faults in the β-IMC can cause branching of the plate structures, as shown in Fig. 9(c) and (d). This branching is a direct consequence of localised solute redistribution and lattice instability during growth.

Trace elements like Mn, Cr, and Sr play a pivotal role in modifying the β-IMC growth kinetics (explained in Section 3.1). These elements can "poison" kink sites along the growth steps, disrupting the step flow mechanism and altering the crystal growth pattern. Mn and Cr, for instance, distort the kink sites, increasing the internal energy of the growing plate structure due to enthalpic contributions [174]. Elevated internal energy enhances solubility at the solid-liquid interface, reducing the degree of supersaturation and slowing the plate's growth.

Sr further modifies the growth of β-IMC plates by promoting the formation of low-energy configurations along the steps, creating localised "dead zones" where growth is inhibited. This results in a higher frequency of faults and twins within the crystal structure, which correlates with another growth mechanism: layer-by-layer propagation influenced by solute redistribution. These imperfections directly affect the morphology and stability of the β-IMC plates [160].

The secondary solidification of the β-IMC is significantly impacted by the preceding growth of α-Al dendrites and the α-IMC. These prior solidification events influence solute availability, leading to localised regions of solute supersaturation. Consequently, by the time β-IMC formation initiates, solute concentrations at the solid-liquid interface may be depleted. This depletion directly affects the nucleation and growth kinetics of the β-IMC plates. Furthermore, extensive research has systematically investigated β-IMC modification by manipulating α-Al grain size and the distribution of solute/residual liquid (detailed in Sections 3.2 and 3.3). This complex interaction between solute availability, diffusion kinetics, and trace elemental incorporation highlights the governing mechanisms for β-IMC growth.

Over the past two decades, extensive research has utilised advanced techniques, such as synchrotron-based methods, to gain real-time insights into the formation of β-IMC in Al alloys [120–127]. These studies have primarily focused on nucleation, growth, and the influence of cooling rate, external fields, and trace elements. High-speed tomographic imaging has revealed a diverse range of nucleation events for the β-IMC in Al–Si alloys, significantly impacting the lateral growth

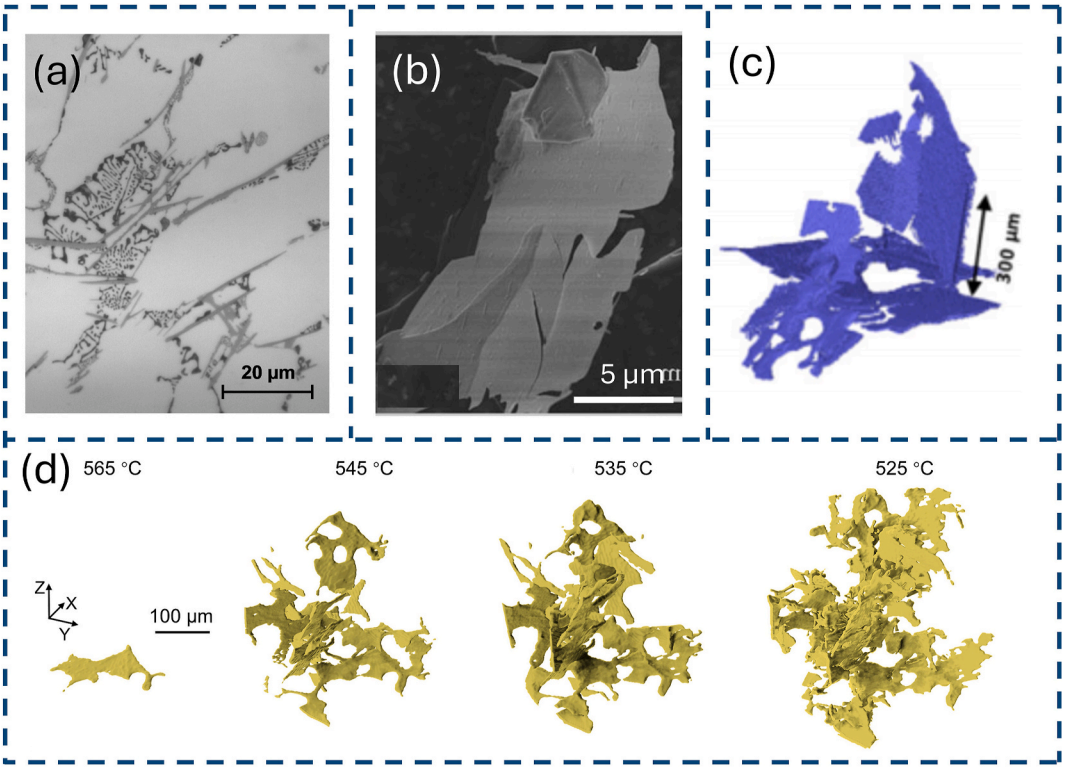

Fig. 9. Two-dimensional (2D) and three-dimensional (3D) morphology of the β-IMC phase: (a) optical micrograph, (b) SEM image of extracted β-IMC, (c) *in-situ* study of the β-IMC during growth [120], and (d) Growth of the β-IMC phase during solidification [159].

direction and morphology. The specific temperature range of nucleation influences the rate, direction, and ultimate microstructure of the β-IMC, highlighting the complex relationship between temperature, nucleation, and growth during solidification. Nucleation of the β-IMC has been observed near the α-Al phase, on oxide nucleation sites, and through self-nucleation via branching. *In-situ* studies have shown that β-IMC can obstruct interdendritic channels, contributing to micro-gap and porosity formation. While direct Fe-bearing IMCs nucleation on pores was not observed, β-IMCs were found to block and hinder pore growth, increasing pore tortuosity [84]. Synchrotron X-ray tomography has explained the intricate morphology of Fe-bearing IMCs, revealing interconnected shrinkage pores and globular pores, with pore sphericity increasing with Fe concentration (0.5–1.0 wt%) [126]. Terzi et al. [120] reported that β-IMC plates in Al–Si alloys can grow and enlarge through branching, sometimes leading to an acicular needle-like morphology. Branching occurs randomly on β-IMC plates, likely due to the interference of Al dendrite arms with IMC growth. Thickening of β-IMC plates often results from ridge lines caused by dendritic enclosure. Additionally, some β-IMC plates exhibit splintered, curved, or arched morphologies due to interactions with dendrite arms during solidification. Notably, trace additions of Sr have been shown to prevent β-IMC formation [125].

Although this section focuses on the β-IMC, research on related Fe-bearing IMCs, such as AlFe, offers valuable comparative insight. For instance, Zhao et al. [175] investigated the influence of Al–5Ti–1B on Fe-containing IMCs in an Al–10Fe alloy. They observed that adding Al–5Ti–1B decreased both the thickness and number of primary Al_3Fe phases while increasing the formation of eutectic Al_6Fe. Primary Fe-bearing phases exhibited lateral growth. The growth rate of these phases was significantly enhanced by the Al–5Ti–1B addition, increasing from 3 to 18 μm/s to 5–45 μm/s. This addition also reduced nucleation undercooling and increased the growth rate of the Fe-bearing IMC. Separately, studies in Al–Cu(-Fe) alloys have shown that increasing the cooling rate five-fold reduces both the length and growth rate of Al_3Fe IMC by approximately half [176]. This is because higher cooling rates limit the diffusion time available for Fe atoms, thus restricting the growth of Fe-bearing IMC and preventing them from attaining larger dimensions. Combined SEM and *in-situ* synchrotron X-ray radiography studies have shown that the addition of Al–Ti–B to both Al–Cu–Fe and Al–Cu–Fe–Si alloys leads to a significant reduction in both the size and number density of primary Al_3(CuFe) phases [177].

2.2.4. δ-IMC phase

The δ-Al_4FeSi_2 (or δ-Al_3FeSi_2) IMC is commonly found in Al–Si based alloys. Although appearing needle-like in two-dimensional views, its true morphology, observed in three dimensions, reveals a faceted plate-like structure similar to the β-IMC (Fig. 10). The δ-IMC typically forms in Al–Si alloys with high Si content or upon the addition of transition elements like Sr [178]. Although δ-IMC formation is typically sensitive to cooling rates, compositional variations can induce formation at lower rates, a behavior similarly noted for β-IMC [42,125,179–181]. The mechanisms underlying this behaviour are detailed in Section 3.4.1.

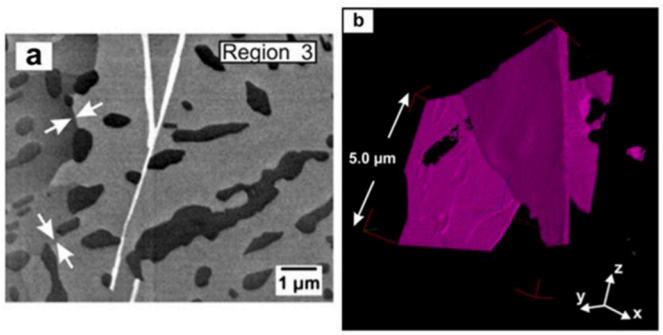

Fig. 10. Two-dimensional (2D) and three-dimensional (3D) morphology of δ-IMC: (a) needle-like appearance in 2D and (b) plate-like structure revealed in 3D [178].

Choi et al. [182] observed that in an Al–20Si–8Fe alloy cooled at 10 °C/s, the δ-IMC formed before Si precipitation. In contrast, under slower cooling conditions, the δ-IMC appeared after Si precipitation and the formation of α-Al. Lu and Dahle et al. [31] suggested that the δ-IMC forms via a reaction at the ternary eutectic point, after Si has solidified, through the eutectic reaction: $L \rightarrow \alpha - Al + (Al - Si) + \delta - Al_4FeSi_2$. This is distinct from the β-IMC, which forms independently during solidification and does not require the completion of the α-Al and Si phases before its nucleation.

The nucleation and growth of the δ-IMC are highly influenced by the Fe:Si ratio and the cooling rate, which control solute distribution and supersaturation in the liquid. The formation of the δ-IMC is favoured at a higher Fe:Si ratio, and the phase itself is often metastable, potentially transforming into more stable phases upon heat treatment [181]. The higher the supersaturation of solute elements in the liquid, the more likely nucleation of the δ-IMC is to occur on dendrite surfaces, oxides, inclusions, GRs, and other IMCs [180,181]. The diffusion of Fe and Si atoms to these nucleation sites is crucial for initiating the formation of δ-IMC.

The formation of the δ-IMC is a diffusion-controlled process, where the rate of solute diffusion, especially that of Fe and Si, plays a critical role in determining the phase's growth rate and morphology. Similar to the β-IMC, rapid cooling rates increase the solute supersaturation in the liquid phase, which promotes faster nucleation and smaller, more densely distributed δ-IMC particles. On the other hand, slower cooling rates allow for more controlled diffusion, leading to a slower nucleation rate and the development of larger, more distinct plate-like structures.

This diffusion-controlled growth mechanism, coupled with the interaction between Fe and Si, emphasises the importance of cooling rate and alloy composition in governing the formation and characteristics of the δ-IMC. Furthermore, the metastability of the δ-phase emphasises the potential for post-solidification transformations under heat treatment, which can affect the overall material properties of the Al–Si alloy.

Contrary to prior understanding, Yu et al. [125,181] found that the δ-IMC can also form in high-Si alloys with low cooling rates. *In-situ* observations revealed that δ-IMC plates primarily nucleate on eutectic Si but can also nucleate on inclusions or oxides within a narrow temperature range (553-551 °C). Critically, solute concentration, rather than substrate potency, was identified as the key factor for δ-IMC nucleation. Branched δ-IMC plates were always present, but branching occurred solely through plate impingement, not nucleation on existing plates. The orientation of δ-IMC plates was determined by the surrounding liquid and nucleation sites, while branching was mainly influenced by plate orientation and blockage by solidifying eutectic Al–Si.

Overall, the nature and morphology of the IMCs can be modified by various factors, including cooling rate, alloy composition, impurities, and targeted additives. However, essential solute diffusion remains a key fundamental process influencing the morphology and distribution of Fe-bearing IMCs, highlighting the need for precise control over cooling rates, alloy composition, and solute levels during the solidification processes.

3. Modification of Fe-bearing intermetallics

The size and distribution of Fe-bearing IMCs significantly influence the mechanical properties of Al alloys. Finer, well-distributed IMCs are generally preferred. Achieving this can be accomplished through various strategies, including chemical modification with alloying elements, application of external fields like ultrasonic or electromagnetic fields during solidification, and precise control of solidification parameters such as thermal gradient and cooling rate.

Table 4
Trace elements atomic number, Bravais lattice and atomic radius.

Transition metal	Atomic number	Bravais lattice	Atomic radius, Å
Ti	22	HCP	1.47
V	23	BCC	1.34
Cr	24	BCC	1.27
Mn	25	SC	1.26
Fe	26	BCC	1.26
Co	27	HCP	1.25
Ni	28	FCC	1.24

3.1. *Effect of alloying elements*

The detrimental impact of Fe impurity on the mechanical properties of Al alloys can be mitigated by the addition of trace elements like Cr, Mn, Co, Sr, Be, Mo, Ni, S, and rare earth elements (REE). These elements, selected for their atomic size similarities to Fe (Table 4), can modify the step edge growth of Fe IMCs by acting as kink blockers, surfactants, incorporators, or step pinners. They possess similar bravais lattices and planar disregistries, facilitating effective interaction with Fe-bearing IMCs. Additionally, Mn, Cr, Ni, Co, and Fe share similar atomic radii and crystal structures, making them particularly influential in modifying Fe-bearing IMCs formation and characteristics [31,183]. Table 5 presents a summary of the effects of different alloying elements on the Fe-bearing IMCs.

3.1.1. *Manganese*

The formation and morphology of Fe-bearing IMCs in Al–Si alloys are significantly influenced by the addition of manganese (Mn) [40,44–47]. The metastable α-AlFeSi phase, which is typically promoted by faster cooling rates, can transform into a script-type or polygonal α-AlFeMnSi phase, such as α-$Al_{19}(FeMn)_4Si_2$ or α-$Al_{15}(Fe,Mn)_3Si_2$, when Mn is introduced across a wide range of cooling conditions [184]. However, achieving complete control over Fe-bearing IMC morphology remains challenging, as the formation of the desired script-type α-IMC does not always occur with increasing Mn content or faster cooling rates [35,42,179,185–187]. The cooling rate and Fe-to-Mn ratio play critical roles in determining the final microstructure (Fig. 11) [42,185]. At low cooling rates (~0.4 °C/s), a higher Mn-to-Fe ratio (~1 wt% Mn and 0.7 wt% Fe) favours the formation of script-like α-IMC, whereas intermediate cooling rates (~5 °C/s) lead to a mixed α and β-IMC structure [42,185,186,188]. At high cooling rates (~65 °C/s), the formation of needle-like β-IMC can reappear despite the presence of Mn (Fig. 11) [185]. Additionally, depending on the solidification conditions, the α-IMC can either nucleate as a primary phase within Al dendrites or form in the eutectic regions after α-Al solidification [42].

Two primary mechanisms have been proposed to explain the evolution of Fe-bearing IMCs with varying Mn levels and cooling rates [35,42,179,185–187]. The first mechanism suggests a peritectic reaction, where the Al_6Fe phase transforms into α-IMC, which can further transition into β-IMC at slower cooling rates [187]. The second mechanism, supported by *in-situ* solidification studies, indicates that β-IMC precipitates directly between 570 °C and 550 °C without an intermediate α-IMC transformation. Furthermore, high cooling rates (>200 °C/s) in Si-rich alloys (>7 wt% Si) have been found to suppress β-IMC formation and extend the stability of α-IMC regions [39,121].

The incorporation of Mn reduces the amount and volume fraction of the harmful β-IMC and refines its structure by substituting Fe atoms [23,31]. This modification alters step edge growth and improves material properties by transforming the morphology of Fe IMCs from plate-like to particulate. However, high Mn additions alongside Fe (up to 3 wt% Mn for 2.5 wt% Fe) promote the precipitation of large, star-like polyhedral α-IMC structures with dendritic morphology, which are detrimental to mechanical properties. In Cu-free alloys, the primary compounds formed are $Al_6(Fe,Mn)$ and $Al_{15}(Fe,Mn)_3Si_2$, while in Cu-bearing alloys, $Al_6(Cu,Fe,Mn)$, $Al_{15}(Cu,Fe,Mn)_3Si_2$, and $Al_{20}Cu_2Mn_3$ are predominant. Mn also promotes the nucleation of Fe-bearing IMCs by favouring the formation of α-IMC over β-IMC, stabilising the α-IMC through both thermodynamic and kinetic effects, especially at lower supersaturation levels in the melt.

Additionally, Mn:Fe ratio optimisation is crucial for achieving favourable IMC morphology without excessively increasing IMC volume fraction. A 1:2 Mn:Fe ratio is often recommended to minimise β-IMC formation, though suppression is not always complete even at 2:1 [42,

Table 5
Effect of trace element additions on Fe-bearing IMC formation and morphology in Al–Si alloys.

Element	Effects on Fe-bearing IMCs	Key observations	Reference(s)
Mn	Transforms β-IMC into script-like α-IMC, refines Fe IMCs, and reduces β-IMC volume fraction.	• At low cooling rates (~0.4 °C/s), high Mn:Fe ratio (~1:1) favours script-like α-IMC formation. • At high cooling rates (~65 °C/s), β-IMC can reappear. • Excess Mn leads to star-like polyhedral α-IMC, affecting mechanical properties.	[40,42,44–47,161,189–191]
Sr	Modifies β-IMC by fragmentation, dissolution, and poisoning of nucleation sites; promotes δ-IMC at high Sr levels.	• 70–300 ppm Sr refines β-IMC needles. • >200 ppm Sr promotes δ-IMC growth. • Sr interacts with P to influence β-IMC nucleation.	[179,208–213]
Cr	Replaces β-IMC with Chinese script α-IMC; excessive Cr leads to sludge formation.	• Optimal Fe:Cr ratio ~3:1 for β-IMC modification. • Enhances dispersoid formation in wrought alloys.	[40,48–51]
Co	Transforms needle-like Al_3Fe into a compact or Chinese script-like structure.	• Fe:Co ratio ~1:1 promotes favourable transformation. • Co reduces solute segregation, improving homogeneity.	[23,48]
K	Lowers eutectic temperature, refines β-IMC.	• Acts as a nucleation aid via potassium oxide formation.	[226]
B	Suppresses β-IMC growth, promotes α-IMC, and enhances nucleation.	• Forms AlB_2 and TiB_2 for grain refinement. • Improves Fe IMC morphology through thermodynamic interactions.	[227,228]
Be	Converts β-IMC into a fine Chinese script or globular morphology.	• 0.2 wt% Be significantly refines β-IMC. • Be–Fe phases serve as nucleation sites for α-Al.	[53,208,229]
Mn + Cr	Synergistically transform β-IMC into α-IMC, preventing needle-like IMCs.	• Enhances mechanical properties by refining Fe IMCs. • Mn:Cr ratio influences morphology and phase stability.	[130]
Mn + Sr	Sr enhances the fragmentation effect of Mn on β-IMC, promoting α-IMC formation.	• Mn and Sr together lead to finer Fe-bearing IMCs. • Sr addition may reduce α-IMC script size.	[209,219]
Mn + Be	Promotes globular α-IMC over β-IMC; excessive Be can form Al–Fe–Be compounds.	• Be enhances Fe-bearing IMC modification, improving ductility.	[208]
Sr + Cr	Cr limits Sr poisoning of nucleation sites, stabilising α-IMC.	• Sr reduces Cr-induced sludge formation.	[54,208,221]
Mn + Cr + Sr	Achieves optimal β-IMC suppression and α-IMC refinement.	• Balancing Mn:Cr:Sr ratios is key to refining IMCs and enhancing mechanical properties.	[54,179,208,221]
REE	Modify Al_xFe_y phases, influence formation temperatures, and refine β-IMC morphology.	• Ce, La, Nd, and Y alter Fe–Si phase formation.	[58–65]

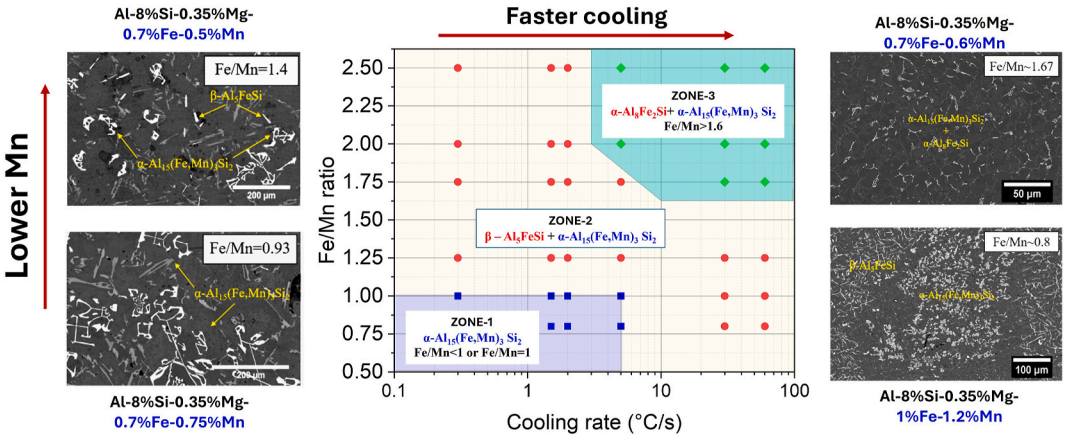

Fig. 11. The figure presents the formation map of Fe-containing IMCs in Al–8Si-0.35Mn-XFe-YMn alloys, illustrating the relationship between the Fe:Mn ratio and cooling rate. Figure redrawn from Ref. [185].

161,189–191]. The optimal Mn:Fe ratio depends on both cooling rate and Si content. Faster cooling (e.g., high-pressure die casting, HPDC) can suppress the peritectic transformation of L + α-Al_8Fe_2Si to β-Al_5FeSi, leading to microstructures with both α-Al_8Fe_2Si and α-$Al_{15}(Fe,Mn)_3Si_2$. In contrast, slower cooling rates (e.g., sand casting) allow the peritectic reaction to proceed, forming β-Al_5FeSi unless sufficient Mn is available to stabilise α-$Al_{15}(Fe,Mn)_3Si_2$.

Achieving optimal microstructures in secondary Al–Si alloys requires careful consideration of several interacting parameters. These include the overall alloy composition (Si content and total transition metal content), and the Mn content relative to total transition metal content. A higher Mn/(Fe + Mn) ratio correlates with an expanded range of intermediate cooling rates where only the α-IMC with a Chinese-script morphology forms, and this is associated with a greater presence of sludge particles [42]. However, Mn additions can increase the overall volume fraction of IMC phases in the bulk material (excluding sludge regions), which may offset the benefits of the improved IMC morphology [130,192–195]. Conversely, lower cooling rates coupled with increasing Mn content increase the propensity for undesirable sludge formation [40,196–201]. While sludge can potentially be removed from the melt [18,196,202–205], its formation alters the remaining alloy composition due to Mn partitioning, consequently affecting the microstructure [196]. Beyond modifying Fe-bearing IMCs, Mn provides additional benefits in Al alloys. It improves corrosion resistance, particularly in Cu-free Al alloys, by influencing both the IMCs and the Al matrix. Mn also enhances ductility, mitigates the negative impact of Fe-bearing IMCs, and improves fatigue resistance. Additionally, it contributes to better casting quality by reducing porosity and refining the microstructure.

3.1.2. *Strontium*

Strontium (Sr) is widely recognised for its role in modifying eutectic Si in Al–Si alloys [206,207], but its influence on Fe-bearing IMCs is complex and still a subject of debate [179,208]. Studies indicate that Sr alters both the nucleation and growth mechanisms of Fe-bearing IMCs, particularly β-IMC, but its effects depend on factors such as Sr concentration, Fe and Mn content, and cooling rate [179,208–211]. The modification of Fe IMCs by Sr can occur through fragmentation [40], dissolution [212,213], poisoning of nucleation sites [209,210,214], or phase transformation mechanisms [212]. However, inconsistencies in reported findings highlight the need for further investigation into the governing thermodynamics and kinetics of these transformations.

One of the primary effects of Sr addition is the refinement of the β-IMC (Fig. 12). Incremental Sr additions (70–300 ppm) at faster cooling rates (~60 °C/S) reduce the size distribution of β-IMC platelets from elongated, branched needles to finer, more fragmented structures [208]. This refinement is attributed to the poisoning of branching sites and the dissolution of thick β-plates, which results in one or more breaks along lengthy β-IMC needles [212,213]. The higher diffusion coefficient of Si in the presence of Sr further destabilises β-IMC platelets, facilitating their fragmentation into shorter, less harmful structures [208,213,215]. Despite the clear evidence of β-IMC refinement, there is no consensus on whether Sr promotes the β to α-IMC transformation [212]. Some studies

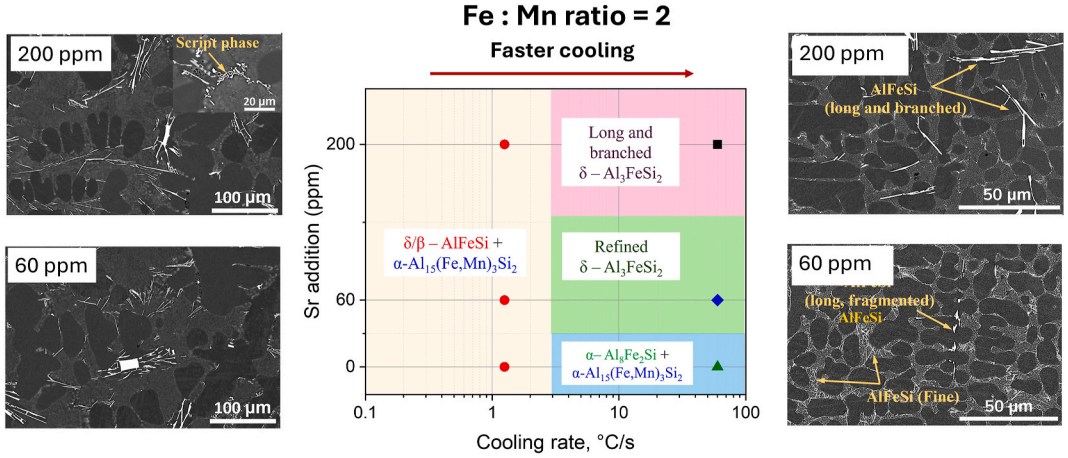

Fig. 12. Phase formation map of Fe-bearing IMCs, including Sr addition at an Fe-to-Mn ratio of 2 under the same casting conditions for Al–9Si–0.6Fe–0.3Mn–0.35 Mg alloys (redrawn from Ref. [179]).

suggest that Sr suppresses β-IMC nucleation in Al alloys by poisoning AlP and oxide particles, which serve as primary β-IMC nucleation sites in Al melts [216,217]. However, the presence of additional nucleation substrates, such as MgO, TiB_2, and SiC, complicates the exact mechanism, as these particles exhibit no strict orientation relationship with β-IMC [34,119]. Interestingly, P has been shown to increase the number density of β-IMC platelets, while Sr addition to a P-containing melt decreases their density, suggesting an interaction between Sr and P in controlling β-IMC formation [86]. The effect of Sr on Fe-bearing IMCs is strongly dependent on the cooling rate [179].

While β-IMC refinement is widely reported, Sr also plays a role in promoting δ-IMC formation, particularly in low-Fe alloys (Fe < 0.6 wt%) [125]. At high cooling rates (~60 °C/s), Sr additions (60 ppm) significantly refine δ-IMC, reducing its length to 3–5 μm and confining it within eutectic regions [216,218]. However, increasing Sr concentration (above 200 ppm) leads to the formation of Al_2Si_2Sr IMC, which influence the nucleation of δ-IMC, promoting its early formation and unrestricted growth into long, branched needle-like structures [216,218]. This observation highlights the dual role of Sr: at lower concentrations (~60 ppm), it refines δ-IMC through poisoning of nucleation sites, whereas at higher concentrations (~200 ppm), it enhances δ-IMC formation and branching through nucleation. The detailed work conducted by Balasubramani et al. [179] on the phase formation map of Fe-bearing IMCs, including Sr addition at an Fe-to-Mn ratio of 2 under identical casting conditions for Al–9Si–0.6Fe–0.3Mn–0.35 Mg alloys, is presented in Fig. 12.

In Mn-containing alloys, Sr can also influence the formation of α-IMC. While Mn is known to transform the acicular β-IMC into a more compact α-IMC, Sr may further promote this transition by altering nucleation conditions [209,219]. However, at lower Sr levels, this effect can be neutralised, leading to a reduction in α-IMC formation [220]. The combined addition of Mn and Sr is generally more effective in refining Fe-bearing IMCs than Sr alone, as it leads to the formation of script-like α-IMC instead of harmful β-IMC platelets [209].

The interaction of Sr with other alloying elements such as Mn, Mg, Ti, Cr, and Ca further complicates its role in Fe-bearing IMCs modification. Mn and Sr together refine β-IMC and promote α-IMC formation, while Cr additions contribute to restricting β-IMC growth and morphology [54,208,221]. Sr also interacts with Ti to refine β-IMC platelets, possibly through a combined effect on nucleation and growth mechanisms [208,222,223]. Additionally, the combination of Sr and Ca enhances eutectic Si modification and reduces β-IMC platelet size [208]. Notably, Sr does not form IMCs with Fe or Mn, indicating that its influence is primarily through nucleation and growth modification rather than phase formation [179]. At higher Sr concentrations (~200 ppm), the formation of Al_2Si_2Sr IMC in the liquid melt (~650–700 °C) suggests that these phases may play a role in β/δ- IMC nucleation, though their exact influence remains uncertain [224].

Unresolved issues persist regarding the precise mechanisms by which Sr influences Fe-bearing IMCs, particularly in distinguishing between fragmentation and nucleation suppression of the β-IMC. While many studies support the fragmentation and refinement of β-IMC needles, a detailed understanding of Sr's effect on nucleation remains elusive, whether it delays β-IMC nucleation by poisoning AlP and oxide particles or promotes early δ-IMC formation at higher Sr concentrations. The optimal Sr concentration for β-IMC refinement remains debated, with conflicting reports on whether Sr primarily suppresses or enhances δ-IMC growth, further complicated by the formation of Al_2Si_2Sr IMC at elevated Sr levels. The influence of cooling rate also lacks clarity, as high Sr (200 ppm) unexpectedly promotes elongated δ-IMC needles rather than refinement under certain conditions.

3.1.3. Chromium

Chromium (Cr), similar to manganese (Mn), can modify the detrimental β-IMC in casting alloys, replacing it with more beneficial phases such as the Chinese script phase, which improves ductility and fracture toughness [40,48–51]. However, excessive Cr can lead to the formation of undesirable sludge phases, including Fe/Cr-containing phases [221]. To balance the beneficial modification of the β-IMC with the risk of sludge formation, an optimal Fe:Cr ratio of approximately 3.0 is often employed. Lower Cr levels (around 0.1 wt%) facilitate the development of both primary Si crystals and the Chinese script phase [48]. In Al-rich Al–Fe–Cr alloys, the equilibrium phases with Al are Al_3Fe and Al_7Cr, with no ternary compounds forming. The Al_3Fe phase can dissolve up to 4 wt% Cr, and the compound $Al_7(Fe,Cr)$ is sometimes observed in these alloys [23]. Addition, Cr is particularly beneficial for the formation of dispersoids (α-Al(Fe,Cr)Si and α′-AlCrSi) during the thermomechanical processing of alloys [225], especially in wrought alloys, where it enhances the stability and distribution of these dispersoids, further improving the material's properties.

3.1.4. Cobalt

In the Al–Fe system, cobalt (Co) does not form ternary phases with Al and Fe but instead leads to the formation of Al_3Fe and Al_9Co_2 [23]. Notably, the Al_3Fe phase can dissolve up to 12.4 wt% Co, and the Al_9Co_2 phase can dissolve up to 10.8 % Fe, represented by the formulas $Al_3(Fe,Co)$ and $Al_9(Fe,Co)_2$, respectively.

A small addition of 0.1 wt% Co in the Al-0.5Fe system significantly transforms the needle-like Al_3Fe morphology into a more compact form. Increasing Co content to 0.2 wt% further modifies the morphology to a Chinese script-like structure. An Fe:Co ratio of approximately 1.0 is crucial for this transformation of the β-IMC platelet phase to the Chinese script morphology [48].

Cobalt's influence on Fe phases stems from its effect on solidification sequences in the ternary [23], $L \rightarrow \alpha - Al + Al_3(Fe,Co) + Al_9(Fe,Co)_2$. A key advantage of Co addition is its ability to reduce solute segregation during solidification, promoting a more homogeneous microstructure.

3.1.5. Potassium

Potassium (K) addition in Al–Si alloys can significantly influence both the eutectic reaction and the formation of Fe-bearing IMCs. Specifically, K lowers the eutectic reaction temperature while increasing the liquidus and crystallisation onset temperatures for the β-IMC [226]. The presence of potassium promotes nucleation by introducing additional particles that serve as nucleation sites, thus reducing the necessary undercooling. These nucleation sites arise from the reaction of K with oxides, forming potassium oxides with planar registries similar to Fe-IMCs. This mechanism can ultimately lead to the refinement of Fe-IMCs in the alloy.

3.1.6. Boron

Boron (B) plays a multifaceted role in refining Fe-bearing IMCs within Al–Si alloys. It achieves this by several interconnected mechanisms. Primarily, B suppresses the growth of detrimental β-IMC platelets and encourages their transformation into the more desirable α-IMC, contributing to a more favourable microstructure. *In-situ* synchrotron X-ray radiography has demonstrated that B significantly lowers the formation temperature of primary Fe-bearing IMC [227,228], indicating its influence on the early stages of solidification. This effect is linked to B's ability to alter the thermodynamic stability of IMCs. By interacting with Fe and Si, B shifts phase equilibria towards the α-IMC, effectively reducing the formation of less desirable phases. The effectiveness of B is further modulated by other alloying elements. For instance, while Mn independently stabilises the α-IMC, B enhances this stabilisation, leading to a refined and more uniform microstructure. Song et al. [227,228] worked with Al–3B master alloys in Al–7Si-1.2Fe alloys illustrating some of these effects. While B effectively refined the grain structure, the formation of Al–AlB_2 during the eutectic reaction limited its impact on the morphology and distribution of Fe-bearing IMCs. However, in alloys with higher Fe content (≥2.36 wt%), B did offer some refinement of primary Fe-IMCs, although it could not completely eliminate the formation of plate-like β-IMC. At the atomic level, B's strong adsorption to

α-Al_2O_3 (0001) crystal planes, compared to Mn and Fe, allows it to act as an active element. B preferentially interacts with the oxide film surface, hindering Fe-bearing phase formation at high temperatures. This not only prevents nucleation at the Al–AlB_2 eutectic temperature but also promotes more controlled phase transformations. First-principle calculations support this, showing that B's higher adsorption energy on nucleation sites, such as α-Al_2O_3, inhibits primary Fe-IMC nucleation above the Al–AlB_2 eutectic temperature, leading to undercooling and a refined microstructure. The Al–AlB_2 eutectic reaction, producing AlB_2 and α-Al, further contributes to refinement through competitive growth, encouraging the transformation of Fe-bearing IMCs into multibranched structures. The *in-situ* synchrotron X-ray radiography, revealing the reduced formation temperature of primary Fe-IMC, reinforces the idea that B enhances α-Al grain nucleation and controls Fe-bearing IMC growth [227,228]. These combined effects of B, encompassing refined phase morphology and improved nucleation control, ultimately enhance the microstructure and boost the overall performance and stability of the alloy.

3.1.7. Beryllium

In Al–Si–Fe alloys, beryllium (Be) plays a crucial role in refining and modifying Fe-bearing IMCs. It transforms the plate-like β-IMC into a Chinese script morphology or fine globules. Notably, 0.2 wt% Be has been shown to significantly refine the β-IMC [53]. The interaction between Mn and Be can result in either fine or coarse Chinese script IMCs, depending on the cooling rate [208]. At low cooling rates, Be neutralisation of Fe-based IMCs promotes the formation of Chinese script structures within the α-Al grains. Murali et al. [53] reported that in an Al–7Si-0.3 Mg alloy with 0.27 wt% Be, Be–Fe phases form within the α-Al matrix, likely due to a peritectic reaction. Similarly, Wang and Xiong [229] observed that in Al–7Si-0.4Mg-0.2Ti alloys, Be–Fe phases may serve as nucleation sites for α-Al during solidification, supporting Murali et al.'s findings [53]. However, under high cooling rates, the number of Be–Fe phases within α-Al decreases, shifting their formation to the interdendritic region. This suggests that Be–Fe phases form at higher temperatures than the β-IMC platelets, which typically precipitate after α-Al and Be–Fe phase formation. At high cooling rates, the growth of Al dendrites dominates, limiting Be–Fe phase formation in interdendritic regions. In Al–7Si-0.3Mg-0.8Fe alloys, the combined addition of 0.15 % Be and 0.15 % Mn promotes the formation of Mn–Fe and Be–Fe Chinese script IMCs, which effectively reduce the overall Fe content by depleting Fe from the matrix.

3.1.8. Rare of earth element (REE)

Rare earth elements (REE), including Ce, La, Nd, and Y, affect the morphology and formation of Fe-bearing IMCs in Al alloys, particularly in phases such as Al_3Fe, Al_6Fe, and β-IMC [58–65]. The addition of Ce and La to Al alloys leads to phase formation shifts, evidenced by changes in the temperatures at which these phases form, though the morphology of eutectic Al_xFe_y phases remains largely unchanged [230,231]. In particular, La has a refining effect on the β-IMC in Al–7Si–4Cu-0.35Mg-0.2Fe alloys. La additions induce the formation of La-rich IMCs like Al_4Cu_2SiLa, which act as nucleation sites for β-IMC [231]. These IMCs promote the nucleation of β-IMC while restricting its growth by altering the solid-liquid interfacial energy and diffusion processes. This results in cross-like and parallel-like growth patterns of β-IMC, controlled by solute concentration and the anisotropy of interfacial energy.

In addition to refining the β-IMC, REE such as Ce and La are also effective in refining the α-Al grains and Fe-bearing IMCs in Al–Fe alloys [230]. For instance, a 0.5 wt% REE addition can reduce the average size of α-Al grains by half compared to alloys without REE, enhancing the structural properties of the material. Similarly, Nd, when added in small amounts (0.03 wt%) to Al–Si–Mg alloys, promotes undercooling and the formation of the π-phase, though excessive Nd can lead to the formation of larger Nd-rich particles that reduce the amount of π-phase formed through peritectic reactions [62]. Y additions in Al–Si–Mg–Fe alloys also refine the acicular β-IMCs and decrease their volume fraction, further improving the alloy's properties [63]. When combined with REE, Mn further stabilises the α-IMC, leading to a more refined and homogeneous microstructure. The combined influence of Mn and REE contributes to a controlled and optimised phase structure, offering substantial improvements in both microstructural uniformity and overall alloy performance.

The casting method and cooling rate also play a crucial role in the formation of Fe-bearing IMCs. In particular, squeeze casting, which involves rapid solidification under pressure, has been shown to refine the microstructure and improve mechanical properties [232]. However, the impact of REE on Fe-bearing IMCs during rapid solidification is still not fully understood.

3.2. Effect of physically induced force

Chemical modification of Al–Si alloys to refine Fe-bearing IMCs can be limited by undesirable side effects like sludge phase formation or poisoning effects. An alternative approach involves physically induced forces, such as high-intensity shear [74–76], low-frequency mechanical mould vibration [81,82], electromagnetic stirring [84], and ultrasonication [66–69,72]. These techniques (Table 6), applicable to both cast and wrought Al alloys, offer advantages like avoiding the formation of detrimental IMCs but may face limitations in terms of scalability.

3.2.1. Effect of high-intensity ultrasonication (UT)

Ultrasonication's (UT) influence on metallic melts is generally explained through the principles of cavitation and acoustic streaming [73]. Cavitation induces the formation, growth, and violent collapse of dissolved gas bubbles within the melt (when the cavitation threshold of the melt is exceeded). The collapse of cavitation bubbles generates localised shockwave pulses nearing 1000 atm and liquid microjets of 100 m/s velocity [71,233]. The cavitation threshold for Al melt, 100 W/cm^2, is far exceeded in melt ultrasonication with estimated energy density of 1500 W/cm^2 reported [234]. Acoustic streaming from ultrasound attenuation induces steady fluid flow dissipating heat and homogenising solute distribution while dispersing nuclei throughout the melt. While microstructural refinement effect is generally attributed to cavitation, the precise mechanisms remain unclear. Suggested contributing factors include dendrite fragmentation from cavitation and subsequent fragment dispersion by acoustic streaming [73], as well as alternative theories on enhanced heterogeneous nucleation through pressure-induced alterations to the freezing point or adiabatic melt cooling at the cavitation bubble surfaces [235,236].

UT has been shown to induce the transformation of both thin β-IMC plates and dendritic (Chinese-script) α-IMC into compact α-IMC of polyhedral form and finer and fragmented β-IMC (Fig. 13). However, the efficacy of this modification is influenced by several parameters besides alloy composition, including treatment temperature, melt volume, sonication duration, melt viscosity, and the distance from the ultrasonic horn. Existing literature indicates that α-IMC can form via peritectic reactions (occurring before α-Al nucleation) [237], a process directly affected by UT. Furthermore, α-IMCs are known to nucleate on oxides [130]. Considering the proposed mechanism of cavitation-assisted forced wetting of inclusions [233,238], it is plausible that cavitation-induced wetting of oxide films increases the number of heterogeneous nucleation sites, contributing to the observed α-IMC nucleation peak under UT. Our findings [239], demonstrated that UT promotes α-IMC nucleation, with a clear reduction of nucleation undercooling in the measured cooling curves. However, growth kinetics continue to play a significant role in the subsequent morphological development of these phases with ultrasound assisted solute homogenisation preventing dendritic growth and leading to compact polygonal particle formation as illustrated in Fig. 13(a–d). Xiang et al. [159] used *in-situ* techniques to study the impact of ultrasound on the solidification

Table 6
Effect of physically induced methods on Fe-bearing IMCs in Al- alloys.

Method	Mechanism	Effect on Fe-bearing IMCs	Key Findings	Reference(s)
UT	Cavitation and acoustic streaming generate localised shockwaves (1000 atm) and microjets (100 m/s).	Transforms β-IMC into particulate α-IMC, refining IMCs.	• Enhances heterogeneous nucleation via oxide wetting. • Increases nucleation rate, leading to finer α-Al and Fe-IMCs. • Reduces Fe-IMC size by ~5 × due to constrained growth space.	[71,159,233, 234,237,238]
EMS	Lorentz forces generate bulk melt flow, affecting nucleation and diffusion.	Alters Al_3Fe and other Fe-IMC morphology; may coarsen or refine IMCs depending on solidification sequence.	• Improves solute distribution, reducing localised supersaturation. • Constrains IMC growth when nucleation occurs after α-Al. • Can coarsen IMCs in hypereutectic alloys via Ostwald ripening.	[83,240,241, 244–247]
Shearing/Stirring	Forced convection via mechanical impellers or mould design.	Promotes compact Fe-IMCs, particularly refining β-IMC morphology.	• Breaks dendrites to finer particles. • Enhances solute and thermal homogenisation. • Disrupts diffusion layer, favouring compact IMC morphologies.	[75,252–255]
Combined chemical physical & methods	Physical treatment followed by chemical stabilization (Mn, Sr, Ti, GR).	Further IMC refinement and improved microstructural control.	• Reduces Fe-IMC size, effective in large melt volume. • TiB_2 dispersion enhanced, restricts Fe-IMC growth. • Balances cost and environmental impact for sustainable recycling.	[264]

of Fe-bearing IMCs nucleated after α-Al formation. Their research demonstrated that brief applications (7 s) of high-frequency ultrasound to the liquid melt generate substantial oscillating pressure and velocity fields, reaching up to 1.5 MPa and 150 mm/s, respectively. These intense fields induce significant homogenisation of the melt's thermal and solute distribution. This homogenisation is a key factor in the observed morphological evolution. The enhanced nucleation under ultrasonication leads to a dramatic refinement of the α-Al dendrite structure, with the average dendrite size reduced approximately five-fold during the initial stages of solidification. This significant microstructural refinement plays a crucial role in controlling the subsequent growth of Fe-bearing phases when these IMCs form later through eutectic reactions (Fig. 13 (e) and (f)). The constrained intergranular growth space imposed by the finer α-Al dendrites ultimately results in a comparable five-fold reduction in the average size of the Fe-bearing phases compared to conventionally solidified samples.

3.2.2. *Effect of electromagnetic stirring (EMS)*

Electromagnetic stirring (EMS), utilising high magnetic fields, has emerged as a promising technique for microstructural modification in Al alloys, affecting α-Al grain size, eutectic structures, and Fe-bearing IMCs [83,240,241]. This method involves the generation of anisotropic magnetic fields to influence the solidification process, offering a different approach compared to other techniques like UT. The application of magnetic fields can significantly alter several key aspects of solidification, including surface tension, diffusion, and undercooling, all of which play crucial roles in crystal nucleation. Furthermore, static magnetic fields are known to modify the morphology of solid/liquid interfaces, induce instability, and influence crystal orientation within the liquid metal [242,243].

Studies on the hypereutectic Al–Fe binary system have provided valuable insights into the effects of magnetic fields on Fe-bearing IMCs [244,245]. These studies have demonstrated that the primary Al_3Fe phase tends to coarsen under the influence of a magnetic field. This coarsening phenomenon is likely attributed to a combination of factors, including enhanced diffusion and potentially reduced undercooling, which facilitate the growth of existing Al_3Fe particles at the expense of smaller ones. Interestingly, despite the coarsening observed in some cases, magnetic field-induced melt stirring can also lead to changes in IMC morphology that are similar to those observed with UT. However, the overall impact of EMS on Fe-bearing IMC modification is often less pronounced than that of UT and also depends on the specific parameters of the applied magnetic field and the alloy system.

The underlying principles of EMS differ significantly from those of UT. While ultrasonication relies on the introduction of high-frequency pressure waves to induce cavitation and acoustic streaming, EMS generates bulk melt flow through Lorentz forces. These forces arise from the interaction between the applied magnetic field and the electric currents induced within the conductive melt. The resulting large-scale melt flow promotes the uniformity in solute and temperature distribution, minimising localised supersaturation and temperature gradients that can influence nucleation and growth [83,246,247]. Additionally, the stirring action can break up existing dendrites or introduce foreign particles into the melt, providing additional heterogeneous nucleation sites. This is analogous to the cavitation-assisted wetting of oxide films proposed for UT, where the increased availability of nucleation sites leads to a higher number density of IMCs.

The impact of EMS on Fe-bearing IMCs is highly dependent on the solidification sequence, specifically the timing of IMC nucleation relative to the α-Al phase. When IMCs nucleate after the α-Al dendrites, the refined α-Al microstructure (due to EMS) can constrain the subsequent growth of the IMCs. This constraint, coupled with the increased number of heterogeneous nucleation sites, can lead to a higher number density of IMCs with smaller individual sizes, similar to the refinement observed with ultrasonication. However, when Fe-bearing IMCs nucleate before the α-Al, EMS can have a different effect. The stirring can break up the primary Fe-IMCs, distributing them throughout the melt (Fig. 14) [241]. This can lead to a more uniform distribution of the IMCs, but it may also coarsen them if the stirring promotes Ostwald ripening, as observed in the hypereutectic Al–Fe system [244,245].

3.2.3. *Effect of stirring or shearing*

The application of stirring or shearing forces during the solidification of metallic alloys, including Fe, Al, Mg, and immiscible alloys has been widely investigated to refine and homogenise microstructures. Early studies in this field concentrated on semi-solid metal (SSM) processing,

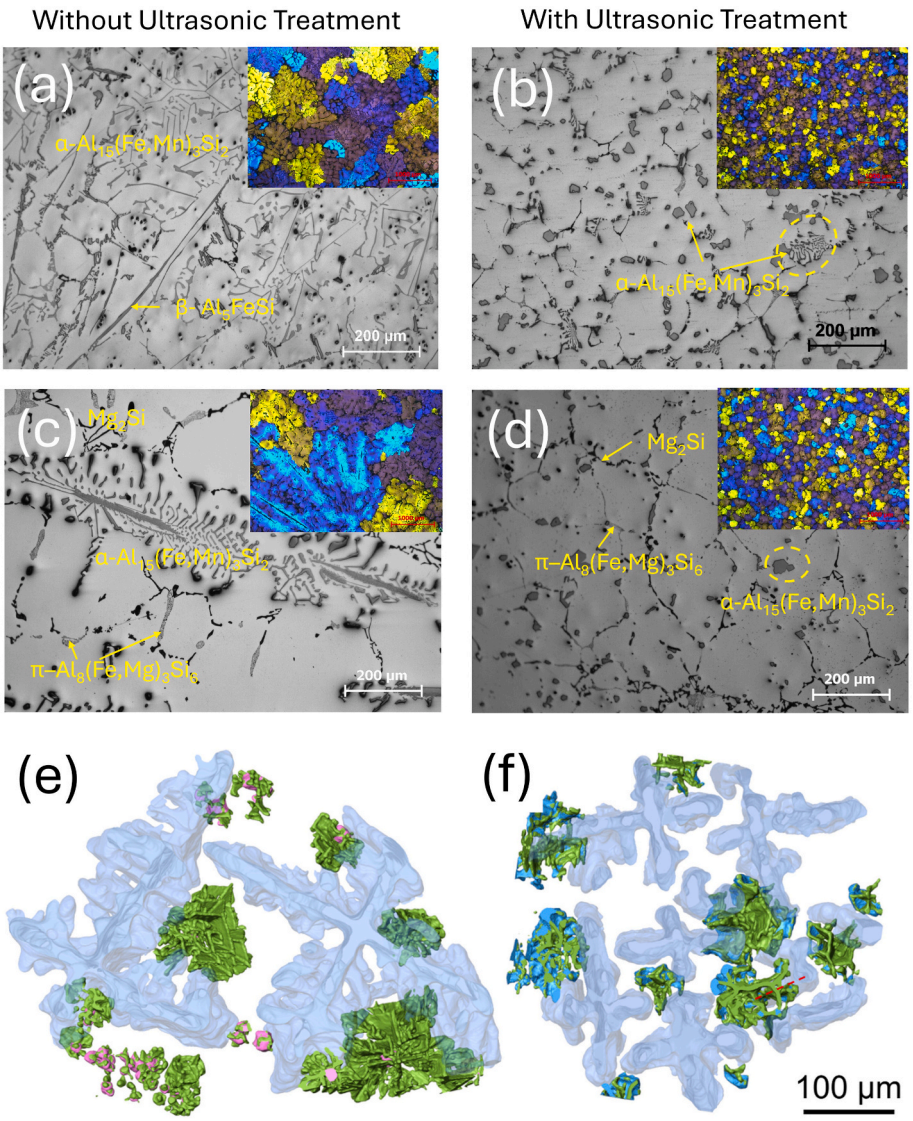

Fig. 13. Effect of ultrasonication on two high-Fe Al alloys: (a, b) Al–2Si–2Mg–1.2Fe–0.5Mn and (c, d) Al–2Si–2Mg–1.2Fe–1Mn. (a, c) represent conventionally cast samples, while (b, d) are ultrasonicated until the end of solidification. Ultrasonication promotes the formation of particulate α-IMCs instead of β-IMC and the Chinese script α-IMC phase (from authors' work). Inserted image shows α-Al grain refinement with ultrasonication. (e, f) 3D spatial relationships between α-Al dendrites and Fe-bearing phases (adopted from Ref. [159]).

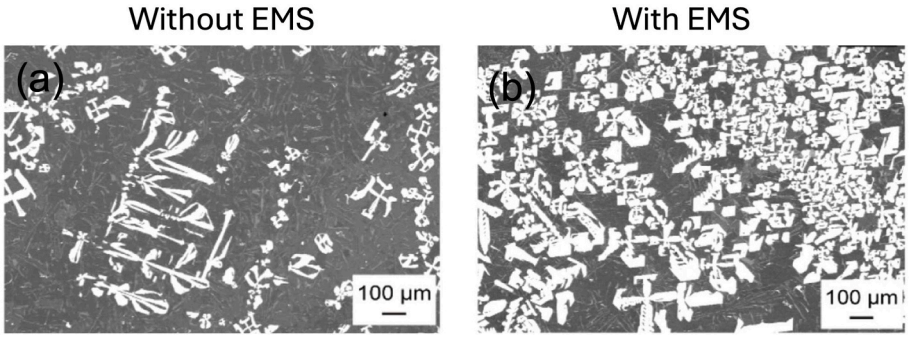

Fig. 14. Al–10Si–2Fe–2Mn alloy solidified (a) without and (b) with EMS, adopted from Ref. [241].

elucidating dendrite fragmentation as the dominant mechanism for achieving microstructural refinement [78–80], distribution of particles [248,249] and immiscible liquid phases [250,251]. However, subsequent studies on shearing Al and Mg alloys melts above their liquidus temperatures have explored the potential for nucleation-driven refinement [252,253], shifting the focus beyond simple fragmentation. Shearing introduces controlled fluid flow within the metallic melts. This forced convection differs fundamentally from the mechanisms involved

in UT and EMS. While UT utilises high-frequency acoustic waves and EMS employs magnetic fields to induce melt movement, stirring and shearing typically involve mechanical means, such as rotating impellers or specially designed mould geometries.

Shearing during solidification offer an alternative route to microstructural refinement in Al alloys, particularly in DC casting [254]. This approach hinges on several key mechanisms. First, similar to UT, shearing can fragment existing dendrites, especially early in solidification. These fragments then act as nuclei, leading to a finer grain structure [254]. However, unlike UT's localised cavitation-induced fragmentation, shearing provides fragmentation of early dendrites throughout the melt [252–254]. Second, mirroring both UT and EMS, the forced convective flow from shearing promotes solute and thermal homogenisation. This reduces localised supersaturation and temperature gradients that may influence IMC nucleation and growth [255]. Third, the shear forces may directly impact nucleation kinetics. They can increase heterogeneous nucleation sites by dispersing particles or enhancing inclusion wetting, depending on the potency of those particles to nucleate Fe-bearing IMCs [252–254]. Finally, and perhaps most significantly, shearing can control IMC growth morphology. High shear rates can disrupt the diffusion boundary layer around growing crystals, preventing directional growth and favouring a more isotropic growth of compact shape [80,256,257]. This spheroidising effect is particularly important for refining plate-like IMCs [75,255].

The effectiveness of shearing depends on several factors, including alloy composition, shearing rate, application temperature, and crucially the solidification sequence of IMCs relative to the α-Al phase. Kotadia et al. [75] demonstrated the impact of near-liquidus casting with shearing on IMC morphology and distribution. They observed a clear shift towards more compact, globular β and α-IMCs (Fig. 15) at high shear rates. This spheroidisation is attributed to the disruption of plate-like β-IMC growth by the shear forces and the promotion of more globular α-IMC growth.

The solidification sequence plays a critical role, much like in UT and EMS. When IMCs nucleate after α-Al dendrite formation, the refined α-Al structure resulting from shearing constrains IMC growth in the smaller liquid pockets. The increased nucleation sites also contribute to a higher number density of smaller IMC particles. Conversely, if IMCs nucleate before α-Al, the shear forces can break up and redistribute the IMCs, preventing large, detrimental clusters. However, this can also lead to coarsening via Ostwald ripening under certain conditions.

3.3. Synergistic strategies: combining chemical and physical methods

While physical methods such as UT and EMS offer significant advantages for refining Fe-bearing IMCs in recycled Al alloys, they are not without limitations. UT, for instance, exhibits high efficacy in small melt volumes, particularly in DC casting where the molten sump is contained and continuously processed. However, scaling UT to large-volume, batch casting operations presents challenges in achieving uniform cavitation and retaining treatment benefits during liquid metal transfer. Furthermore, the selection of horn materials for UT is critical, requiring resistance to molten Al to prevent contamination and minimise replacement costs. While non-contact UT shows promise [258–260], its large-scale applicability remains to be thoroughly investigated.

EMS, effective for reducing segregation and promoting α-IMC formation, faces limitations in highly viscous melts and complex geometries. Similarly, intensive shearing, though beneficial for inclusion dispersion and primary Fe-IMC refinement, struggles with large melt volumes and demands precise operational control to prevent equipment wear. These limitations underscore the need for a more comprehensive approach to Fe-bearing IMC management.

Conversely, chemical methods, relying on alloying additions, also have inherent limitations. While elements like Mn and Cr can effectively stabilise the α-IMC, excessive additions can negatively impact alloy properties, such as ductility and electrical conductivity [261]. Furthermore, the introduction of alloying elements increases material costs and may complicate recycling processes due to compositional changes. Precise control over alloying additions is also crucial, as deviations from optimal compositions can lead to unintended phase formation and microstructural defects. Additionally, chemical methods can generate secondary waste streams, necessitating careful consideration of environmental impact. Furthermore, the "poisoning effect" and cross-interactions among alloying elements in Al alloys pose significant challenges, particularly in recycled materials where impurity levels fluctuate. For example, excessive Si can weaken the efficacy of Mn in promoting the beneficial α-IMC [35]. Specifically, when the Fe: Si ratio is low, such as below 1:2, Si favours the formation of the brittle β-IMC, even with adequate Mn additions. Similarly, high Fe levels, coupled with insufficient Mn, can lead to the formation of undesirable Fe-bearing IMCs like β-IMC [189]. These interactions can ultimately result in the formation of phases that negatively impact mechanical properties, such as ductility and fracture toughness. Moreover, the presence of other elements, like Ti, can be affected by Si; high Si content can promote Al_3Ti formation over the intended TiB_2 [262]. Additionally, in near-eutectic Al–Si alloys containing both Sr and B, the formation of Sr_3B_4 leads to a stoichiometric depletion of these elements from the melt, showing minimal effect on microstructural refinement [263].

To maximise the benefits of both physical and chemical methods and mitigate their respective drawbacks, a synergistic strategy combining these routes is proposed. Physical techniques like UT or EMS can be strategically employed to refine α-Al grains and homogenise melt composition and temperature, thereby inhibiting the formation of large, plate-like IMCs. Subsequently, alloying elements such as Mn or Cr can be judiciously introduced to stabilise the α-IMC, leveraging the strengths of both approaches while minimising their individual weaknesses. Our recent work [264] demonstrated the combined effect of UT and growth-restricting elements (Ti) in refining α-Al grains and subsequently

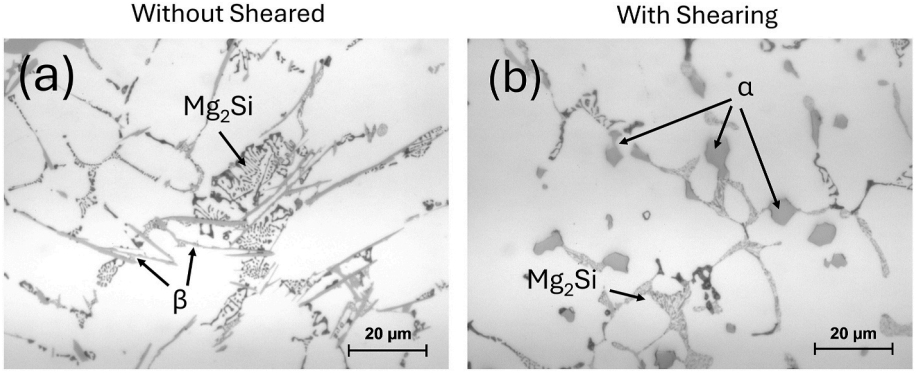

Fig. 15. Modification of Fe-bearing IMC morphology under intensive shearing [75].

influencing the morphology and distribution of Fe-bearing IMCs. The study revealed the significantly refined Al-grain structure leading to the finest and most uniformly distributed Fe-IMCs in treated ingots, even when these compounds formed outside the application regime of ultrasonication. When UT was applied in conjunction with Ti or GR additions, the size of Fe-IMCs was further reduced compared to the use of chemical treatments alone. The most notable refinement of Fe-IMCs was observed in alloys treated with both GR and UT, which also exhibited better dispersion of residual TiB_2 particles in intergranular regions. The synergy between UT and GR was critical in controlling the distribution of intergranular liquid pockets, which appeared to be the predominant factor influencing the growth and size of Fe-IMCs. By reducing the size and improving the uniformity of these liquid pockets through combined application of UT and GR, the growth of coarse Fe-IMCs was restricted (even though they solidified following ultrasound withdrawal), thereby improving the microstructural homogeneity of the alloy. This combined approach offers a scalable and effective solution for high-quality recycling processes as confining ultrasound application only during the early stages of solidification may address the practical limitations in process development. Furthermore, this combined strategy balances cost and environmental considerations, leveraging the strengths of each approach to overcome their respective limitations. While physical methods are particularly effective for refining and homogenising the melt without introducing additional materials, chemical methods enable precise phase transformations and compositional adjustments. Together, they offer a comprehensive solution for managing Fe-bearing IMCs in recycled alloys, paving the way for more efficient and sustainable large-scale recycling processes.

3.4. Effect of cooling, superhating and post-solidification heat treatment

3.4.1. The effect of cooling rate

Al alloys can be cast using various techniques, including gravity casting, high-pressure die casting (HPDC), and direct chill (DC) casting. Each technique offers a distinct range of cooling rates, influenced by factors like mould material and design, casting volume, and distance from the centre to the mould walls. DC casting typically exhibits cooling rates between 0.1 and 20 °C/s [102], while HPDC can achieve rates up to 1000 °C/s [74]. Gravity casting cooling rates can also reach 60 °C/s. It is important to note that rapid solidification, as observed in HPDC, can significantly impact the resulting microstructure, leading to increased solute solubility, decreased grain size, altered microsegregation patterns, and the potential formation of metastable phases.

The influence of cooling rate on the formation and stability of Fe-bearing IMCs in Al–Si alloys has been investigated extensively [91,104,265–268]. Increasing the cooling rate has been shown to promote the formation of metastable phases while suppressing the formation of stable IMCs. For instance, the Al_3Fe phase can be replaced by the metastable Al_6Fe phase at higher cooling rates, and the Fe content in the eutectic decreases with increasing cooling rate [104,265,266].

In the ternary Al–Si–Fe alloy, various metastable phases, including Al_3Fe, Al_6Fe, and Al_mFe, have been observed in the eutectic at high cooling rates [102]. Moreover, increasing the cooling rate from 6 to 8 °C/s led to the formation of Al_6Fe, α-AlFeSi, and α'-AlFeSi phases. Notably, the Al_3Fe phase, prevalent at low cooling rates, was absent at higher cooling rates [102]. In the Al-0.5Fe-0.2Si alloy system, Griger et al. [269] observed the substitution of $Al_{13}Fe_4$ by the α-IMC at cooling rates of 2.3 °C/s.

Dutta et al. [99] investigated the effects of cooling rate (0.04–3.5 °C/s) on the eutectic fraction, dendritic arm spacing, and refinement of Fe-bearing IMCs in Al–Si–Fe alloys. They found that higher cooling rates decrease the Fe:Si ratio in the eutectic, promoting the formation of metastable Al_6Fe and/or α-IMCs while suppressing the Al_3Fe phase. The size of secondary phases is also influenced by the bulk alloy composition and repeated nucleation during eutectic solidification. Further research is needed to understand the composition of the liquid eutectic and its impact on phase selection. Belmares-Perales et al. [270] observed the disappearance of the β-IMC at both high (>3.5 °C/s) and low (<0.1 °C/s) cooling rates, hypothesising that this is related to growth kinetics and chemical composition.

Becker et al. [42] observed a cooling rate window for α-IMC formation and plate-shaped particle (β and δ-IMC) suppression, bounded at both low and high cooling rates, and expanding with increasing Mn content. The δ-IMC fraction increases significantly with increased cooling rate and slightly with Mn content, while the β-IMC fraction decreases. At 0.05 °C/s, β-IMC dominates; at 200 °C/s, δ-IMC becomes the major phase. This phase dominance shift occurs at both low and high, but not intermediate, cooling rates. The coexistence of β and δ-IMC within single particles suggests multiple formation mechanisms: (1) incomplete δ-to-β transformation or (2) direct as-solidified δ and β regions. Both relate to how cooling rate affects the reaction pathway kinetically, leading to different microstructures. Rapid cooling can suppress nucleation, growth, and diffusion, favouring non-equilibrium phases. This implies that primary phase crystallisation regions may differ significantly from equilibrium predictions, altering the solidification path. Experimental result has shown that in hypoeutectic Al–Si alloys under non-equilibrium solidification, the melt's Si content rises, approaching the δ-IMC region. Thus, δ-IMC can solidify at β-IMC particle peripheries. The β and δ-IMC structural similarity makes β a good δ-IMC nucleation site. Local compositional variations (e.g., higher Si) can cause deviations from the overall path, leading to δ-IMC formation on β-IMC even at low cooling rates. Higher cooling rates extend the δ-IMC region to lower Si concentrations, increasing the δ-IMC fraction, a trend enhanced by Mn. Also noted that with increasing cooling rate, α-Al phase sludge particles transition from bulky polyhedral to coarse dendritic with their volume fraction decreasing. This concentrates IMCs in the bulk. Balancing plate-shaped particle suppression against increased bulk IMC content (including sludge) is crucial, not only with Mn additions [40,190,194], but also with Mn:Fe ratio adjustments. At 200 °C/s, smaller, mainly δ-IMC plate-shaped particles appear in eutectic regions. At very high cooling rates, sludge is suppressed. However, plate-shaped particles can reappear, depending on the Mn:Fe ratio. If these particles are within the Al–Si eutectic, their negative impact may be negligible [191,271,272], likely due to smaller size.

The cooling rate significantly influences the solidification process, grain structures, and morphology of Fe-bearing IMCs in AA6063 Al alloys [109,110,134]. Slower cooling rates led to larger, more interconnected IMCs, while faster rates resulted in smaller, less interconnected ones. The interconnectivity, size, and morphology of the IMCs are determined by the α-Al grain structure and the solute-rich liquid surrounding the grain boundaries. While changes in α-Al grain structure do not directly affect phase selection, the cooling rate can dictate the dominant precipitation of β-IMC (lower rates, 1.1 °C/s) or α-IMC (higher rates, 16.6 °C/s) [110]. Fe-bearing IMCs solidify at the intergranular region. The solute-rich liquid around these grain boundaries governs the interconnectivity and morphology of Fe-bearing IMCs [134]. Coarse feathery α-Al grains result in a less interconnected network of coarser IMCs, whereas globular structures increase their interconnectivity along with some refinement (Fig. 16). Conversely, a fine dendritic microstructure enhances chemical uniformity and minimises liquid pockets, favouring the formation of a fine, less interconnected α-IMC, that can be further refined through solutionising heat treatment [134,264].

3.4.1.1. The effect of rapid solidification. Rapid solidification processing (RSP) techniques, characterised by extremely high cooling rates, offer a powerful approach to modify the microstructure and properties of Al alloys. Recent research has focused on the potential of high Fe-containing Al alloys produced via additive manufacturing (AM) processes like Laser Powder Bed Fusion (L-PBF) to achieve superior high-temperature mechanical properties compared to conventional cast and

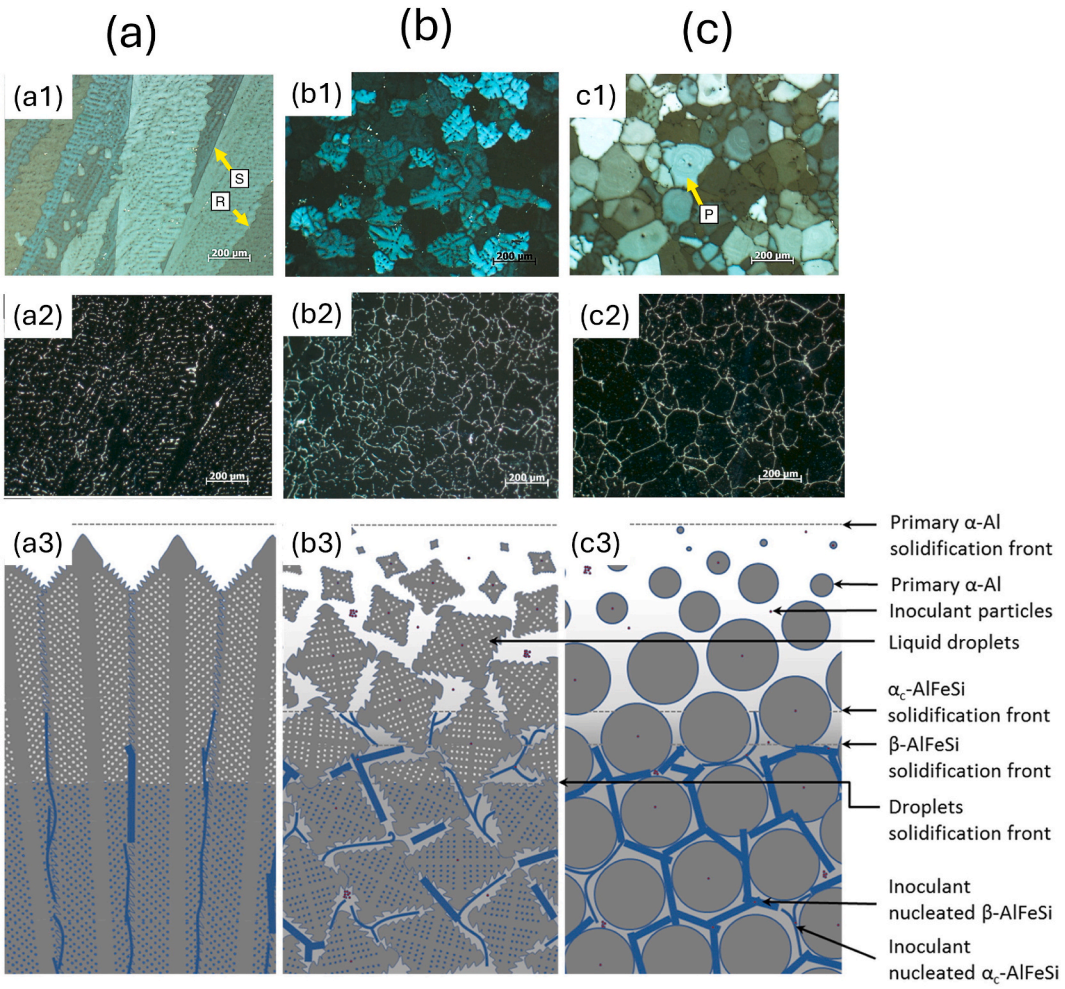

Fig. 16. Optical microstrucure and schematic illustration of the solidification process, depicting different α-Al morphologies: (a) feathery-dendritic structure with a significant β-IMC volume fraction, (b) equiaxed dendritic structure refining both α and β-IMCs, and (c) equiaxed-globular structure with fine β-IMC and small volume of eutectic Chinese script α phase. The refinement of IMCs in (b) and (c) is achieved through increasing nucleation sites for IMCs using an inoculant and changing the liquid pockets between α-Al. Polarised (a1, b1, c1) and dark field (a2, b2, c2) light microscopy images showing different α-Al grain morphologies and corresponding positions of the secondary phases in the same area. It is important to note that this schematic is not drawn to scale. Figure adopted from Ref. [134].

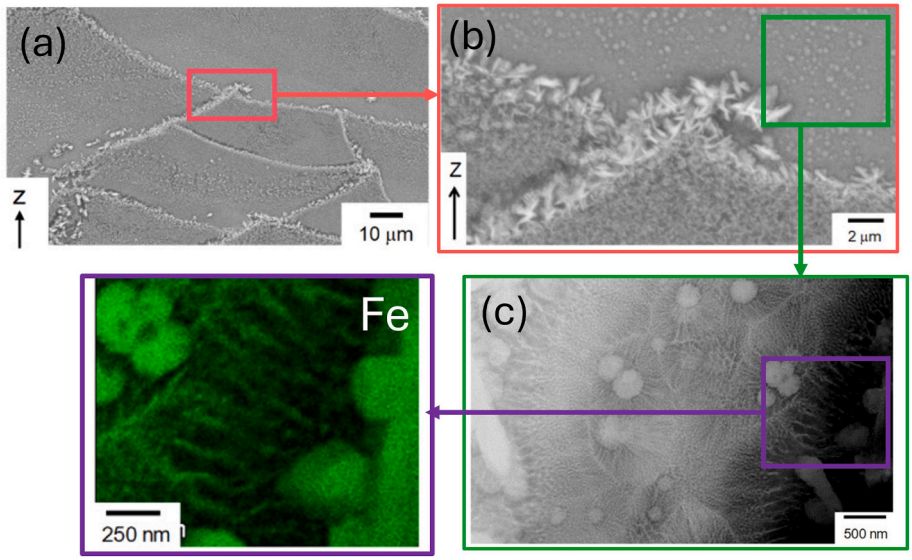

Fig. 17. SEM and TEM image of LPBF-built Al–15Fe alloy samples confirming the presence of nano-scaled Al–Fe phases in grain boundary and within α-Al. Adopted from Ref. [274].

wrought processing [273–279].

The incorporation of Fe in Al alloys is known to enhance high-temperature strength, creep resistance, and fatigue life. This enhancement is significantly amplified by the rapid cooling rates (reaching up to 10^7 °C/s) achievable with L-PBF [280]. These extreme cooling rates induce several microstructural modifications:

(1) The RSP suppresses the formation of coarse and equilibrium Fe-bearing IMCs typically observed in conventionally processed alloys. Instead, it promotes the formation of a fine dispersion of nano to micron-sized Al–Fe phases (as illustrated in Fig. 17). This fine dispersion provides effective strengthening through mechanisms like precipitation hardening and Orowan strengthening, where the fine particles impede dislocation movement.
(2) RSP extends the solid solubility of Fe in the Al matrix beyond the equilibrium limits. This supersaturation of Fe in the α-Al matrix can further enhance precipitation hardening during subsequent heat treatments or high-temperature service.
(3) Under extreme cooling conditions, metastable phases, which are not thermodynamically stable under equilibrium conditions, can form. These metastable phases can have unique crystal structures and properties that can contribute to improved mechanical performance.
(4) The unique thermal history (repeated heating and cooling) of L-PBF results in microstructures that are distinct from those obtained through traditional casting and wrought thermomechanical processes.

As shown in Fig. 17(c), L-PBF can generate unique strengthening phases within the α-Al matrix that are not typically observed in conventional alloys. These phases, often with intricate morphologies and distributions, can significantly contribute to the overall mechanical properties, especially at elevated temperatures. RSP can also involve refinement of grain structure, formation of cellular or dendritic microstructures with fine IMC networks, or even formation of amorphous regions. For example, L-PBF-processed Al–9Si–3Cu, which contained 1 wt% Fe, exhibited significantly finer IMC dispersions compared to its cast counterpart with 0.65 wt% Fe [278]. This refinement led to a remarkable increase in elongation at fracture from 0.6 % (cast) to 5.3 % (L-PBF), along with a near doubling of the yield strength. Similarly, Yamasaki et al. [279] demonstrated that Al–12Si–1Cu–1Mg–1Ni alloys with Fe concentrations up to 5 wt% retained superior strength and ductility when processed by L-PBF. These findings suggest that impurity-tolerant alloy design could be particularly effective in AM applications.

3.4.2. *The effect of melt superheating*

Superheating influences the characteristics of Fe-bearing IMCs in Al alloys, impacting their morphology, size, and distribution. A key benefit of superheating is the observed transformation of the detrimental β-IMC into α-IMC. This transformation, coupled with RSP, leads to a cascade of microstructural improvements: reduced interdendritic spacing, refined eutectic constituents, and decreased grain size, ultimately enhancing mechanical properties as shown in Fig. 18 [281–284].

While high superheating temperatures (above 500 °C) decrease the number and size of nucleation sites, they do not eliminate them entirely [281]. The β-IMC has a propensity to nucleate on fine γ-Al_2O_3 inclusions, while α-Al_2O_3 inclusions appear to be less conducive to its formation. This suggests that the transformation of γ-Al_2O_3 to α-Al_2O_3 during superheating might play a role in suppressing β-IMC formation [285]. However, it's important to acknowledge that superheating can also introduce challenges, such as increased hydrogen and oxide inclusion concentrations in the melt, potentially affecting overall alloy quality.

Superheating has proven particularly effective in refining the α-IMC, even surpassing the effects of Mn additions in alloys with 1 % Fe [271, 286]. Experiential evidence demonstrates that relatively high melt

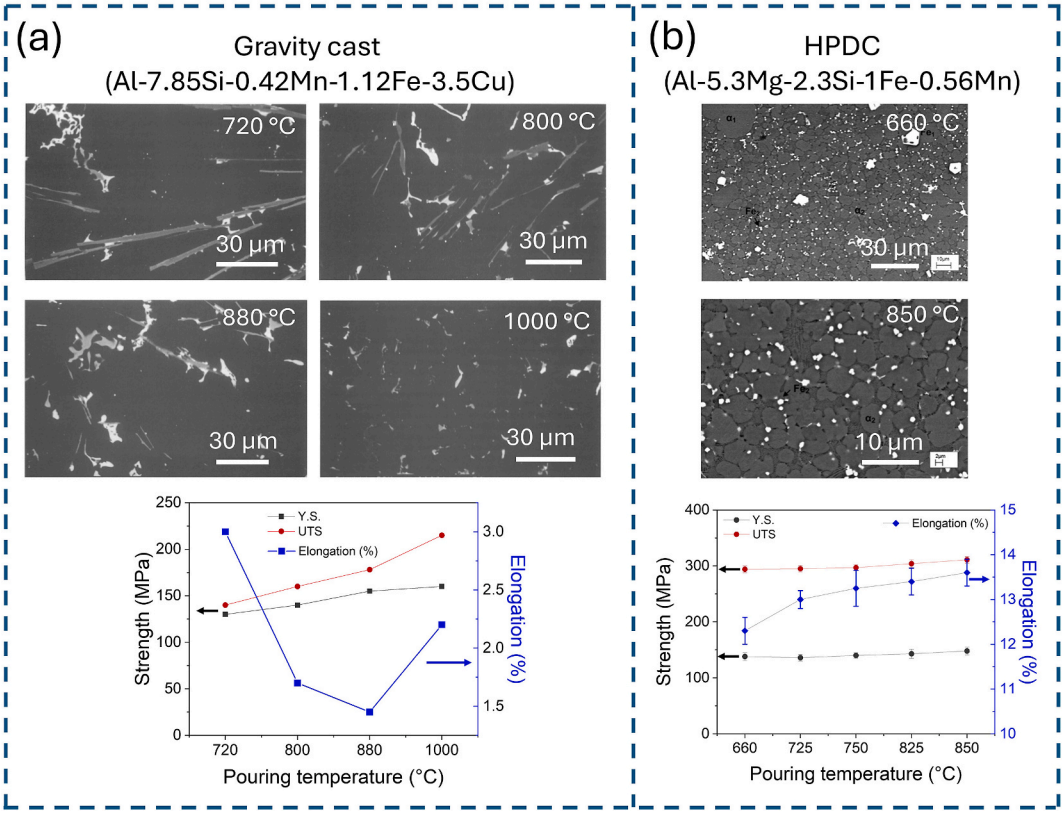

Fig. 18. Microstructural and mechanical properties comparison of two Fe containing alloys cast in (a) metal gravity casting and (b) HPDC, demonstrating a significant reduction in the size and distribution of Fe-bearing IMCs. Figure redrawn from Refs. [283,284].

superheating enhances the mechanical properties of Al–Mg–Si–Mn alloys. Improvements in yield strength, ultimate tensile strength, and elongation are observed as a result of the refined Fe-bearing IMCs and α-Al grains. Studies on alloys with 1.12 % and 1.94 % iron content, across a melt temperature range of 720 °C–1000 °C, confirm that superheating transforms coarse β-IMC plates into more compact, globular structures, leading to substantial gains in strength and ductility in the cast alloys (Fig. 18(a)) [284]. At the atomic level, higher melt temperatures reduce the size of atomic clusters and diminish the number of heterogeneous nucleation sites. This promotes greater undercooling and increased nucleation rates, which, in turn, drive simultaneous grain growth, reduce solidification time, and refine the as-cast microstructure. In HPDC, the significantly higher cooling rates (up to 1000 °C/s) in the die cavity compared to gravity casting further amplify undercooling and promote the formation of fine Fe-bearing IMC particles (Fig. 18(b)) [283].

3.4.3. *The effect of post-solidification heat treatment*

Post-solidification heat treatment, including solutionising, homogenisation, and aging plays a crucial role in modifying the morphology, stability, and mechanical impact of Fe-bearing IMCs in Al alloys. These processes enhance microstructural refinement, improve mechanical properties, and optimise the alloy's performance.

Solution heat treatment (SHT) significantly alters the morphology of Fe-bearing IMCs in cast Al–Si–Cu alloys. At high solutionising temperatures, β-IMC plates dissolve and fragment, reducing their width and thickness, which refines the microstructure [286]. Conversely, lower solutionising temperatures induce necking and splitting of β-IMC plates, shortening their length without altering their thickness (Fig. 19) [287]. These transformations mitigate the detrimental effects of coarse Fe-bearing IMCs, improving the alloy's ductility and toughness. In addition, solid-state transformations between different Fe-bearing IMCs can occur during SHT. Studies on 2xxx series Al–Cu cast alloys have demonstrated the transformation of Al_mFe to β-Al_7Cu_2Fe, driven by nucleation and growth mechanisms. These transformations are crucial for breaking up large Fe-bearing IMC particles, enhancing hot workability, and refining the microstructure.

Homogenisation heat treatment further refines Fe-bearing phases by promoting the transformation of β into α-IMC. This transformation occurs through a eutectoid decomposition mechanism, where β-IMC decomposes into α-IMC and an Al solid solution. The nucleation of the α-IMC at the particle–matrix interfaces is followed by rapid growth, effectively replacing the β-IMC [288]. Mn acts as a catalyst, accelerating diffusion and facilitating the formation of the α-IMC, which is beneficial for mechanical properties [288]. Experimental studies have demonstrated that intermediate homogenisation temperatures lead to the transformation of fragmented plate-like Fe-bearing IMCs into the α-IMC. However, prolonged heat treatment can induce coarsening of the α-IMC and spheroidisation of the β-IMC. Ibrahim et al. [289] reported that homogenisation promotes the transformation of fragmented Fe-bearing IMCs into α-IMC structures, leading to a more uniform microstructure. Similarly, Tanihata et al. [290] observed that at 858 K for 54 ks, a substantial amount of the α-IMC remained, but extending the treatment to 2400 ks resulted in the formation of an α' phase and a reduction in β-IMC content. These findings indicate that optimising homogenisation parameters is essential for achieving a refined and stable microstructure.

The thermal stability of Fe-bearing IMCs is particularly relevant in ultrafine-grained (UFG) Al alloys. In Al–2 %Fe alloys, severe plastic deformation (SPD) followed by heat treatment can lead to the partial dissolution of metastable Al_6Fe particles, forming a Fe-supersaturated solid solution [291]. During annealing, nanoscale Fe-bearing precipitates nucleate and pin grain boundaries, preventing excessive grain growth. This process stabilises the fine-grained structure, preserving grain sizes as small as 300 nm even after exposure to 250 °C for 1 h. Strengthening mechanisms in heat-treated alloys include grain boundary strengthening, dislocation hardening, and precipitation hardening. In UFG Al alloys, grain boundaries and dislocations each contribute approximately 40 % to microhardness, while nanoscale Fe particles and solid solution strengthening account for the remainder. Aging further modifies Fe-bearing IMCs, with Al_6Fe particles undergoing limited growth and $Al_{13}Fe_4$ precipitating at defects. Strain-induced defects, such as dislocations and grain boundaries, enhance diffusion and accelerate precipitation kinetics, improving the alloy's mechanical performance.

In wrought Al alloys, Fe-bearing IMCs influence mechanical properties through their morphology and transformation behaviour [106, 292–294]. The Chinese-script α-IMC morphology is preferred due to its superior dissolution characteristics during homogenisation, resulting in a more uniform microstructure. Processing conditions including temperature, time, and cooling rate significantly impact the dissolution and transformation of Fe-bearing IMCs. By optimising these parameters,

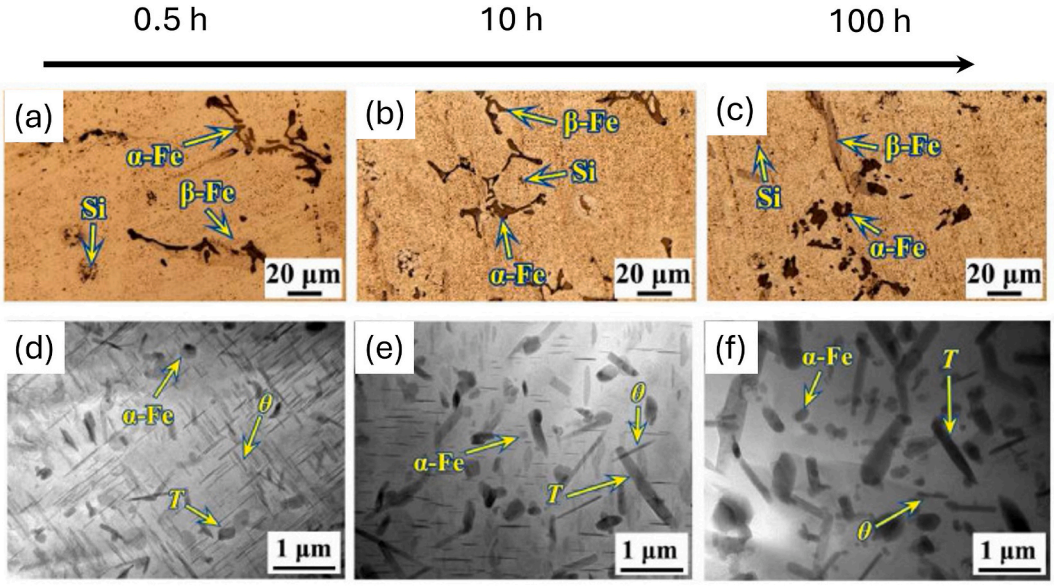

Fig. 19. Effect of solution treatment on α and β-IMC of Al-6.5Cu–1Si-0.6Mn-0.5F: (a) to (c) optical microstructure and (d) to (f) TEM microstructure with increasing solutionisation and heat treatment time. Increasing solutionisation time led to reduction of IMC particle size through dissolution, coarsening and fragmentation. Heat treatment led to precipitation within Al matrix (θ (Al_2Cu), T ($Al_{20}Cu_2Mn_3$), and α-Fe phases). Figure adopted from Ref. [287].

post-solidification heat treatment effectively refines Fe-bearing IMCs, enhances microstructural homogeneity, and improves alloy performance [295].

4. Role of Fe-bearing intermetallics in porosity development

Porosity formation is a common occurrence in commercial Al alloys during casting, influenced by a set of factors including the casting process, mould design, thermal and environmental conditions, melt feeding, riser/gate design, and applied pressure [296–298]. The presence of hydrogen, inclusions, trace elements, and minor elements can also play a role in porosity development. Notably, several studies have correlated increased porosity with the presence of β-IMC platelets [25, 31,299]. Given the prevalence of Fe in Al–Si alloys and its impact on porosity, extensive research has explored the underlying mechanisms and proposed various theories to explain this phenomenon.

4.1. Intermetallics role in obstructing feeding

The prevailing theory suggests that the formation of β-IMC platelets in the interdendritic regions is the primary cause of porosity development in Al alloys [31]. These platelets can obstruct liquid feeding, leading to hot tearing and voids (Fig. 20). However, Taylor et al. [297, 298] found no direct correlation between porosity and shrinkage-induced micro-gaps, proposing instead that the β-IMC influences the nucleation and growth of eutectic Si. While some studies have observed a direct relationship between porosity and Fe content, this correlation appears limited to alloys containing trace elements like Cu, Mn, and Sr, which can alter the solidification sequence [297,298]. An *in-situ* study further supports this observation [121], highlighting the complex relationship between various factors in porosity formation.

4.2. Pore nucleation and growth restraint

Roy et al. [299] proposed that the presence of Fe in Al–Si alloys increases porosity, with β-IMC platelets acting as nucleation sites for pores. They suggested a linear relationship between the volume fraction of β-IMC platelets and porosity levels, implying that more β-IMC platelets lead to more nucleation sites and consequently, increased porosity. However, this theory requires further investigation due to limited understanding of how porosity forms as a function of β-IMC platelet volume fraction, and insufficient observations on the impact of β-IMC platelets on pore nucleation.

In-situ experiments have revealed that while the β-IMC itself does not nucleate porosity, pores tend to grow along its surface [121]. This is due to the β-IMC's lower interfacial energy with the gas-solid interface compared to α-Al, promoting pore growth. Moreover, while IMCs do not directly nucleate pores, they obstruct interdendritic channels, thereby decreasing shrinkage feeding and porosity permeability. This highlights the complex relationship of factors influencing porosity formation in Al–Si alloys, extending beyond the role of β-IMC platelets alone.

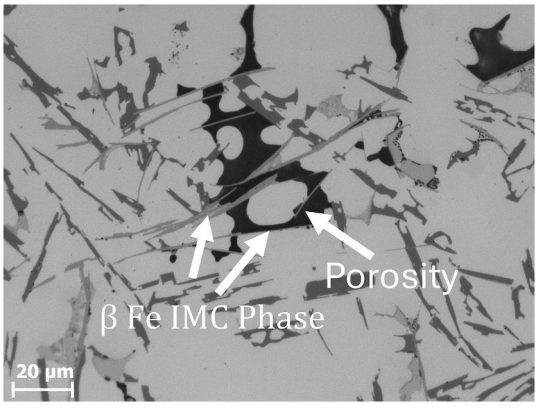

Fig. 20. Shrinkage porosity formation surrounded by β-Al_5FeSi platelets (from authors' work).

4.3. Nucleation of the Al–Si eutectic by intermetallics

Taylor et al. [296–298] proposed that porosity development in Al–Si alloys is linked to β-IMC platelets acting as nucleation sites for eutectic Si. Their analysis of the ternary Al–Si–Fe phase diagram (Fig. 21) highlighted a correlation between Fe content and porosity, specifically related to the formation of the Al–Si–Al_5FeSi ternary eutectic. They found that critical Fe content, defined by a specific Fe and Si composition line, led to the most permeable structures due to fine Al–Si eutectic nucleation on β-IMC platelets. The solidification path and directional changes at the ternary eutectic point were identified as influential factors in porosity susceptibility. However, it is important to note that defects can still arise under poor casting conditions, regardless of Fe content.

Taylor's model [296–298] predicted low porosity permeability at critical Fe levels in Al alloys, but subsequent studies have yielded varying results. For instance, Al–10Si–1Cu alloy castings with approximately 0.7 wt% Fe exhibited low porosity, while Al–5Si–1Cu castings showed higher porosity. Otte et al. [300] modified Taylor's theory, finding that porosity in Al–9Si-0.5Mg–3Cu castings was not directly linked to eutectic grain nucleation on β-IMC platelets and that no minimum Fe content was required for porosity formation in this specific alloy. They suggested that the solid/liquid interface morphology may directly influence porosity, with high Fe concentrations in Al–Si eutectic grains leading to increased interfacial area and decreased porosity permeability. The discrepancies between Taylor's and Otte's models may be attributed to differences in Cu concentrations.

4.4. Effect of alloying elements

The concentration of Fe and Si in Al alloys significantly influences the formation of residual liquids, which, in turn, enrich β-IMC platelets and promote the development of solid fractions prior to the Al–Si-β ternary eutectic reaction. This ternary eutectic, composed of 11.5 % Si and 0.8 % Fe, is a critical point in the solidification process. Any alteration in the solidification sequence, particularly those affecting interdendritic permeability, can lead to porosity formation.

The addition of trace elements like Cu and Mn to Al–Si foundry alloys can further modulate porosity levels. While Mn has been observed to increase porosity [201], Cu tends to reduce it. However, the interplay

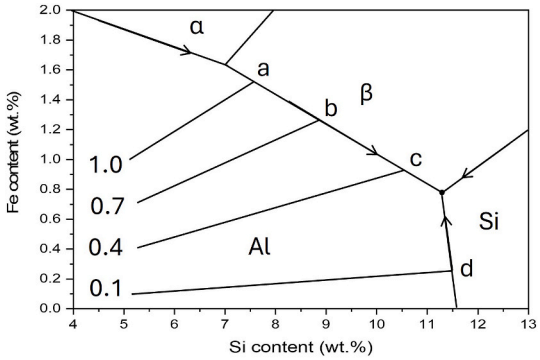

Fig. 21. The calculated segregation lines (freezing/solidification paths) across the liquidus surface of the Al–Si–Fe ternary phase diagram. These calculations are based on three different solidification models for AA309 alloy, varying in iron content. The fraction solid values at the eutectic trough intersections (points a, b, c, and d) are roughly 35, 46, 57, and 61 %, respectively. Figure redrawn from Ref. [297].

between Fe, the specific solidification sequence, and trace elements such as Mn, Ca, Sr, and Be adds complexity to understanding the precise mechanisms underlying porosity formation. Although high Fe levels are generally associated with increased porosity, further research is needed to fully explain the specific relationship between Fe content and porosity levels in Al–Si alloys, considering the complex interactions with other alloying elements and solidification parameters.

5. Influence of Fe-bearing intermetallics on properties

5.1. Mechanical properties

The presence, morphology, and distribution of Fe-bearing IMCs exert a significant influence on the mechanical properties of Al alloys, particularly in cast and wrought Al alloys [1,2,25–27]. Plate-like IMCs, especially the β-IMC, are detrimental to ductility, fatigue resistance, formability, and processability [33]. Beyond their direct impact on mechanical properties, these IMCs can also exacerbate porosity formation, as discussed earlier. During thermomechanical processing (e.g., extrusion, rolling), Fe-bearing IMCs can act as stress concentrators, contributing to the formation of cavities or cracks. While any form of IMC can reduce ductility, morphology is crucial. The finer, more rounded α-IMC is generally preferred over the plate-like β-IMC in both cast and wrought alloys. Refined IMCs facilitate slip movement, as dislocations can bypass small, rounded particles more easily than faceted structures.

Fe-bearing IMCs are inherently brittle and prone to fracture under tensile loading [301,302]. As shown in in-situ tensile testing (Fig. 22 (a)), microcracks initiate frequently around these IMCs, and their subsequent propagation can lead to ultimate material failure [162–166, 303]. Studies have shown a strong correlation between particle size distribution and fracture strain [304]. Smaller average particle sizes lead to higher fracture strains, with particles larger than 5 μm being particularly susceptible to fracture [305]. Furthermore, coarser particles (>3–4 μm) are prone to multiple fractures, increasing the local crack density and accelerating damage propagation. The mechanism of particle failure is either by fracture or decohesion from the matrix [304], depending on factors like morphology, size, alignment, and the stress mismatch between the IMC and the matrix. Specifically, as illustrated in Fig. 22(b), the size of β-IMCs plays a crucial role in determining the strength of the material. Matrix hardness also plays a role; in softer matrices debonding is favoured while in harder matrices particle fracture is more common [306]. Both decohesion and cracking increase with plastic strain, but in hard matrices, cracking occurs at lower strains and increases sharply with further strain. Particle morphology significantly affects strain localisation and damage mechanisms. Plate-like β-IMC is more detrimental than round α-IMC due to its elongated shape [307, 308]. β-IMC particles aligned parallel to the loading direction tend to fracture easily, while those perpendicular, along with α-IMC, typically lead to void nucleation through debonding. Generally, particles with a long axis at an angle >45° to the loading direction tend to decohere, while those at smaller angles crack. Larger plate-like particles often fracture into multiple fragments [307]. Increased Fe generally reduces ductility while slightly increasing yield strength [100]. Low Fe content (<0.06 wt%) can increase toughness due to dispersoids, but higher Fe content (~0.3 wt%) decreases it due to coarse IMC formation [100, 888]. Furthermore, the quantitative impact of Fe-bearing IMCs on mechanical properties varies across alloy types. In cast Al–Si alloys, each 0.1 wt% increase in Fe content can increase tensile and yield strength by 3–5 MPa but reduce elongation by approximately 2 % (Fig. 22 (c)) [309]. Coarse β-IMC can substantially reduce yield strength by up to 20 % compared to alloys containing only fine α-IMC particles. An increase in the volume fraction of β-IMC in these alloys negatively impacts fracture toughness. Conversely, modifying the morphology of Fe-bearing IMCs from plate-like to script-like can improve fatigue life by 10–20 % [164,310–312].

As discussed previously, modifying Fe-bearing IMCs through alloying additions or any other means offers a pathway to alter mechanical properties. For example, Co additions, while influencing Fe distribution through the formation of $Al_7(Fe,Co)Cu_2$, can increase the volume fraction of plate-like IMCs, leading to decreased mechanical properties (e.g., a reduction from 385.7 MPa to 309.6 MPa) [261]. Mn additions, on the

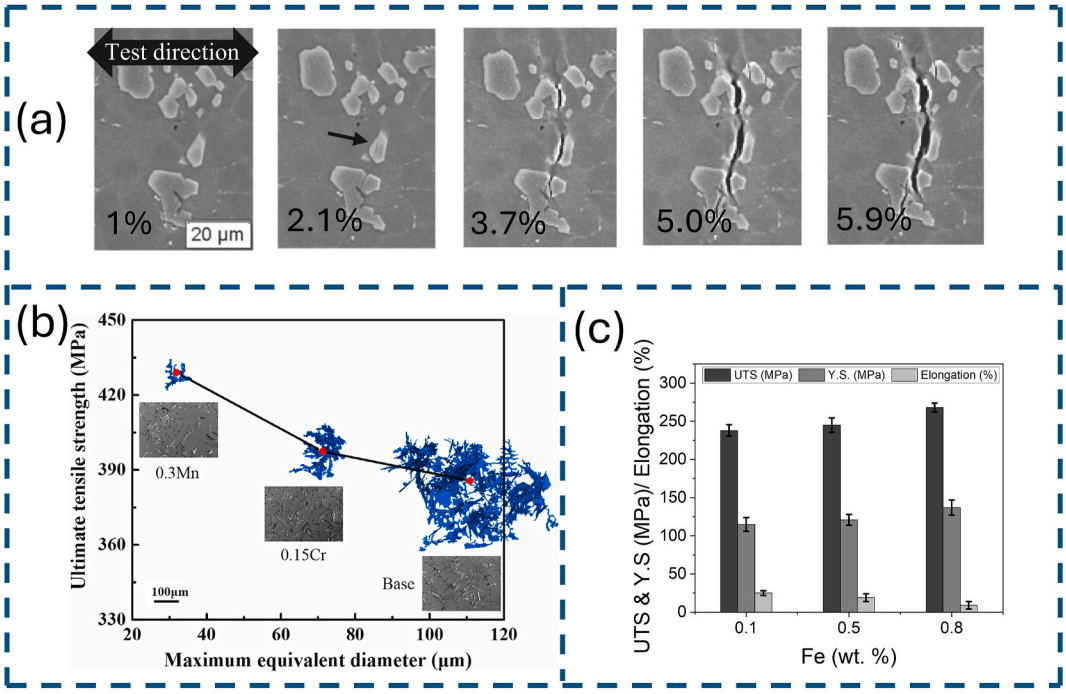

Fig. 22. (a) Progression of cracking in the Al-8.5Si-0.84Fe-0.92Mn alloy with increasing elongation [303]. (b) Ultimate tensile strength (UTS) as a function of the maximum Fe-bearing IMC particle equivalent diameter in the Al-7.3Si-3.5Cu-0.3Mg-0.75Ti alloy with modification [261]. (c) Variation in mechanical properties with increasing Fe content (wt.%) in Al–3Mg-0.9Mn-xFe based alloys [309].

other hand, refine the size of Fe-bearing IMCs and promote the β-to-α IMC transformation, generally improving mechanical properties (e.g., an increase from 385.7 MPa to 427.9 MPa). Cr additions, by influencing Fe distribution through $Al_{13}Cr_4$ and Al_7(Fe,Cr) formation, have a less pronounced effect than Mn (e.g., a 3.1 % improvement). Combined additions can also have complex effects. Be, Ca, and Sr additions to Al–7Si-0.3Mg-0.8Fe alloys improve impact strength [208] by modifying eutectic Si and refining β-IMCs. However, combining these elements with Mn (Be + Mn, Ca +Mn, Sr + Mn) reduces impact strength compared to individual additions [205], highlighting the need for careful optimisation. In wrought Al alloys, Fe-bearing IMCs significantly influence mechanical properties. Increased Fe content generally reduces ductility while slightly increasing yield strength [46]. While low Fe content (<0.06 wt%) can improve toughness due to dispersoids, higher Fe content (~0.3 wt%) leads to a decrease in toughness due to the formation of coarse IMCs [46,313]. Lower Si content enhances the spheroidisation of these IMCs [12]. Mg content, while not significantly affecting Fe-bearing IMCs, influences the formation of Mg_2Si particles and can promote the formation of π-$Al_8FeMg_3Si_6$, which exhibits a Chinese-script morphology [308]. In 5xxx and 6xxx alloys, course and flake shaped IMCs can decrease fatigue life by 20–35 % compared to alloys with predominantly fine and well distributed particles [314,315]. AM alloys can increase strength up 950 MPa, however, ductility reduced to around 3 % [316]. High-strength 2xxx and 7xxx series alloys are also affected. Large, blocky Al_7Cu_2Fe IMC can decrease tensile strength by 10–15 % compared to alloys with smaller IMCs or less Fe containing alloys [317]. However, modifying the morphology of IMCs from plate-like to script-like in these alloys can notably improve fracture toughness by 15 %. These quantitative examples highlight the importance of controlling the formation and morphology of IMCs to tailor the mechanical properties of Al alloys for specific applications. Therefore, controlling the morphology and distribution of Fe-bearing IMCs, through alloying and processing techniques like those discussed previously (UT, EMS, shearing), is crucial for tailoring the mechanical properties of Al alloys.

5.2. Corrosion properties

The presence and morphology of Fe-bearing IMCs significantly influence the corrosion behaviour of Al alloys, with varying impacts observed across different alloy types [12,26–30,113,318–325].

In cast Al–Si alloys, Fe-bearing IMCs, particularly the β-IMC, play a crucial role in determining corrosion behaviour [323]. The β-IMC exhibits a higher corrosion potential (nobility) compared to the Al matrix. In aggressive environments, the combination of the Al matrix and the β-IMC leads to the formation of a microgalvanic cell, wherein the Al matrix acts as the anode (undergoing oxidation) and the β-IMC serves as the cathode (site of the reduction reactions) [318,319]. The oxidation of the Al matrix surrounding the β-IMC results in its dissolution into the environment. Once the Al matrix in the vicinity of the IMC is completely dissolved, the β-IMC detaches from the matrix. This detachment exposes a new Al matrix surface, leading to the formation of a secondary microgalvanic cell, where the newly exposed Al matrix acts as the anode, and the Al passive film functions as the cathode, initiating pit formation. This type of localised corrosion, known as galvanic corrosion, arises from the galvanic cell formation within the alloy. The detachment of the β-IMC or other IMCs during galvanic corrosion disrupts the passive film, compromising its integrity and further accelerating corrosion (Fig. 23). The plate-like morphology of the β-IMC exacerbates this effect by providing a large cathodic surface area.

In common cast Al–Si alloys, increased Fe content has been linked to reduced corrosion resistance due to the higher area fraction of Fe-bearing IMCs [323]. The extent and rate of galvanic corrosion are amplified by an increased cathodic/anodic area ratio. Additionally, the presence of coarse β-IMC platelets has been associated with greater susceptibility to pitting corrosion, as these IMCs can serve as initiation sites for localised corrosion attacks.

In wrought Al alloys, the effect of Fe-bearing IMCs on corrosion is less pronounced but still significant. In wrought 6061 Al alloy, Park et al. [324] observed that corrosion pits initiate at Al_3Fe sites in Al-6061 when exposed to aerated 0.6 M NaCl solution. Al_3Fe also contributes to microgalvanic cell formation due to its cathodic effect on the Al matrix. In 2xxx series alloys, the presence of AlFeMnSi dispersoids can enhance

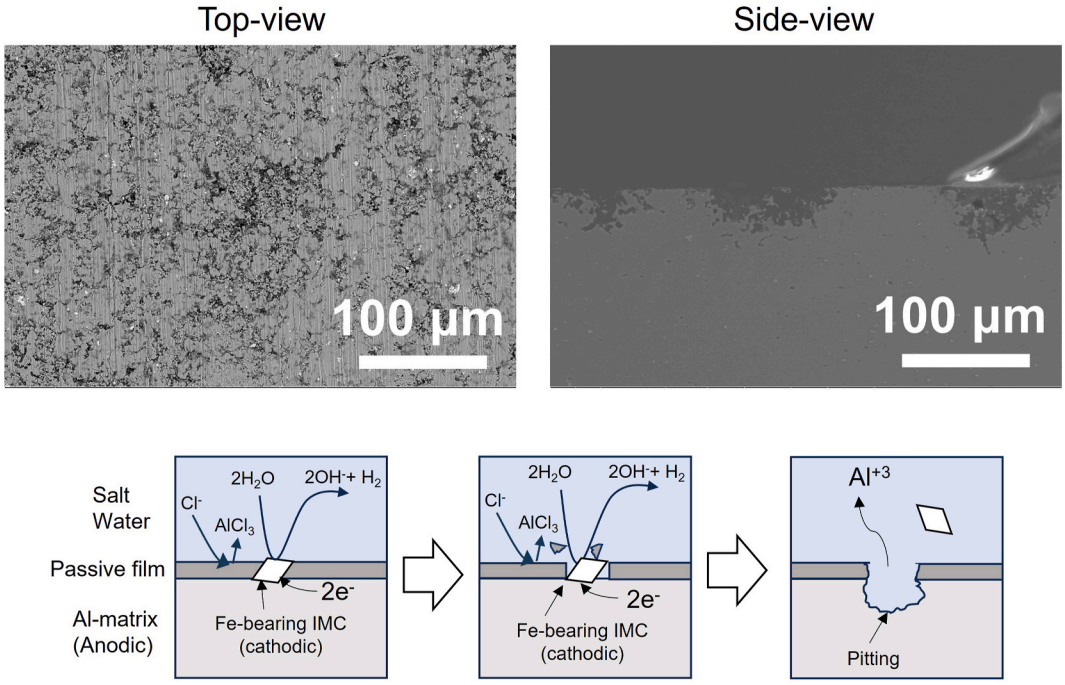

Fig. 23. Wrought 5182 Al alloy after Potentiodynamic Polarisation test (exposed to 0.6 M of sodium chloride) showing pitting corrosion initiation through Fe-bearing IMC (from authors' work).

pitting corrosion resistance by acting as barriers to pit growth. These dispersoids contribute to the formation and stability of the passive film. Additionally, Al–Mg alloys containing Sr and Zr, produced through AM, exhibit improved corrosion resistance due to the presence of fine IMCs [321]. Sr and Zr promote the formation and enhance the stability of the Al passive film [321]. However, in high-strength 7xxx series alloys, large Al_7Cu_2Fe IMCs can be detrimental to corrosion resistance due to their significant electrochemical potential difference relative to the matrix, leading to localised galvanic corrosion. The rate of galvanic corrosion increases with greater potential differences between phases [322].

Generally, fine and well-dispersed IMCs are less detrimental than coarse, plate-like ones. The specific impact of IMCs is influenced by their type, morphology, and distribution, as well as the alloy composition and environmental conditions. Understanding these effects is crucial for developing corrosion-resistant Al alloys and optimising their performance in various applications.

6. Outlook for aluminium recycling

Al recycling presents a far more sustainable and energy-efficient alternative to primary Al production. Recycling Al consumes only about 5 % of the energy required for primary production, resulting in significant energy savings. The recycling process typically requires 3–6 MJ/kg of Al, while primary Al production demands 60–80 MJ/kg. In addition, recycling significantly lowers the carbon emission to only 0.5–1.0 kg CO_2 per kg of Al as compared to 12–16.6 kg CO_2 per kg for primary production [10]. This highlights the substantial environmental benefits of Al recycling, especially as the global manufacturing industry pushes for greater sustainability.

The Al recycling process involves several stages, each with varying energy requirements and emissions, depending on scrap quality and the technologies employed. Closed-loop recycling of high-quality, low-contaminant scrap stands out as one of the most energy-efficient approaches (Fig. 24) [11]. Such scrap is more predictable and easier to process, requiring less sorting, improving material quality, and leading to higher recycling rates. A prime example of efficient closed-loop recycling is the beverage can industry. Used beverage cans, which are cleaned and melted down to produce new cans, have a high recycling rate up to 70 % or more in some regions [326]. The consistent quality of the scrap and established collection systems make this a highly sustainable and energy-efficient recycling method.

In the automotive industry, a shift has occurred toward recycling production scrap, such as those generated during forming or punching operations (e.g., car doors). This scrap is directly supplied to Al manufacturers before being mixed with other alloys. By recycling this manufacturing waste through closed-loop systems, the industry enhances recycling efficiency and reduces the need for additional sorting and processing, contributing to lower energy consumption and carbon emissions.

Closed-loop recycling also plays a significant role in stabilising Al prices and reducing price volatility, benefiting Original Equipment Manufacturers (OEMs). Al prices can fluctuate due to global supply and demand, energy costs, and geopolitical factors. Such price shifts create uncertainty, making it difficult for OEMs to manage production costs effectively. By adopting closed-loop recycling, OEMs can secure a consistent and cost-effective supply of Al, particularly from high-quality scrap like beverage cans and automotive production waste. This reduces dependence on primary Al, which is more vulnerable to price fluctuations, helping manufacturers maintain predictable costs and avoid hesitation in using Al in production. Moreover, the closed-loop system ensures a steady supply of Al, allowing OEMs to plan material needs with greater certainty, thereby ensuring competitive pricing and minimising production delays.

Effective sorting of general Al scrap is crucial for maximising recycling efficiency and ensuring the quality of the final product, which can be achieved using technologies like X-ray transmission. However, recycling companies often classify scrap into broad categories, such as cast and wrought alloys, based on product type and scrap volume. This general sorting often leads to downcycling, which reduces the potential value of the recycled material. Cast alloys are more impurity-tolerant and easier to recycle, while wrought alloys lose significant value due to the introduction of impurities during recycling and corresponding degradation of mechanical properties. The inefficiency of sorting can diminish the quality of the recycled material and limit its use in high-value applications. Although sorting and shredding in the recycling process are energy-efficient compared to primary production, the loss of material quality and value due to inadequate sorting remains a key limitation. Innovations in sorting and separation technologies are needed to enhance the efficiency of recycling processes. Technologies such as sensor-based sorting, advanced eddy current separation, and machine learning algorithms can more accurately identify and separate different Al alloys, minimising contamination and improving the quality of the recycled material. These innovations could significantly reduce downcycling and increase the value of recycled Al. This will also help prevent cross-contamination with other alloys, such as steel, where Al and Cu must be avoided during recycling.

The global trade of Al exhibits a complex flow, with developed nations frequently importing primary Al while simultaneously exporting Al scrap, often to developing countries. This two-way trade presents significant economic and environmental sustainability concerns. Economically, developed nations generally receive lower market value for the exported scrap compared to the value of primary Al or semi-finished products. Environmentally, the long-distance maritime transport inherent in this trade pattern generates substantial carbon emissions, exacerbating the overall lifecycle carbon footprint of Al production and consumption. This practice thus undermines global efforts towards a

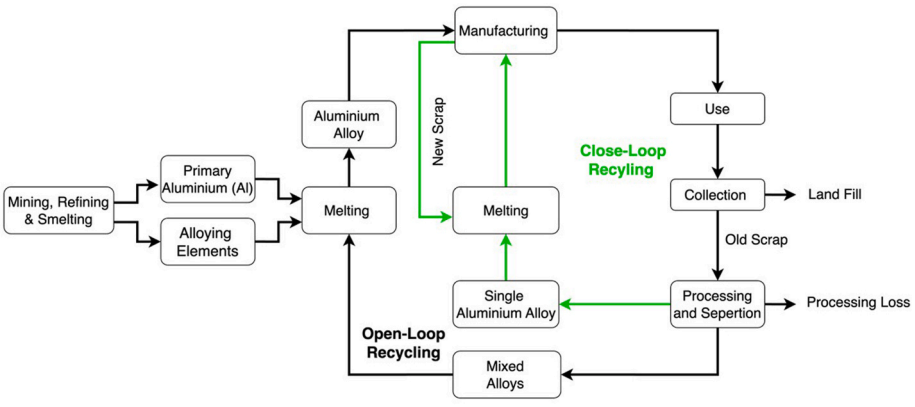

Fig. 24. Aluminium production process, illustrating both open-loop and closed-loop recycling.

circular economy and sustainable resource management.

Collaboration between Al manufacturers, OEMs, and recycling companies is essential to improve recycling rates and create more efficient closed-loop systems. By adopting *Design for Recycling* (DFR) principles, OEMs can design products with end-of-life recyclability in mind, ensuring that materials are easier to disassemble and separate during recycling. This can improve the efficiency of recycling operations and reduce contamination. Al manufacturers can provide guidance to OEMs on the recyclability of materials and help standardise alloy composition to facilitate smoother recycling processes. Recycling companies, in turn, can invest in advanced sorting technologies to enhance the quality of the recycled material, ensuring that more Al can be used in high-value applications.

Ultimately, the success of closed-loop recycling depends on creating a more circular supply chain, where Al products are continuously recycled back into production processes. By fostering collaboration across the entire value chain from product design to recycling, stakeholders can help overcome current limitations and increase recycling rates, making Al production more sustainable and cost-effective. Such collaborations will not only improve recycling efficiency but also reduce the reliance on primary Al, supporting a circular economy that prioritises sustainability and resource efficiency. Incorporating DFR principles, improving recycling technologies, and enhancing communication between stakeholders will allow the Al industry to transition toward a more sustainable, closed-loop system. These efforts will not only promote environmental benefits but also make Al manufacturing more competitive and less reliant on volatile primary production, contributing to a more sustainable and resilient global economy.

6.1. Designing impurity-tolerant alloys for sustainable manufacturing

The push for sustainability in metal manufacturing necessitates innovative strategies for alloy design that can accommodate higher impurity levels while maintaining or even enhancing performance. Traditionally, impurities in Al alloys have been regarded as detrimental, affecting phase equilibria, mechanical and corrosion properties, and recyclability, as discussed in the previous sections. However, emerging research suggests that certain impurity elements, particularly Fe, can be leveraged to develop impurity-tolerant alloys suitable for both conventional and advanced manufacturing processes such as AM. These strategies can significantly reduce reliance on high-purity primary Al, facilitating the use of secondary (recycled) Al and contributing to lower carbon emissions. Following approaches can be explored to design next generation impurity tolerant alloys:

(1) **Microstructural refinement via RSP/AM:** Investigations into L-PBF processed Al alloys with higher Fe impurity levels demonstrate that RSP significantly refines Fe-bearing IMCs, as detailed in Section 3.4.1.1. This microstructural refinement effectively mitigates the detrimental effects of increased Fe and other residual elements, leading to enhanced mechanical properties. Consequently, L-PBF enables the development of tailored Al–Fe alloys with superior properties for high-temperature applications in aerospace, automotive, and energy sectors. Optimal control of L-PBF parameters and alloy composition is crucial for achieving the desired balance of strength, creep resistance, and fatigue life. However, the specific IMC phases and their morphology remain dependent on precise alloy composition and L-PBF parameters, necessitating further research to comprehensively understand their complex interplay. Future AM research could explore the incorporation of peritectic-forming elements, such as Zr, to induce the formation of novel IMCs that refine α-Al grains. These IMCs can enhance microstructural stability and improve high-temperature properties above 200 °C, expanding the potential applications of impurity-tolerant Al alloys in aerospace and automotive industries. Leveraging advanced alloy design in AM allows for systematic control of impurity-driven phase formation, ultimately enabling superior mechanical performance in recycled Al-based components

(2) **Strategies for trace alloying elements:** Beyond AM, the strategic incorporation of Fe and Mn into Al alloys has shown significant potential for enhancing mechanical properties while maintaining processability. Patent disclosures from AMAG Casting GmbH and AUDI AG [327] demonstrate that adding 0.5–1 wt. % Fe to Mn-modified wrought Al alloys in the 5xxx, 6xxx, and 7xxx series leads to improvements in tensile strength, elongation, and resistance to hot cracking. These findings suggest that controlled Fe additions, when combined with Mn, can enhance alloy performance while expanding the use of secondary Al. Additionally, research indicates that the addition of elements such as Sr, Ti, and GR, in conjunction with cooling rate control and external field applications, significantly influences the modification of Fe-bearing IMCs. This is particularly important because, as is well known, impurities are often found to become accumulated in dispersoids, in IMCs, in the bulk, and at grain boundaries, posing challenges to the use of recycled materials. To fully exploit these strategies, systematic investigations are necessary to establish the complete processing window and maximise impurity tolerance. A deeper understanding of phase transformations is essential for optimising alloy design, enabling more effective impurity management in recycled and secondary Al alloys.

(3) **Crossover and multi-purpose alloy development:** An alternative strategy involves developing “crossover alloys” that bridge traditionally distinct alloy classes to enhance impurity tolerance and recyclability. Research on 5xxx-7xxx crossover alloys [12], for instance, has explored the combined addition of Zn and Cu to 5xxx series Al, enabling age hardening without compromising formability. This approach not only improves strength but also enhances recyclability by reducing the number of distinct alloy compositions used in manufacturing. This concept can be further extended to 6xxx and 2xxx series alloys, offering additional benefits in strength, processability, and sustainability. For instance, incorporating Cu into 6xxx series alloys can enhance strength while maintaining extrudability, whereas integrating Mg–Si into 2xxx series alloys can improve weldability and reduce quench sensitivity. A key challenge in crossover alloy development is managing impurity tolerance, particularly the influence of Fe and Si on mechanical properties. Strategies to suppress detrimental β-IMCs through controlled additions of Mn, Cr, or REE elements could be instrumental in optimising alloy performance. Additionally, advancements in processing techniques, such as controlled solidification, thermomechanical treatments, and external field applications (e.g., UT, EMS), offer new pathways to refine Fe-bearing IMCs and improve overall alloy quality. To accelerate the design of these multi-purpose alloys, computational thermodynamics and machine learning models can be leveraged to predict phase stability and optimise composition-processing-property relationships. A systematic, multi-disciplinary approach, combining alloy development, advanced processing methods, and recyclability assessments, will be crucial in creating high-performance, impurity-tolerant Al alloys that align with the demands of both industry and sustainable manufacturing.

(4) **Process optimisation for sustainable recycling:** Research has also explored novel processing techniques to accommodate impurities in Al alloys. For example, high-speed twin-roll casting has been investigated as a method for integrating higher impurity levels into recycled Al streams without significantly degrading mechanical performance. This method has shown that alloys such as 5182 can tolerate up to 2 wt% Si while retaining good drawability and ductility, suggesting potential pathways for broader

industrial adoption [328]. Advanced solidification control methods, such as ultrasonic melt treatment and electromagnetic stirring, have demonstrated effectiveness in breaking up Fe-bearing IMCs, leading to finer and more dispersed phases. To complement these approaches, gradient thermal treatments are being explored to optimise phase transformations, particularly in high-impurity 5xxx, 6xxx, and 2xxx alloys. Also, the strong dependence of the nature and morphology of Fe-bearing IMCs on the prevalent cooling rate during solidification, as discussed in previous sections, allows process optimisation for controlling Fe-IMCs. Precise control and tailoring of cooling rates during conventional casting-based processing can improve material performance in recycled Al alloys. By integrating computational alloy design and machine learning, researchers are accelerating the development of impurity-tolerant processing pathways, ensuring efficient adaptation to high-recycled-content Al streams.

Despite these promising developments, key gaps remain in the widespread implementation of impurity-tolerant alloys. Most current studies focus on mechanical performance, with limited research on how impurity levels impact corrosion resistance, fatigue behaviour, and long-term stability in different processing environments. Moreover, while AM techniques like L-PBF demonstrate high impurity tolerance, their scalability and cost-effectiveness for mass production remain challenging. Additional research is needed to establish grade-specific impurity thresholds for various alloy families, ensuring consistent performance across different manufacturing conditions.

Furthermore, while impurity-tolerant alloy design offers clear sustainability benefits, industrial adoption will require alignment with existing standards and regulatory frameworks. The integration of crossover alloys into mainstream manufacturing will depend on demonstrating their long-term performance, recyclability, and cost-effectiveness compared to traditional alloys.

7. Summary and outlook

Al is a key material for a sustainable future due to its recyclability, lightweight, strength, and durability. As the demand for Al continues to grow in industries like construction, automotive, aviation, and packaging, its role in the circular economy becomes even more critical. By 2050, the amount of recycled Al is projected to double, underscoring the need to address challenges and seize opportunities in Al recycling. Recycling Al not only conserves natural resources but also offers significant energy savings (95 %) and helps reduce greenhouse gas emissions.

A major challenge in Al recycling is the accumulation of impurities, particularly Fe, which complicates the recycling process due to the harmful effect of Fe-based IMCs on the mechanical and chemical properties of Al, especially in the presence of common alloying elements like Si. Significant research on the formation of such IMCs has identified complex interdependencies on the alloy chemistry and processing parameters, with a comprehensive understanding in mitigating their detrimental impact still remaining elusive. The mixing of different Al grades during recycling further complicates the task. To address these challenges, future research should prioritise a comprehensive, integrated approach to Fe mitigation in Al alloys. Strategies encompassing processing, alloying, physical methods, solidification control, and heat treatment require further refinement. Specifically, the influence of cooling rate modulation in advanced manufacturing techniques such as HPDC and AM on Fe-bearing IMC formation necessitates detailed investigation. Solidification control, leveraging increased cooling rates and peritectic elements like Zr, Ti, or GR, offers promising avenues for minimising IMC growth. Optimised heat treatment protocols are crucial for further refining IMC microstructures. A critical focus should be placed on elucidating the complex multi-elemental effects on IMC modification. Leveraging thermodynamic data and machine learning techniques will enable predictive modeling and optimisation of alloying strategies, minimising elemental usage while maximising Fe tolerance. Physical methods, such as ultrasonication, hold potential for large-scale IMC refinement, but require further optimisation and strategy for industrial implementation.

Beyond these processing-focused strategies, several key areas demand deeper investigation. Firstly, the nucleation mechanisms of Fe-bearing IMCs on inoculants require detailed study to understand the influence of alloying elements on interfacial atomic arrangements and nucleation substrates. Secondly, a more quantitative understanding of Fe's impact on mechanical and corrosion properties, considering weight percentage, phase type, and morphology, is essential for establishing informed composition requirements and facilitating broader recycled Al utilisation. Thirdly, the integration of AI-driven sensor technology for scrap separation and sorting offers significant potential for enhancing Al recycling efficiency and improving lifecycle assessments. Finally, optimisation of established Fe removal techniques, such as gravity separation and foam ceramic filtration, is necessary for achieving industrial-scale effectiveness.

Developing high-quality Al-alloys with improved tolerance to impurities is crucial. These advanced alloys will enable greater utilisation of recycled Al, especially in high-end applications that require strict performance standards. Additionally, designing alloys specifically for recycling, such as reducing the use of multiple alloys in applications (e.g., in automobiles), will make it easier to separate and recycle materials effectively, thus contributing to the circular economy.

In conclusion, addressing the challenges associated with Fe-bearing IMCs and improving the efficiency of Al recycling will play a vital role in advancing the circular economy. By focusing on designing alloys that are more impurity-tolerant, promoting cleaner recycling processes, and leveraging advanced technologies can improve the quality of recycled Al. This will contribute to achieving Sustainable Development Goals (SDG #12, #13, #9), supporting a more sustainable future for Al production and recycling.

CRediT authorship contribution statement

H.R. Kotadia: Writing – original draft, Investigation, Funding acquisition, Data curation, Conceptualization. **N. Bareker:** Writing – review & editing. **M.H. Khan:** Writing – review & editing. **J.I. Ahuir-Torres:** Writing – review & editing. **A. Das:** Writing – review & editing, Conceptualization.

Dr A. Das - participated in extensive discussions with H. R. Kotadia.

Declaration of competing interest

The authors declare that they have no known competing financial interests or personal relationships that could have appeared to influence the work reported in this paper.

Acknowledgment

This research was funded by the Industrial Cooperative Awards in Science & Technology (Industrial CASE,EP/R51214X/1).

Data availability

Data will be made available on request.

References

[1] I. Polmear, Light Alloys: from Traditional Alloys to Nanocrystals, fourth ed., Butterworth-Heinemann, 2005.
[2] J. Davis, ASM Specialty Handbook: Aluminum and Aluminum Alloys, ASM International, Ohio, 1993, p. 351, 316.
[3] B.K. Reck, T.E. Graedel, Challenges in metal recycling, Science 337 (6095) (2012) 690–695.

[4] T.E. Graedel, J. Allwood, J.-P. Birat, M. Buchert, C. Hagelüken, B.K. Reck, S. F. Sibley, G. Sonnemann, What do we know about metal recycling rates? J. Ind. Ecol. 15 (3) (2011) 355–366.
[5] Aluminium in Cars: Unlocking the Light-Weighting Potential, European Aluminium Association, 2020.
[6] Opportunities for Aluminium in A Post-Covid Economy, International Aluminium Institute (IAI), 2022.
[7] I.A. Institute, Global Aluminium Cycle, 2016.
[8] D. Raabe, C.C. Tasan, E.A. Olivetti, Strategies for improving the sustainability of structural metals, Nature 575 (7781) (2019) 64–74.
[9] A. Gupta, B. Basu, Sustainable primary aluminium production: technology status and future opportunities, Trans. Indian Inst. Met. 72 (2019) 2135–2150.
[10] International Aluminium Institute, Statistics (2024). https://international-aluminium.org/statistics-overview/.
[11] International Aluminium Institute publishes global recycling data. www.world-aluminium.org, 2024.
[12] D. Raabe, D. Ponge, P.J. Uggowitzer, M. Roscher, M. Paolantonio, C. Liu, H. Antrekowitsch, E. Kozeschnik, D. Seidmann, B. Gault, F. De Geuser, A. Deschamps, C. Hutchinson, C. Liu, Z. Li, P. Prangnell, J. Robson, P. Shanthraj, S. Vakili, C. Sinclair, L. Bourgeois, S. Pogatscher, Making sustainable aluminum by recycling scrap: the science of "dirty" alloys, Prog. Mater. Sci. 128 (2022) 100947.
[13] G. Gaustad, E. Olivetti, R. Kirchain, Improving aluminum recycling: a survey of sorting and impurity removal technologies, Resour. Conserv. Recycl. 58 (2012) 79–87.
[14] M. Bertram, K.J. Martchek, G. Rombach, Material flow analysis in the aluminum industry, J. Ind. Ecol. 13 (5) (2009).
[15] S. Capuzzi, G. Timelli, Preparation and melting of scrap in aluminum recycling: a review, Metals 8 (4) (2018) 249.
[16] K. Daehn, R. Basuhi, J. Gregory, M. Berlinger, V. Somjit, E.A. Olivetti, Innovations to decarbonize materials industries, Nat. Rev. Mater. 7 (4) (2022) 275–294.
[17] Van Der Donk, Recycling of metals and engineered materials, 3rd international symposium (1995) 651–661. Alabama; USA.
[18] A. Flores-V, M. Sukiennik, A.H. Castillejos-E, F.A. Acosta-G, J.C. Escobedo-B, A kinetic study on the nucleation and growth of the Al8FeMnSi2 intermetallic compound for aluminum scrap purification, Intermetallics 6 (3) (1998) 217–227.
[19] H. Matsubara, N. Izawa, M. Nakanishi, Macroscopic segregation in Al–11 mass% Si alloy containing 2 mass%Fe solidified under centrifugal force, J. Jpn. Inst. Light Metals 48 (2) (1998) 93–97.
[20] L. Zhang, L.N. Damoah, Current technologies for the removal of iron from aluminium alloys, in: Stephen J. Lindsay (Ed.), Light Met. (2011) 101–106.
[21] J.W. Gao, D. Shu, J. Wang, B.D. Sun, Effects of Na2B4O7 on the elimination of iron from aluminum melt, Scr. Mater. 57 (3) (2007) 197–200.
[22] H.L. de Moraes, J. de Oliveira, Roberto eacute, D.C.R. Espinosa, oacute Ten, J.A. S. rio, Removal of iron from molten recycled aluminum through intermediate phase filtration, Mater. Trans. 47 (7) (2006) 1731–1736.
[23] N.A. Belov, A.A. Aksenov, D.G. Eskin, Iron in Aluminium Alloys : Impurity and Alloying Element, CRC Press, Taylor & Francis Ltd, 2002.
[24] H.W.L. Phillips, Annotated Equilibrium Diagrams of Some Aluminium Alloy Systems, The Institute of Metals, London, 1959.
[25] J.A. Taylor, Iron-containing intermetallic phases in Al-Si based casting alloys, Procedia Materials Science 1 (2012) 19–33.
[26] L. Zhang, J. Gao, L.N.W. Damoah, D.G. Robertson, Removal of iron from aluminum: a review, Miner. Process. Extr. Metall. Rev. 33 (2) (2012) 99–157.
[27] I.N. Fridlyander, O.A. Noskova, N.B. Kuznetsova, Effect of iron and silicon impurities on the mechanical properties of an alloy in the system Al−Zn−Mg−Cu, Met. Sci. Heat Treat. 29 (6) (1987) 439–440.
[28] H. Shen, W.D. Yang, H. Liang, G.C. Yao, Research advance in harmful effects and removal of impurity Fe from Al and Al alloys, Adv. Mater. Res. 295–297 (2011) 751–759.
[29] Y. Tang, Y. Tomita, Z. Horita, Mechanical properties and microstructures of highly Fe-containing Al–Mg–Si alloys processed by severe plastic deformation under high pressure, Mater. Trans. 64 (2) (2023) 448–457.
[30] J. Lazaro-Nebreda, J.B. Patel, I.T.H. Chang, I.C. Stone, Z. Fan, Solidification processing of scrap Al-alloys containing high levels of Fe, IOP Conf. Ser. Mater. Sci. Eng. 529 (1) (2019) 012059.
[31] L. Lu, A.K. Dahle, Iron-rich intermetallic phases and their role in casting defect formation in hypoeutectic Al-Si alloys, Metall. Mater. Trans. 36 (3) (2005) 819–835.
[32] P.N. Crepeau, Effect of iron in Al-Si casting alloys: a critical review, Trans. Am. Foundrymen's Soc. 103 (1995) 361–366.
[33] T.O. Mbuya, B.O. Odera, S.P. Ng'ang'a, Influence of iron on castability and properties of aluminium silicon alloys: literature review, Int. J. Cast Metals Res. 16 (5) (2003) 451–465.
[34] W. Khalifa, F.H. Samuel, Gm-Nserc-Uqac, J.E. Gruzleski, H.W. Doty, S. Valtierra, Nucleation of Fe-intermetallic phases in the Al-Si-Fe alloys, Metall. Mater. Trans. 36 (4) (2005) 1017–1032.
[35] W. Khalifa, F.H. Samuel, J.E. Gruzleski, Iron intermetallic phases in the Al corner of the Al-Si-Fe system, Metall. Mater. Trans. 34 (13) (2003) 807–825.
[36] O. Kubaschewski, IRON—Binary Phase Diagrams, Springer Verlag, Berlin, 1982.
[37] S.E. Williams, J. Tien-Chien, Intermetallics Formation and their effect on mechanical properties of Al-Si-X alloys, in: A. Mahmood (Ed.), Intermetallic Compounds, IntechOpen, Rijeka, 2018. Ch. 2.
[38] Z. Que, C.L. Mendis, Formation of θ-Al13Fe4 and the multi-step phase transformations to α-Al8Fe2Si, β-Al5FeSi and δ-Al4FeSi2 in Al–20Si-0.7Fe alloy, Intermetallics 127 (2020) 106960.
[39] J. Wang, P.D. Lee, R.W. Hamilton, M. Li, J. Allison, The kinetics of Fe-rich intermetallic formation in aluminium alloys: in situ observation, Scr. Mater. 60 (7) (2009) 516–519.
[40] S.G. Shabestari, The effect of iron and manganese on the formation of intermetallic compounds in aluminum–silicon alloys, Mater. Sci. Eng., A 383 (2) (2004) 289–298.
[41] A. Couture, Iron in aluminium casting alloys- A literature survey, International cast metals journal 6 (4) (1981) 9–17.
[42] H. Becker, T. Bergh, P.E. Vullum, A. Leineweber, Y. Li, Effect of Mn and cooling rates on α-, β- and δ-Al–Fe–Si intermetallic phase formation in a secondary Al–Si alloy, Materialia 5 (2019) 100198.
[43] M.H. Khan, A. Das, Z. Li, H.R. Kotadia, Effects of Fe, Mn, chemical grain refinement and cooling rate on the evolution of Fe intermetallics in a model 6082 Al-alloy, Intermetallics 132 (2021) 107132.
[44] A.N. Lakshmanan, S.G. Shabestari, J.E. Gruzleski, Microstructure control of iron intermetallics in Al-Si casting alloys, Z. Metallkd. 86 (7) (1995) 457–467.
[45] P. Donnadieu, G. Lapasset, T.H. Sanders, Manganese-induced ordering in the α-(Al-Mn-Fe-Si) approximant phase, Philos. Mag. Lett. 70 (5) (1994) 319–326.
[46] S. Ji, W. Yang, F. Gao, D. Watson, Z. Fan, Effect of iron on the microstructure and mechanical property of Al–Mg–Si–Mn and Al–Mg–Si diecast alloys, Mater. Sci. Eng., A 564 (2013) 130–139.
[47] D. Song, Y. Zhao, Y. Jia, R. Li, N. Zhou, K. Zheng, Y. Fu, W. Zhang, Study of the evolution mechanisms of Fe-rich phases in Al-Si-Fe alloys with Mn modification using synchrotron X-ray imaging, J. Alloys Compd. 915 (2022) 165378.
[48] M. Mahta, M. Emamy, A. Daman, A. Keyvani, J. Campbell, Precipitation of Fe rich intermetallics in Cr- and Co-modified A413 alloy, Int. J. Cast Metals Res. 18 (2) (2005) 73–79.
[49] G. Timelli, F. Bonollo, The influence of Cr content on the microstructure and mechanical properties of AlSi9Cu3(Fe) die-casting alloys, Mater. Sci. Eng., A 528 (1) (2010) 273–282.
[50] G. Gustafsson, T. Thorvaldsson, G.L. Dunlop, The influence of Fe and Cr on the microstructure of cast Al-Si-Mg alloys, Metall. Trans. A 17 (1) (1986) 45–52.
[51] L.F. Mondolfo, Aluminum Alloys: Structure and Properties, Butterworths, 1976.
[52] A. Pennors, A.M. Samuel, F.H. Samuel, H.W. Doty, Precipitation of beta-Al5FeSi iron intermetallic in Al-6 % Si-3. 5 % Cu(319) type alloys: role of Sr and P, Trans. Am. Foundrymen's Soc. 106 (1998) 251–264.
[53] S. Murali, K.S. Raman, K.S.S. Murthy, Effect of trace additions (beryllium, chromium, manganese and cobalt) on the mechanical properties and fracture toughness of iron-containing Al-7Si-0.3Mg alloy, Ljevarstvo 37 (1995) 3–14.
[54] F.H. Samuel, A.M. Samuel, P. Ouellet, H.W. Doty, Effect of Mg and Sr additions on the formation of intermetallics in Al-6 Wt pct Si-3.5 Wt pct Cu-(0.45) to (0.8) Wt pct Fe 319-type alloys, Metall. Mater. Trans. 29 (12) (1998) 2871–2884.
[55] S. Bercovici, Control of Solidification Structure and Properties of Al-Si Alloys, Presentation at 45th International Foundry Congress, 1978.
[56] Z. Zhang, G. Li, X.G. Chen, Effect of nickel and vanadium on iron bearing intermetallic phases in AA 5657 simulated DC castings, Mater. Sci. Technol. 30 (8) (2014) 951–961.
[57] C.B. Basak, A. Meduri, N. Hari Babu, Influence of Ni in high Fe containing recyclable Al-Si cast alloys, Mater. Des. 182 (2019) 108017.
[58] W. Jiang, Z. Fan, Y. Dai, C. Li, Effects of rare earth elements addition on microstructures, tensile properties and fractography of A357 alloy, Mater. Sci. Eng., A 597 (2014) 237–244.
[59] K. Nogita, S.D. McDonald, A.K. Dahle, Eutectic modification of Al-Si alloys with rare earth metals, Mater. Trans. 45 (2) (2004) 323–326.
[60] Y.-C. Tsai, C.-Y. Chou, S.-L. Lee, C.-K. Lin, J.-C. Lin, S. Lim, Effect of trace La addition on the microstructures and mechanical properties of A356 (Al–7Si–0.35 Mg) aluminum alloys, J. Alloys Compd. 487 (1–2) (2009) 157–162.
[61] Q. Zheng, L. Zhang, H. Jiang, J. Zhao, J. He, Effect mechanisms of micro-alloying element La on microstructure and mechanical properties of hypoeutectic Al-Si alloys, J. Mater. Sci. Technol. 47 (2020) 142–151.
[62] Q. Tang, J. Zhao, T. Wang, J. Chen, K. He, The effects of neodymium addition on the intermetallic microstructure and mechanical properties of Al-7Si-0.3 Mg-0.3 Fe alloys, J. Alloys Compd. 741 (2018) 161–173.
[63] B. Wan, W. Chen, L. Liu, X. Cao, L. Zhou, Z. Fu, Effect of trace yttrium addition on the microstructure and tensile properties of recycled Al–7Si–0.3 Mg–1.0 Fe casting alloys, Mater. Sci. Eng., A 666 (2016) 165–175.
[64] B. Zhao, S. Xing, H. Sun, G. Yan, W. Gao, L. Ou, Effect of rare-earth La on microstructure and mechanical properties of Al7Si4CuMg alloys prepared by squeeze casting, J. Mater. Sci. 57 (25) (2022) 12064–12083.
[65] C. Fan, S.-y. Long, H.-d. Yang, X. Wang, J. Zhang, Influence of Ce and Mn addition on α-Fe morphology in recycled Al-Si alloy ingots, Int. J. Miner. Metall. Mater. 20 (2013) 890–895.
[66] A. Das, H.R. Kotadia, Effect of high-intensity ultrasonic irradiation on the modification of solidification microstructure in a Si-rich hypoeutectic Al–Si alloy, Mater. Chem. Phys. 125 (3) (2011) 853–859.
[67] H.R. Kotadia, A. Das, Modification of solidification microstructure in hypo- and hyper-eutectic Al–Si alloys under high-intensity ultrasonic irradiation, J. Alloys Compd. 620 (Supplement C) (2015) 1–4.
[68] H. Kotadia, A. Das, Modification of Fe Rich Intermetallics through Ultrasonic (Unpublished work).
[69] Y. Osawa, S. Takamori, T. Kimura, K. Minagawa, H. Kakisawa, Morphology of intermetallic compounds in Al-Si-Fe alloy and its control by ultrasonic vibration, Mater. Trans. 48 (9) (2007) 2467–2475.
[70] H.R. Kotadia, A. Das, E. Doernberg, R. Schmid-Fetzer, A comparative study of ternary Al–Sn–Cu immiscible alloys prepared by conventional casting and casting

under high-intensity ultrasonic irradiation, Mater. Chem. Phys. 131 (1) (2011) 241–249.
[71] H.R. Kotadia, M. Qian, D.G. Eskin, A. Das, On the microstructural refinement in commercial purity Al and Al-10wt% Cu alloy under ultrasonication during solidification, Mater. Des. 132 (Supplement C) (2017) 266–274.
[72] H.R. Kotadia, M. Qian, A. Das, Solidification of aluminium alloys under ultrasonication: an overview, Trans. Indian Inst. Met. 71 (11) (2018) 2681–2686.
[73] G.I. Eskin, Ultrasonic Treatment of Light Alloy Melts, CRC press, 1998.
[74] H.R. Kotadia, N. Hari Babu, H. Zhang, S. Arumuganathar, Z. Fan, Solidification behavior of intensively sheared hypoeutectic Al-Si alloy liquid, Metall. Mater. Trans. 42 (4) (2011) 1117–1126.
[75] H.R. Kotadia, J.B. Patel, H.T. Li, F. Gao, Z. Fan, Microstructure evolution in melt conditioned direct chill (MC-DC) casting of Fe-rich Al-alloy, Adv. Mater. Res. 1019 (2014) 90–95.
[76] H.R. Kotadia, N. Hari Babu, H. Zhang, Z. Fan, Microstructural refinement of Al–10.2 %Si alloy by intensive shearing, Mater. Lett. 64 (6) (2010) 671–673.
[77] M.C. Flemings, Solidification processing, Metall. Trans. A 5 (10) (1974) 2121–2134.
[78] Z. Fan, Semisolid metal processing, Int. Mater. Rev. 47 (2) (2002) 49–85.
[79] M.C. Flemings, Behavior of metal alloys in the semisolid state, Metall. Trans. A B 22 (3) (1991) 269–293.
[80] A. Das, S. Ji, Z. Fan, Morphological development of solidification structures under forced fluid flow: a Monte-Carlo simulation, Acta Mater. 50 (18) (2002) 4571–4585.
[81] K. Kocatepe, C.F. Burdett, Effect of low frequency vibration on macro and micro structures of LM6 alloys, J. Mater. Sci. 35 (13) (2000) 3327–3335.
[82] N. Abu-Dheir, M. Khraisheh, K. Saito, A. Male, Silicon morphology modification in the eutectic Al–Si alloy using mechanical mold vibration, Mater. Sci. Eng., A 393 (1) (2005) 109–117.
[83] S. Nafisi, D. Emadi, M.T. Shehata, R. Ghomashchi, Effects of electromagnetic stirring and superheat on the microstructural characteristics of Al–Si–Fe alloy, Mater. Sci. Eng., A 432 (1) (2006) 71–83.
[84] C. Vives, Electromagnetic refining of aluminum alloys by the CREM process: Part I. Working principle and metallurgical results, Metall. Trans. A B 20 (5) (1989) 623–629.
[85] F.H. Samuel, G. Pucella, C. Villeneuve, A.M. Samuel, H.W. Doty, S. Valtierra, Microstructural observations on Fe-intermetallics in unmodified and Sr-modified Al-Si-Cu (A380.1) die casting alloy, Int. J. Cast Metals Res. 12 (3) (1999) 197–210.
[86] A.M. Samuel, A. Pennors, C. Villeneuve, F.H. Samuel, H.W. Doty, S. Valtierra, Effect of cooling rate and Sr-modification on porosity and Fe-intermetallics formation in Al-6.5 % Si-3.5 % Cu-Fe alloys, Int. J. Cast Metals Res. 13 (4) (2000) 231–253.
[87] S. Onurlu, A. Tekin, Effect of heat treatment on the insoluble intermetallic phases present in an AA 6063 alloy, J. Mater. Sci. 29 (6) (1994) 1652–1655.
[88] S. Zajac, B. Hutchinson, A. Johansson, L.O. Gullman, Microstructure control and extrudability of Al–Mg–Si alloys microalloyed with manganese, Mater. Sci. Technol. 10 (4) (1994) 323–333.
[89] United Nations: General assembly economic and social council, Sustainable Development Goals.
[90] M.C. Flemings, Solidification Processing, Materials Science and Technology, Wiley-VCH Verlag GmbH & Co. KGaA2006.
[91] S.J. Maggs, PhD Thesis: Intermetallic Phase Selection in Dilute AI-Fe-Si Alloys, The University of Leeds, School of Materials, 1996.
[92] P. Liu, T. Thorvaldsson, G.L. Dunlop, Formation of intermetallic compounds during solidification of dilute Al–Fe–Si alloys, Mater. Sci. Technol. 2 (10) (1986) 1009–1018.
[93] P. Skjerpe, Intermetallic phases formed during DC-casting of an Al−0.25 Wt Pct Fe−0.13 Wt Pct Si alloy, Metall. Trans. A 18 (2) (1987) 189–200.
[94] I.R. Hughes, H. Jones, Coupled eutectic growth in Al-Fe alloys, J. Mater. Sci. 11 (10) (1976) 1781–1793.
[95] R. Elliott, Eutectic Solidification Processing: Crystalline and Glassy Alloys, first ed., Butterworth-Heinemann, 1983.
[96] R.C. Hudd, W.H. Taylor, The structure of Co4Al13, Acta Crystallogr. 15 (5) (1962) 441–442.
[97] P. Black, The structure of FeAl3. I, Acta Crystallogr. 8 (1) (1955) 43–48.
[98] P. Black, The structure of FeAl3. II, Acta Crystallogr. 8 (3) (1955) 175–182.
[99] B. Dutta, M. Rettenmayr, Effect of cooling rate on the solidification behaviour of Al–Fe–Si alloys, Mater. Sci. Eng., A 283 (1) (2000) 218–224.
[100] A. Griger, V. Stefániay, E. Kovács-Csetényi, T. Turmezey, Formation and transformation of binary intermetallic phases in high purity Al-Fe alloys, Key Eng. Mater. 44–45 (1991) 17–30.
[101] H. Kosuge, I. Mizukami, Formation of fir-tree structure in DC cast ingots of Al-0.06 %Fe alloys Journal of Japan Institute of Light, Metals 25 (2) (1975) 48–58.
[102] P. Skjerpe, Intermetallic phases formed during DC-casting of an Al−0.25 Wt Pct Fe−0.13 Wt Pct Si alloy, Metall. Mater. Trans. 18 (2) (1987) 189–200.
[103] C.J. Simensen, R. Vellasamy, Determination of phases present in cast material of an Al-0. 5 Fe-0. 2 Wt per cent Si alloy, Zeitschrift fur Metallkunde 68 (6) (1977) 428–431.
[104] C.M. Allen, K.A.Q. O'Reilly, B. Cantor, P.V. Evans, Intermetallic phase selection in 1XXX Al alloys, Prog. Mater. Sci. 43 (2) (1998) 89–170.
[105] D. Panahi, Precipitation of Intermetallic Phases from Rapidly Solidfying Aluminium Alloys, MCMAser University, 2009. MSc Thesis.
[106] B. Lin, W.W. Zhang, Effect of heat treatment on morphology of Fe-rich intermetallics in Al–Cu alloys, Mater. Sci. Technol. 33 (6) (2017) 738–743.
[107] K. Liu, X.G. Chen, Evolution of intermetallics, dispersoids, and elevated temperature properties at various Fe contents in Al-Mn-Mg 3004 alloys, Metall. Mater. Trans. B 47 (6) (2016) 3291–3300.
[108] O. Engler, K. Kuhnke, J. Hasenclever, Development of intermetallic particles during solidification and homogenization of two AA 5xxx series Al-Mg alloys with different Mg contents, J. Alloys Compd. 728 (2017) 669–681.
[109] S. Kumar, P.S. Grant, K.A.Q. O'Reilly, Evolution of Fe bearing intermetallics during DC casting and homogenization of an Al-Mg-Si Al alloy, Metall. Mater. Trans. 47 (6) (2016) 3000–3014.
[110] A. Verma, S. Kumar, P.S. Grant, K.A.Q. O'Reilly, Influence of cooling rate on the Fe intermetallic formation in an AA6063 Al alloy, J. Alloys Compd. 555 (2013) 274–282.
[111] F.H. Samuel, A.M. Samuel, H.W. Doty, S. Valtierra, Decomposition of Fe-intermetallics in Sr-modified cast 6XXX type aluminum alloys for automotive skin, Metall. Mater. Trans. 32 (8) (2001) 2061–2075.
[112] L. X.-M., M. Starink, Effect of compositional variations on characteristics of coarse intermetallic particles in overaged 7000 aluminium alloys, Mater. Sci. Technol. 17 (11) (2001) 1324–1328.
[113] Y. Zhu, K. Sun, G.S. Frankel, Intermetallic phases in aluminum alloys and their roles in localized corrosion, J. Electrochem. Soc. 165 (11) (2018) C807.
[114] Y. Langsrud, Silicon in commercial aluminium alloys - what becomes of it during DC-casting? Key Eng. Mater. 44–45 (1991) 95–116.
[115] N.C.W. Kuijpers, F.J. Vermolen, C. Vuik, P.T.G. Koenis, K.E. Nilsen, S.v.d. Zwaag, The dependence of the β-AlFeSi to α-Al(FeMn)Si transformation kinetics in Al–Mg–Si alloys on the alloying elements, Mater. Sci. Eng., A 394 (1) (2005) 9–19.
[116] X. Cao, J. Campbell, The solidification characteristics of Fe-rich intermetallics in Al-11.5Si-0.4Mg cast alloys, Metall. Mater. Trans. 35 (5) (2004) 1425–1435.
[117] Z. Que, Y. Wang, Z. Fan, Formation of the Fe-containing intermetallic compounds during solidification of Al-5Mg-2Si-0.7Mn-1.1Fe alloy, Metall. Mater. Trans. 49 (6) (2018) 2173–2181.
[118] Y.L. Liu, S.B. Kang, The solidification process of Al–Mg–Si alloys, J. Mater. Sci. 32 (6) (1997) 1443–1447.
[119] X. Cao, J. Campbell, The nucleation of Fe-Rich phases on oxide films in Al-11.5Si-0.4Mg cast alloys, Metall. Mater. Trans. 34 (7) (2003) 1409–1420.
[120] S. Terzi, J.A. Taylor, Y.H. Cho, L. Salvo, M. Suéry, E. Boller, A.K. Dahle, In situ study of nucleation and growth of the irregular α-Al/β-Al5FeSi eutectic by 3-D synchrotron X-ray microtomography, Acta Mater. 58 (16) (2010) 5370–5380.
[121] C. Puncreobutr, A.B. Phillion, J.L. Fife, P. Rockett, A.P. Horsfield, P.D. Lee, In situ quantification of the nucleation and growth of Fe-rich intermetallics during Al alloy solidification, Acta Mater. 79 (2014) 292–303.
[122] C. Puncreobutr, P.D. Lee, K.M. Kareh, T. Connolley, J.L. Fife, A.B. Phillion, Influence of Fe-rich intermetallics on solidification defects in Al–Si–Cu alloys, Acta Mater. 68 (2014) 42–51.
[123] S. Feng, E. Liotti, A. Lui, M.D. Wilson, T. Connolley, R.H. Mathiesen, P.S. Grant, In-situ X-ray radiography of primary Fe-rich intermetallic compound formation, Acta Mater. 196 (2020) 759–769.
[124] J. Cao, S. Shuai, C. Huang, T. Hu, C. Chen, J. Wang, Z. Ren, 4D synchrotron X-ray tomographic study of the influence of transverse magnetic field on iron intermetallic compounds precipitation behavior during solidification of Al–Si–Fe alloy, Intermetallics 143 (2022) 107471.
[125] J.M. Yu, N. Wanderka, A. Rack, R. Daudin, E. Boller, H. Markötter, A. Manzoni, F. Vogel, T. Arlt, I. Manke, J. Banhart, Influence of impurities, strontium addition and cooling rate on microstructure evolution in Al-10Si-0.3Fe casting alloys, J. Alloys Compd. 766 (2018) 818–827.
[126] Y. Zhao, Z. Wang, C. Zhang, W. Zhang, Synchrotron X-ray tomography investigation of 3D morphologies of intermetallic phases and pores and their effect on the mechanical properties of cast Al-Cu alloys, J. Alloys Compd. 777 (2019) 1054–1065.
[127] Z. Song, O.V. Magdysyuk, L. Tang, T. Sparks, B. Cai, Growth dynamics of faceted Al13Fe4 intermetallic revealed by high-speed synchrotron X-ray quantification, J. Alloys Compd. 861 (2021) 158604.
[128] G.K. Sigworth, Determining grain size and eutectic modification in aluminum alloy castings, Mod. Cast. 77 (7) (1987) 23–25.
[129] Y.H. Cho, H.-C. Lee, K.H. Oh, A.K. Dahle, Effect of strontium and phosphorus on eutectic Al-Si nucleation and formation of β-Al5FeSi in hypoeutectic Al-Si foundry alloys, Metall. Mater. Trans. 39 (10) (2008) 2435–2448.
[130] A. Bjurenstedt, D. Casari, S. Seifeddine, R.H. Mathiesen, A.K. Dahle, In-situ study of morphology and growth of primary α-Al(FeMnCr)Si intermetallics in an Al-Si alloy, Acta Mater. 130 (2017) 1–9.
[131] Z. Que, Y. Wang, C.L. Mendis, C. Fang, J. Xia, X. Zhou, Z. Fan, Understanding Fe-containing intermetallic compounds in Al alloys: an overview of recent advances from the LiME research hub, Metals 12 (10) (2022) 1677.
[132] A. Lui, P.S. Grant, I.C. Stone, K.A.Q. O'Reilly, The role of grain refiner in the nucleation of AlFeSi intermetallic phases during solidification of a 6xxx aluminum alloy, Metall. Mater. Trans. 50 (11) (2019) 5242–5252.
[133] K. Liu, X. Cao, X.-G. Chen, Solidification of iron-rich intermetallic phases in Al-4.5Cu-0.3Fe cast alloy, Metall. Mater. Trans. 42 (7) (2011) 2004–2016.
[134] S. Kumar, K.A.Q. O'Reilly, Influence of Al grain structure on Fe bearing intermetallics during DC casting of an Al-Mg-Si alloy, Mater. Char. 120 (2016) 311–322.
[135] D.M. Stefanescu, R. Ruxanda, in: G.F. Vander Voort (Ed.), Fundamentals of Solidification Metallography and Microstructures, ASM International, 2004, pp. 1–24.
[136] V. Stefániay, Á. Griger, T. Turmezey, Intermetallic phases in the aluminium-side corner of the AlFeSi-alloy system, J. Mater. Sci. 22 (2) (1987) 539–546.

[137] Y. Zhang, Y. Liu, Y. Han, C. Wei, Z. Gao, The role of cooling rate in the microstructure of Al–Fe–Si alloy with high Fe and Si contents, J. Alloys Compd. 473 (1) (2009) 442–445.
[138] H. Kosuge, I. Mizukami, Behavior of "fir-tree" structure in Al-Fe-Si alloy ingots soaking at elevated temperatures, J. Jpn. Inst. Light Metals 22 (7) (1972) 437–444.
[139] A. Douglas, The structure of Co2Al9, Acta Crystallogr. 3 (1) (1950) 19–24.
[140] E.H. Hollingsworth, G.R. Frank Jr., R.E. Willett, Identification of a new Al-Fe constituent, FeAl6, Trans. TMS-AIME 224 (1962) 188–189.
[141] L. Walford, The structure of the intermetallic phase FeAl6, Acta Crystallogr. 18 (2) (1965) 287–291.
[142] A. Nicol, The structure of MnAl6, Acta Crystallogr. 6 (3) (1953) 285–293.
[143] P.J. Black, O.S. Edwards, J.B. Forsyth, The structure of [alpha] (Al-Cu-Fe), Acta Crystallogr. 14 (9) (1961) 993–998.
[144] R.M.K. Young, T.W. Clyne, An Al-Fe intermetallic phase formed during controlled solidification, Scripta Metall. 15 (11) (1981) 1211–1216.
[145] M. Cooper, The crystal structure of the ternary alloy [alpha](AlFeSi), Acta Crystallogr. 23 (6) (1967) 1106–1107.
[146] M. Cooper, K. Robinson, The crystal structure of the ternary alloy α(AlMnSi), Acta Crystallogr. 20 (5) (1966) 614–617.
[147] V.G. Rivlin, G.V. Raynor, 4: critical evaluation of constitution of aluminium-Iran-silicon system, Int. Met. Rev. 26 (1) (1981) 133–152.
[148] K. Robinson, P.J. Black, CXLVI. An X-Ray examination of an α (Al-Fe-Si) ternary compound, London, Edinburgh Dublin Phil. Mag. J. Sci. 44 (359) (1953) 1392–1397.
[149] H. Westengen, Formation of intermetallic compounds during DC-casting of a commercial purity Al-Fe-Si alloy, Zeitschrift fur Metallkunde 73 (6) (1982) 360–368.
[150] P. Liu, T. Thorvaldsson, G.L. Dunlop, SCANDEM 85 35.
[151] R. Höier, Citedby, A.L. Dons, Z. Metallkde 76 (2) (1985) 151–153.
[152] G. PhragmŽn, On the phases occurring in alloys of aluminium with copper, magnesium, manganese, iron and silicon, J. Inst. Met. 77 (1950) 489–552.
[153] D. Munson, A clarification of the phases occurring in aluminium-rich aluminium-iron-silicon alloys, with particular reference to the ternary phase alpha-AlFeSi, J. Inst. Met. 95 (1967) 217–219.
[154] A. Fabrizi, G. Timelli, S. Ferraro, F. Bonollo, Evolution of Fe-rich compounds in a secondary Al–Si–Cu alloy: influence of cooling rate, Int. J. Mater. Res. 106 (7) (2015) 719–724.
[155] I. Sunagawa, Crystals Growth, Morphology, & Perfection, Cambridge University Press, 2005.
[156] C. Li, Y.Y. Wu, H. Li, X.F. Liu, Morphological evolution and growth mechanism of primary Mg2Si phase in Al–Mg2Si alloys, Acta Mater. 59 (3) (2011) 1058–1067.
[157] B. Kim, L. Sangmok, H. Yasuda, Morphological variation in of the Fe/Cr-containing intermetalic phase in the Al-Si cast alloy as a function of cooling rate: time-resolved radiography, Mater. Sci. Forum 654–656 (2010) 974–977.
[158] T. Gao, Y. Wu, C. Li, X. Liu, Morphologies and growth mechanisms of α-Al(FeMn)Si in Al–Si–Fe–Mn alloy, Mater. Lett. 110 (2013) 191–194.
[159] K. Xiang, L. Qin, Y. Zhao, S. Huang, W. Du, E. Boller, A. Rack, M. Li, J. Mi, Operando study of the dynamic evolution of multiple Fe-rich intermetallics of an Al recycled alloy in solidification by synchrotron X-ray and machine learning, Acta Mater. 279 (2024) 120267.
[160] M. Tachibana, Beginner's Guide to Flux Crystal Growth, Springer, 2017.
[161] H. Becker, N. Bulut, J. Kortus, A. Leineweber, β-Al4.5FeSi: hierarchical crystal and defect structure: reconciling experimental and theoretical evidence including the influence of Al vs. Si ordering on the crystal structure, J. Alloys Compd. 911 (2022) 165015.
[162] D. Song, Y. Zhao, Z. Wang, Y. Jia, H. Huang, D. Zhang, W. Zhang, Effect of Mn/Fe ratio on Fe removal efficiency and tensile ductility of an Al–7.0Si–2.4Fe alloy, J. Mater. Res. 36 (6) (2021) 1357–1366.
[163] Y. Zhao, W. Zhang, C. Yang, D. Zhang, Z. Wang, Effect of Si on Fe-rich intermetallic formation and mechanical properties of heat-treated Al–Cu–Mn–Fe alloys, J. Mater. Res. 33 (8) (2018) 898–911.
[164] Y. Kuroki, T. Tanaka, T. Sato, A. Kamio, Effects of defects and Fe intermetallic compounds on fatigue properties of Al-Si-Cu-Mg alloy castings, Mater. Trans. 42 (11) (2001) 2339–2344.
[165] Z. Ma, A.M. Samuel, H.W. Doty, S. Valtierra, F.H. Samuel, Effect of Fe content on the fracture behaviour of Al–Si–Cu cast alloys, Mater. Des. 57 (2014) 366–373.
[166] M. Emamy, A.R. Emami, R. Khorshidi, M.R. Ghorbani, The effect of Fe-rich intermetallics on the microstructure, hardness and tensile properties of Al–Mg2Si die-cast composite, Mater. Des. 46 (2013) 881–888.
[167] T. Homma, T. Honma, D. Terada, M. Hoshino, Effects of extrusion speed and compounds on surface defects in extruded-AA7003 alloy, Mater. Sci. Technol. 37 (8) (2021) 785–793.
[168] H. Zhu, M.J. Couper, A.K. Dahle, Effect of process variables on the formation of streak defects on anodized aluminum extrusions: an overview, High Temp. Mater. Process. 31 (2) (2012) 105–111.
[169] M.V. Kral, A crystallographic identification of intermetallic phases in Al–Si alloys, Mater. Lett. 59 (18) (2005) 2271–2276.
[170] J.G. Zheng, R. Vincent, J.W. Steeds, Crystal structure of an orthorhombic phase in β-(Al-Fe-Si) precipitates determined by convergent-beam electron diffraction, Philos. Mag. A 80 (2) (2000) 493–500.
[171] M.V. Kral, P.N.H. Nakashima, D.R.G. Mitchell, Electron microscope studies of Al-Fe-Si intermetallics in an Al-11 Pct Si alloy, Metall. Mater. Trans. 37 (6) (2006) 1987–1997.
[172] C.M. Fang, Z.P. Que, Z. Fan, Crystal chemistry and electronic structure of the β-AlFeSi phase from first-principles, J. Solid State Chem. 299 (2021) 122199.
[173] S. Feng, Z. Jin, W. Du, I. Han, A. Lui, X. Zhou, P.R. Shearing, P.S. Grant, E. Liotti, The mechanism of Fe-rich intermetallic compound formation and growth on inoculants revealed by electron backscattered diffraction and X-ray imaging, Mater. Des. 232 (2023) 112110.
[174] J.J. De Yoreo, P.G. Vekilov, Principles of crystal nucleation and growth, Rev. Mineral. Geochem. 54 (1) (2003) 57–93.
[175] Y. Zhao, W. Zhang, D. Song, B. Lin, F. Shen, D. Zheng, C. Xie, Z. Sun, Y. Fu, R. Li, Nucleation and growth of Fe-rich phases in Al-5Ti-1B modified Al-Fe alloys investigated using synchrotron X-ray imaging and electron microscopy, J. Mater. Sci. Technol. 80 (2021) 84–99.
[176] Y. Zhao, W. He, D. Song, W. Zhang, F. Shen, B. Ma, Y. Jia, Z. Sun, Y. Fu, R. Fernández, In-situ synchrotron X-ray radiography study of primary Fe-rich phases growth in Al-Fe(Cu) alloys, Mater. Char. 195 (2023) 112539.
[177] Y. Zhao, D. Song, H. Wang, X. Li, L. Chen, Z. Sun, Z. Wang, T. Zhai, Y. Fu, Y. Wang, S. Liu, Y. Du, W. Zhang, Revealing the nucleation and growth mechanisms of Fe-rich phases in Al–Cu–Fe(-Si) alloys under the influence of Al–Ti–B, Intermetallics 146 (2022) 107584.
[178] M. Timpel, N. Wanderka, R. Grothausmann, J. Banhart, Distribution of Fe-rich phases in eutectic grains of Sr-modified Al–10wt.% Si–0.1wt.% Fe casting alloy, J. Alloys Compd. 558 (2013) 18–25.
[179] N. Balasubramani, M. Moodispaw, E. Cinkilic, J. Miao, A.A. Luo, Strontium effects on the formation of iron-intermetallic phases in secondary Al–9Si–0.6Fe alloys, Metall. Mater. Trans. 55 (2) (2024) 550–568.
[180] W. Khalifa, A.M. Samuel, F.H. Samuel, H.W. Doty, S. Valtierra, Metallographic observations of β-AlFeSi phase and its role in porosity formation in Al–7 %Si alloys, Int. J. Cast Metals Res. 19 (3) (2006) 156–166.
[181] J.M. Yu, N. Wanderka, A. Rack, R. Daudin, E. Boller, H. Markötter, A. Manzoni, F. Vogel, T. Arlt, I. Manke, J. Banhart, Formation of intermetallic δ phase in Al-10Si-0.3Fe alloy investigated by in-situ 4D X-ray synchrotron tomography, Acta Mater. 129 (2017) 194–202.
[182] Y.S. Choi, J.S. Lee, W.T. Kim, H.Y. Ra, Solidification behavior of Al-Si-Fe alloys and phase transformation of metastable intermetallic compound by heat treatment, J. Mater. Sci. 34 (9) (1999) 2163–2168.
[183] A.O. Mekhrabov, M.V. Akdeniz, Effect of ternary alloying elements addition on atomic ordering characteristics of Fe–Al intermetallics, Acta Mater. 47 (7) (1999) 2067–2075.
[184] X. Zhang, D. Wang, H. Nagaumi, Y. Zhou, W. Yu, X. Chong, X. Li, H. Zhang, Morphology, thermal stability, electronic structure and mechanical properties of α-AlFeMnSi phases with varying Mn/Fe atomic ratios: experimental studies and DFT calculations, J. Alloys Compd. 901 (2022) 163523.
[185] E. Cinkilic, C.D. Ridgeway, X. Yan, A.A. Luo, A formation map of iron-containing intermetallic phases in recycled cast aluminum alloys, Metall. Mater. Trans. 50 (12) (2019) 5945–5956.
[186] E. Cinkilic, M. Moodispaw, J. Zhang, J. Miao, A.A. Luo, A new recycled Al–Si–Mg alloy for sustainable structural die casting applications, Metall. Mater. Trans. 53 (8) (2022) 2861–2873.
[187] A. Gorny, J. Manickaraj, Z. Cai, S. Shankar, Evolution of Fe based intermetallic phases in Al–Si hypoeutectic casting alloys: influence of the Si and Fe concentrations, and solidification rate, J. Alloys Compd. 577 (2013) 103–124.
[188] L. Wang, M. Makhlouf, D. Apelian, Aluminium die casting alloys: alloy composition, microstructure, and properties-performance relationships, Int. Mater. Rev. 40 (6) (1995) 221–238.
[189] Z. Zhang, E. Kobayashi, H. Tezuka, T. Sato, Influence of the Fe content, Mn/Fe ratio and cooling rate on the modification process of Fe intermetallic compounds in hypoeutectic Al-Si alloys. 13th International Conference on Aluminum Alloys (ICAA13), 2012, pp. 1451–1456.
[190] S. Seifeddine, S. Johansson, I.L. Svensson, The influence of cooling rate and manganese content on the β-Al5FeSi phase formation and mechanical properties of Al–Si-based alloys, Mater. Sci. Eng., A 490 (1) (2008) 385–390.
[191] E. Samuel, A.M. Samuel, H.W. Doty, S. Valtierra, F.H. Samuel, Intermetallic phases in Al–Si based cast alloys: new perspective, Int. J. Cast Metals Res. 27 (2) (2014) 107–114.
[192] S. Ferraro, G. Timelli, Influence of sludge particles on the tensile properties of die-cast secondary aluminum alloys, Metall. Mater. Trans. B 46 (2015) 1022–1034.
[193] L.B. Otani, J. Soyama, G. Zepon, A. Costa e Silva, C.S. Kiminami, W.J. Botta, C. Bolfarini, Predicting the formation of intermetallic phases in the Al-Si-Fe system with Mn additions, J. Phase Equilibria Diffus. 38 (2017) 298–304.
[194] J. Hwang, H. Doty, M. Kaufman, Crystallographic studies on the iron-containing intermetallic phases in the 319-type aluminium casting alloys, Philos. Mag. 88 (4) (2008) 607–619.
[195] D. Ferdian, C. Josse, P. Nguyen, N. Gey, N. Ratel-Ramond, P. De Parseval, Y. Thebault, B. Malard, J. Lacaze, L. Salvo, Chinese script vs plate-like precipitation of beta-Al 9 Fe 2 Si 2 phase in an Al-6.5 Si-1Fe alloy, Metall. Mater. Trans. 46 (2015) 2814–2818.
[196] H. Becker, A. Thum, B. Distl, M.J. Kriegel, A. Leineweber, Effect of melt conditioning on removal of Fe from secondary Al-Si alloys containing Mg, Mn, and Cr, Metall. Mater. Trans. 49 (2018) 6375–6389.
[197] J. Jorstad, Understanding sludge, die casting engineer 30 (6) (1986).
[198] R. Dunn, Aluminum melting problems and their influence on furnace selection, DIE CAST, ENG, B 9 (5) (1965) 8.
[199] G. Timelli, S. Capuzzi, A. Fabrizi, Precipitation of primary Fe-rich compounds in secondary AlSi9Cu3 (Fe) alloys, J. Therm. Anal. Calorim. 123 (2016) 249–262.
[200] T. Murat, J. Cambell, G. Byczynski, Shape Casting: 5th International Symposium 2014, John Wiley & Sons, 2014, p. 278.

[201] C.M. Dinnis, J.A. Taylor, A.K. Dahle, Interactions between iron, manganese, and the Al-Si eutectic in hypoeutectic Al-Si alloys, Metall. Mater. Trans. 37 (11) (2006) 3283–3291.
[202] B.G. Dietrich, H. Becker, M. Smolka, A. Keßler, A. Leineweber, G. Wolf, Intermetallic sludge formation in Fe containing secondary Al–Si alloys influenced by Cr and Mn as preparative tool for metal melt filtration, Adv. Eng. Mater. 19 (9) (2017) 1700161.
[203] H.L. de Moraes, J.R. de Oliveira, D.C.R. Espinosa, J.A.S. Tenório, Removal of iron from molten recycled aluminum through intermediate phase filtration, Mater. Trans. 47 (7) (2006) 1731–1736.
[204] A. Pitsch, New experimental approach in the search of intermetallic compounds for Fe, Mn, and Si removal in aluminium recycling, Light Met. 2005 (2005) 1191–1195.
[205] P. Ashtari, K. Tetley-Gerard, K. Sadayappan, Removal of iron from recycled aluminium alloys, Can. Metall. Q. 51 (1) (2012) 75–80.
[206] R.W. Kraft, Controlled eutectics, JOM 18 (2) (1966) 192–200.
[207] S.Z. Lu, A. Hellawell, The mechanism of silicon modification in aluminum-silicon alloys: impurity induced twinning, Metall. Trans. A 18 (10) (1987) 1721–1733.
[208] S.S. Sreeja Kumari, R.M. Pillai, T.P.D. Rajan, B.C. Pai, Effects of individual and combined additions of Be, Mn, Ca and Sr on the solidification behaviour, structure and mechanical properties of Al–7Si–0.3Mg–0.8Fe alloy, Mater. Sci. Eng., A 460–461 (2007) 561–573.
[209] P. Ashtari, H. Tezuka, T. Sato, Influence of Sr and Mn additions on intermetallic compound morphologies in Al-Si-Cu-Fe cast alloys, Mater. Trans. 44 (12) (2003) 2611–2616.
[210] M. Zamani, PhD Thesis: Al-Si Cast Alloys - Microstructure and Mechanical Properties at Ambient and Elevated Temperature, School of Engineering, Jönköping University Dissertation Series No. 7, 2015.
[211] S. Yaneva, N. Stoichev, Z. Kamenova, S. Budurov, Quaternary iron-containing phases in Al-Si cast alloys, Zeitschrift fur metallkunde 75 (1984) 395–398.
[212] A.M. Samuel, F.H. Samuel, H.W. Doty, Observations on the formation of β-Al5FeSi phase in 319 type Al-Si alloys, J. Mater. Sci. 31 (20) (1996) 5529–5539.
[213] C. Villeneuve, F. Samuel, Fragmentation and dissolution of β-Al5FeSi phase during solution heat treatment of Al-13wt% Si-Fe alloys, Int. J. Cast Metals Res. 12 (3) (1999) 145–160.
[214] Q. Li, J. Wang, C. Xue, Y. Miao, Q. Hou, X. Yang, Y. Meng, Z. Yang, G. Tian, H. Su, X. Li, Effects of Sr on Fe-rich intermetallics in recycled Al–Si–Cu alloys, J. Mater. Sci. 59 (25) (2024) 11572–11595.
[215] M.H. Mulazimoglu, A. Zaluska, J.E. Gruzleski, F. Paray, Electron microscope study of Al-Fe-Si intermetallics in 6201 aluminum alloy, Metall. Mater. Trans. 27 (4) (1996) 929–936.
[216] Y. Cho, H.-C. Lee, K. Oh, A. Dahle, Effect of strontium and phosphorus on eutectic Al-Si nucleation and formation of β-Al 5 FeSi in hypoeutectic Al-Si foundry alloys, Metall. Mater. Trans. 39 (2008) 2435–2448.
[217] J. Campbell, J. Campbell, Casting Alloys, Complete Casting Handbook, 2011, pp. 255–390.
[218] W. Yi, G. Liu, Z. Lu, J. Gao, L. Zhang, Efficient alloy design of Sr-modified A356 alloys driven by computational thermodynamics and machine learning, J. Mater. Sci. Technol. 112 (2022) 277–290.
[219] E. Vandersluis, C. Ravindran, D. Sediako, A. Elsayed, G. Byczynski, Strontium-modification in the stepwise solidification of A319 Al alloy: an in-situ neutron diffraction study, J. Alloys Compd. 792 (2019) 240–249.
[220] S. Shabestari, M. Mahmudi, M. Emamy, J. Campbell, Effect of Mn and Sr on intermetallics in Fe-rich eutectic Al-Si alloy, Int. J. Cast Metals Res. 15 (1) (2002) 17–24.
[221] W. Eidhed, Modification of β-Al5FeSi compound in recycled Al-Si-Fe cast alloy by using Sr, Mg and Cr additions, J. Mater. Sci. Technol. 24 (1) (2008).
[222] B. Suárez-Peña, J. Asensio-Lozano, Influence of Sr modification and Ti grain refinement on the morphology of Fe-rich precipitates in eutectic Al–Si die cast alloys, Scr. Mater. 54 (9) (2006) 1543–1548.
[223] J.E. Hatch, Aluminum: Properties and Physical Metallurgy, ASM International, 1984.
[224] Alan Prince and MSIT® Materials Science International Team, Al-Fe-Sr ternary phase diagram evaluation phase diagrams, crystallographic and thermodynamic data: datasheet from MSI eureka in SpringerMaterials, MSI Materials Science International Services GmbH (1993).
[225] M. Kenyon, The Effect of Chromium on the Evolution of Dispersoids in Al-Mg-Si Alloys, School of Material Science, University of Manchester, 2018.
[226] P. Ashtari, H. Tezuka, T. Sato, Modification of Fe-containing intermetallic compounds by K addition to Fe-rich AA319 aluminum alloys, Scr. Mater. 53 (8) (2005) 937–942.
[227] D. Song, Y. Zhao, Y. Jia, G. Huang, Z. Zhang, N. Zhou, X. Li, K. Zheng, Y. Fu, W. Zhang, Effect of B addition on the formation of Fe-rich phases in Al-Si-Fe alloys, J. Alloys Compd. 930 (2023) 167426.
[228] D. Song, Y. Zhao, Y. Jia, X. Li, Y. Fu, W. Zhang, Synergistic effects of Mn and B on iron-rich intermetallic modification of recycled Al alloy, J. Mater. Res. Technol. 24 (2023) 527–541.
[229] Y. Wang, Y. Xiong, Effects of beryllium in Al–Si–Mg–Ti cast alloy, Mater. Sci. Eng., A 280 (1) (2000) 124–127.
[230] Y. Liang, Z. Shi, G. Li, R. Zhang, M. Li, Effects of rare earth modification on microstructure refinement and mechanical properties of Al-2 wt% Fe alloys, Mater. Res. Express 6 (10) (2019) 106504.
[231] B. Zhao, S. Xing, A. Shan, G. Yan, X. Jiang, Influence of La addition on Fe-rich intermetallic phases formation and mechanical properties of Al-7Si-4Cu-0.35Mg-0.2Fe alloys prepared by squeeze casting, Intermetallics 153 (2023) 107783.
[232] M. Ghomashchi, A. Vikhrov, Squeeze casting: an overview, J. Mater. Process. Technol. 101 (1–3) (2000) 1–9.
[233] G.I. Eskin, D.G. Eskin, Ultrasonic Treatment of Light Alloys Metals, second ed., CRS Press, 2014.
[234] H.R. Kotadia, M. Qian, D.G. Eskin, A. Das, On the microstructural refinement in commercial purity Al and Al-10wt% Cu alloy under ultrasonication during solidification, Mater. Des. 132 (2017) 266–274.
[235] B. Chalmers, Principles of solidification, in: Applied Solid State Physics, Springer, 1964, pp. 161–170.
[236] J. Hunt, K. Jackson, Nucleation of solid in an undercooled liquid by cavitation, J. Appl. Phys. 37 (1) (1966) 254–257.
[237] M. Warmuzek, K. Rabczak, J. Sieniawski, The course of the peritectic transformation in the Al-rich Al–Fe–Mn–Si alloys, J. Mater. Process. Technol. 162 (2005) 422–428.
[238] Y. Tsunekawa, H. Suzuki, Y. Genma, Application of ultrasonic vibration to in situ MMC process by electromagnetic melt stirring, Mater. Des. 22 (6) (2001) 467–472.
[239] H.R. Kotadia, M. Qian, A. Das, Microstructural modification of recycled aluminium alloys by high-intensity ultrasonication: observations from custom Al–2Si–2Mg–1.2Fe–(0.5,1.0)Mn alloys, J. Alloys Compd. 823 (2020) 153833.
[240] Y. Li, Z. Wang, X. Zhou, H. Xiao, Q. Yue, A review of electromagnetic stirring on solidification characteristics of molten metal in continuous casting, Metallurgical Research & Technology 121 (3) (2024) 312.
[241] K. Shiga, T. Fujiwara, Y. Murakami, N. Omura, In situ X-ray imaging of α-Al (FeMn)Si grain evolution during solidification of an Al-Si alloy with electromagnetic stirring, J. Alloys Compd. 1004 (2024) 175866.
[242] C. Vivès, Effects of forced electromagnetic vibrations during the solidification of aluminum alloys: Part I. solidification in the presence of crossed alternating electric fields and stationary magnetic fields, Metall. Mater. Trans. B 27 (3) (1996) 445–455.
[243] C. Vivès, Effects of forced electromagnetic vibrations during the solidification of aluminum alloys: Part II. solidification in the presence of colinear variable and stationary magnetic fields, Metall. Mater. Trans. B 27 (3) (1996) 457–464.
[244] C.Y. Ban, X. Zhang, P. Qian, Y. Han, J.Z. Cui, Study on the solidification structures of Al-Fe-Si alloy under DC and AC magnetic fields, Adv. Mater. Res. 189–193 (2011) 4477–4482.
[245] Y. Han, C.Y. Ban, S.J. Guo, Q.X. Ba, J.Z. Cui, Morphology and distribution of in Al-Fe alloy under an alternating magnetic field, Mater. Sci. Forum 546–549 (2007) 933–936.
[246] R. Guan, C. Ji, M. Zhu, Modeling the effect of combined electromagnetic stirring modes on macrosegregation in continuous casting blooms, Metall. Mater. Trans. B 51 (3) (2020) 1137–1153.
[247] P.J. Prescott, F. Incropera, The Effect of Turbulence on Solidification of a Binary Metal Alloy with Electromagnetic Stirring, 1995.
[248] S. Tzamtzis, N.S. Barekar, N. Hari Babu, J. Patel, B.K. Dhindaw, Z. Fan, Processing of advanced Al/SiC particulate metal matrix composites under intensive shearing – a novel Rheo-process, Compos. Appl. Sci. Manuf. 40 (2) (2009) 144–151.
[249] N.S. Barekar, S. Tzamtzis, N. Hari Babu, Z. Fan, B.K. Dhindaw, Processing of ultrafine-size particulate metal matrix composites by advanced shear technology, Metall. Mater. Trans. 40 (3) (2009) 691–701.
[250] H.R. Kotadia, E. Doernberg, J.B. Patel, Z. Fan, R. Schmid-Fetzer, Solidification of Al-Sn-Cu based immiscible alloys under intense shearing, Metall. Mater. Trans. 40 (9) (2009) 2202–2211.
[251] H.R. Kotadia, J.B. Patel, Z.Y. Fan, E. Doernberg, R. Schmid-Fetzer, Processing of Al-45Sn-10Cu based immiscible alloy by a rheomixing process, Solid State Phenom. 141–143 (2008) 529–534.
[252] H.T. Li, Y. Wang, Z. Fan, Mechanisms of enhanced heterogeneous nucleation during solidification in binary Al–Mg alloys, Acta Mater. 60 (4) (2012) 1528–1537.
[253] Z. Fan, Y. Wang, M. Xia, S. Arumuganathar, Enhanced heterogeneous nucleation in AZ91D alloy by intensive melt shearing, Acta Mater. 57 (16) (2009) 4891–4901.
[254] S.M. K.M, N.S. Barekar, J. Lazaro-Nebreda, J.B. Patel, Z. Fan, In-situ microstructural control of A6082 alloy to modify second phase particles by melt conditioned direct chill (MC-DC) casting process – a novel approach, J. Mater. Process. Technol. 295 (2021) 117170.
[255] J. Lazaro-Nebreda, J.B. Patel, K. Al-Helal, F. Gao, I. Stone, I.T.H. Chang, G. M. Scamans, Z. Fan, De-ironing of aluminium alloy melts by high shear melt conditioning technology: an overview, Metals 12 (10) (2022) 1579.
[256] A. Das, Z. Fan, A Monte Carlo simulation of solidification structure formation under melt shearing, Mater. Sci. Eng., A 365 (1) (2004) 330–335.
[257] A. Das, Effects of atomic processes occurring at or near solid/liquid interface on morphological evolution of solidification microstructure – Monte Carlo simulation, Int. J. Cast Metals Res. 20 (3) (2007) 113–121.
[258] C.E.H. Tonry, G. Djambazov, A. Dybalska, W.D. Griffiths, C. Beckwith, V. Bojarevics, K.A. Pericleous, Acoustic resonance for contactless ultrasonic cavitation in alloy melts, Ultrason. Sonochem. 63 (2020) 104959.
[259] G. Ludtka, J. Wilgen, R. Kisner, R. Jaramillo, G. Mackiewicz-Ludtka, Non-Contact Ultrasonic Treatment of Metals in a Magnetic Field, TMS Annual Meeting, 2007.
[260] K. Pericleous, V. Bojarevics, G. Djambazov, A. Dybalska, W.D. Griffiths, C. Tonry, Contactless ultrasonic cavitation in alloy melts, Materials 12 (21) (2019) 3610.
[261] B. Wang, J. Wang, X. Liu, Q. Li, X. Liu, Uncovering the effects of neutralizing elements (Co, Mn and Cr) on the Fe-rich intermetallic formation in Al–Si–Cu alloys, Mater. Sci. Eng., A 858 (2022) 144090.
[262] Y. Li, B. Hu, B. Liu, A. Nie, Q. Gu, J. Wang, Q. Li, Insight into Si poisoning on grain refinement of Al-Si/Al-5Ti-B system, Acta Mater. 187 (2020) 51–65.

[263] H. Liao, G. Sun, Mutual poisoning effect between Sr and B in Al–Si casting alloys, Scr. Mater. 48 (8) (2003) 1035–1039.
[264] M.H. Khan, A. Das, T.I. Khan, Z. Li, H.R. Kotadia, Microstructural modification in an Al-Mg-Si (6082) alloy with high Fe content using inoculation and/or high-intensity ultrasonication, J. Alloys Compd. 1012 (2025) 178500.
[265] P.V. Evans, J. Worth, A. Bosland, S.C. Flood, Solidification Processing, 1997. Sheffield, UK.
[266] R.W. Thomas, H. Cama, P.V. Evans, J.D. Hunt, Solidification Processing, 1997. Sheffield, UK.
[267] D.G. Eskin, Physical Metallurgy of Direct Chill Casting of Aluminum Alloys, CRC Press 1st Edition, 2008.
[268] I. Miki, H. Kosuge, K. Nagahama, Supersaturation and decomposition of Al-Fe alloys during solidification, J. Jpn. Inst. Light Metals 25 (1) (1975) 1–9.
[269] A. Griger, V. Stefaniay, A. Lendvai, T. Turmezey, Possible modification of cast structure by continuous casting technology in AlFeSi alloys Part III: intermetallic phases, Aluminium 10 (1989) 1049.
[270] S. Belmares-Perales, M. Castro-Román, M. Herrera-Trejo, L.E. Ramírez-Vidaurri, Effect of cooling rate and Fe/Mn weight ratio on volume fractions of α-AlFeSi and β-AlFeSi phases in Al−7.3Si−3.5Cu alloy, Met. Mater. Int. 14 (3) (2008) 307–314.
[271] L.A. Narayanan, F.H. Samuel, J.E. Gruzleski, Crystallization behavior of iron-containing intermetallic compounds in 319 aluminum alloy, Metall. Mater. Trans. 25 (8) (1994) 1761–1773.
[272] L. Bäckerud, G. Chai, J. Tamminen, Solidification Characteristics of Aluminum Alloys, 1990. Solidification Characteristics of Aluminum Alloys: Foundry alloys.
[273] X. Qi, N. Takata, A. Suzuki, M. Kobashi, M. Kato, Laser powder bed fusion of a near-eutectic Al–Fe binary alloy: processing and microstructure, Addit. Manuf. 35 (2020) 101308.
[274] W. Wang, N. Takata, A. Suzuki, M. Kobashi, M. Kato, Formation of multiple intermetallic phases in a hypereutectic Al–Fe binary alloy additively manufactured by laser powder bed fusion, Intermetallics 125 (2020) 106892.
[275] X. Qi, N. Takata, A. Suzuki, M. Kobashi, M. Kato, Change in microstructural characteristics of laser powder bed fused Al–Fe binary alloy at elevated temperature, J. Mater. Sci. Technol. 97 (2022) 38–53.
[276] Y. Wang, R. Li, T. Yuan, L. Zou, M. Wang, H. Yang, Microstructure and mechanical properties of Al-Fe-Sc-Zr alloy additively manufactured by selective laser melting, Mater. Char. 180 (2021) 111397.
[277] W. Wang, N. Takata, A. Suzuki, M. Kobashi, M. Kato, Design of Al–Fe–Mn alloy for both high-temperature strength and sufficient processability of laser powder bed fusion, Addit. Manuf. 68 (2023) 103524.
[278] J. Suchy, L. Pantelejev, D. Palousek, D. Koutny, J. Kaiser, Processing of AlSi9Cu3 alloy by selective laser melting, Powder Metall. 63 (3) (2020) 197–211.
[279] S. Yamasaki, T. Okuhira, M. Mitsuhara, H. Nakashima, J. Kusui, M. Adachi, Effect of Fe addition on heat-resistant aluminum alloys produced by selective laser melting, Metals 9 (4) (2019) 468.
[280] H.R. Kotadia, G. Gibbons, A. Das, P.D. Howes, A review of laser powder bed fusion additive manufacturing of aluminium alloys: microstructure and properties, Addit. Manuf. 46 (2021) 102155.
[281] J.G. Barlock, L.F. Mondolfo, Structure of some aluminium-iron-magnesium-manganese-silicon alloys, Int. J. Mater. Res. 66 (10) (1975) 605–611.
[282] H.W. Doty, E. Samuel, A.M. Samuel, E. Elsharkawi, V. Songmene, F.H. Samuel, Effect of Fe concentration and superheating on the microstructure and tensile properties of high Mg 413.0-type alloys: role of Sr, Be, P, and La, Materials 18 (2) (2025) 249.
[283] W. Yang, X. Yang, S. Ji, Melt superheating on the microstructure and mechanical properties of diecast Al-Mg-Si-Mn alloy, Met. Mater. Int. 21 (2) (2015) 382–390.
[284] R. Ahmad, R.I. Marshall, Effect of superheating on iron-rich plate-type compounds in Aluminium-Silicon alloys, Int. J. Cast Metals Res. 15 (5) (2003) 497–504.
[285] P. Crepeau, Effect of iron in Al-Si casting alloys: a critical review (95-110), Trans. Am. Foundrymen's Soc. 103 (1995) 361–366.
[286] L.A. Narayanan, F.H. Samuel, J.E. Gruzleski, Dissolution of iron intermetallics in Al-Si Alloys through nonequilibrium heat treatment, Metall. Mater. Trans. 26 (8) (1995) 2161–2174.
[287] L. Bo, H. Xiangxiang, X. Rui, Z. Yuliang, L. Yemao, X. Huaqiang, Evolution of iron-rich intermetallics and its effect on the mechanical properties of Al–Cu–Mn–Fe–Si alloys after thermal exposure and high-temperature tensile testing, J. Mater. Res. Technol. 23 (2023) 2527–2541.
[288] A.G. Avalos, J.T. Torres, A. Flores Valdés, Effect of the Fe/Mn ratio on the microstructural evolution of the AA6063 alloy with homogenization heat treatment interruption, Metals 14 (4) (2024) 373.
[289] M.F. Ibrahim, S.A. Alkahtani, K.A. Abuhasel, F.H. Samuel, Effect of intermetallics on the microstructure and tensile properties of aluminum based alloys: role of Sr, Mg and Be addition, Mater. Des. 86 (2015) 30–40.
[290] H. Tanihata, T. Sugawara, K. Matsuda, S. Ikeno, Effect of casting and homogenizing treatment conditions on the formation of Al–Fe–Si intermetallic compounds in 6063 Al–Mg–Si alloys, J. Mater. Sci. 34 (6) (1999) 1205–1210.
[291] A. Duchaussoy, X. Sauvage, K. Edalati, Z. Horita, G. Renou, A. Deschamps, F. De Geuser, Structure and mechanical behavior of ultrafine-grained aluminum-iron alloy stabilized by nanoscaled intermetallic particles, Acta Mater. 167 (2019) 89–102.
[292] N. Bayat, T. Carlberg, M. Cieslar, In-situ study of phase transformations during homogenization of 6005 and 6082 Al alloys, J. Alloys Compd. 725 (2017) 504–509.
[293] C. Liu, H. Azizi-Alizamini, N. Parson, W. Poole, Q. Du, Microstructure evolution during homogenization of Al-Mg-Si-Mn-Fe alloys: modelling and experimental results, Trans. Nonferrous Metals Soc. China 27 (4) (2017) 747–753.
[294] G. Mrówka-Nowotnik, J. Sieniawski, Influence of heat treatment on the microstructure and mechanical properties of 6005 and 6082 aluminium alloys, J. Mater. Process. Technol. 162–163 (2005) 367–372.
[295] H. Yang, S. Ji, Z. Fan, Effect of heat treatment and Fe content on the microstructure and mechanical properties of die-cast Al–Si–Cu alloys, Mater. Des. 85 (2015) 823–832.
[296] J.A. Taylor, G.B. Schaffer, D.H. StJohn, The role of iron in the formation of porosity in Al-Si-Cu-based casting alloys: Part I. Initial experimental observations, Metall. Mater. Trans. 30 (6) (1999) 1643–1650.
[297] J.A. Taylor, G.B. Schaffer, D.H. StJohn, The role of iron in the formation of porosity in Al-Si-Cu-based casting alloys: Part II. A phase-diagram approach, Metall. Mater. Trans. 30 (6) (1999) 1651–1655.
[298] J.A. Taylor, G.B. Schaffer, D.H. StJohn, The role of iron in the formation of porosity in Al-Si-Cu-based casting alloys: Part III. A microstructural model, Metall. Mater. Trans. 30 (6) (1999) 1657–1662.
[299] N. Roy, A.M. Samuel, F.H. Samuel, Porosity formation in AI-9 Wt Pct Si-3 Wt Pct Cu alloy systems: metallographic observations, Metall. Mater. Trans. 27 (2) (1996) 415–429.
[300] M. Otte, S. Mcdonald, J. Taylor, D. St John, W. Schneider, Controlling porosity-related casting rejects: understanding the role of iron in Al-Si alloys, 103rd Annual Meeting of the American-Foundrymen's-Society, St Louis Mo, Mar 13-16, (1999) 1999.
[301] C.H. Cáceres, J.A. Taylor, Enhanced ductility in Al-Si-Cu-Mg foundry alloys with high Si content, Metall. Mater. Trans. B 37 (6) (2006) 897–903.
[302] C.H. Cáceres, I.L. Svensson, J.A. Taylor, Strength-ductility behaviour of Al-Si-Cu-Mg casting alloys in T6 temper, Int. J. Cast Metals Res. 15 (5) (2003) 531–543.
[303] A. Bjurenstedt, E. Ghassemali, S. Seifeddine, A.K. Dahle, The effect of Fe-rich intermetallics on crack initiation in cast aluminium: an in-situ tensile study, Mater. Sci. Eng., A 756 (2019) 502–507.
[304] F. Hannard, T. Pardoen, É. Maire, C. Le Bourlot, R. Mokso, A. Simar, Characterization and micromechanical modelling of microstructural heterogeneity effects on ductile fracture of 6xxx aluminium alloys, Acta Mater. 103 (2016) 558–572.
[305] F. Hannard, S. Castin, E. Maire, R. Mokso, T. Pardoen, A. Simar, Ductilization of aluminium alloy 6056 by friction stir processing, Acta Mater. 130 (2017) 121–136.
[306] L. Babout, E. Maire, R. Fougeres, Damage initiation in model metallic materials: X-ray tomography and modelling, Acta Mater. 52 (8) (2004) 2475–2487.
[307] D. Lassance, D. Fabregue, F. Delannay, T. Pardoen, Micromechanics of room and high temperature fracture in 6xxx Al alloys, Prog. Mater. Sci. 52 (1) (2007) 62–129.
[308] L. Sweet, S.-M. Zhu, S. Gao, J. Taylor, M. Easton, The effect of iron content on the iron-containing intermetallic phases in a cast 6060 aluminum alloy, Metall. Mater. Trans. 42 (2011) 1737–1749.
[309] Y. Zhao, D. Song, H. Wang, Y. Jia, B. Lin, Y. Tang, Y. Tang, D. Shu, Z. Sun, Y. Fu, W. Zhang, Revealing the influence of Fe on Fe-rich phases formation and mechanical properties of cast Al-Mg-Mn-Fe alloys, J. Alloys Compd. 901 (2022) 163666.
[310] L. Kuchariková, D. Medvecká, E. Tillová, J. Belan, M. Kritikos, M. Chalupová, M. Uhríčik, The effect of the β-Al5FeSi phases on microstructure, mechanical and fatigue properties in A356.0 cast alloys with higher Fe content without additional alloying of Mn, Materials 14 (8) (2021) 1943.
[311] L. Ceschini, I. Boromei, A. Morri, S. Seifeddine, I.L. Svensson, Microstructure, tensile and fatigue properties of the Al–10 %Si–2 %Cu alloy with different Fe and Mn content cast under controlled conditions, J. Mater. Process. Technol. 209 (15) (2009) 5669–5679.
[312] D. Závodská, L. Kuchariková, E. Tillová, M. Guagliano, M. Chalupová, M. Uhríčik, J. Belan, The effect of iron content on fatigue lifetime of AlZn10Si8Mg cast alloy, Int. J. Fatig. 128 (2019) 105189.
[313] J. Blind, J. Martin, The effect of dispersoids on the ductile fracture toughness of Al Mg Si alloys, Mater. Sci. Eng. 57 (1) (1983) 49–54.
[314] R.R. McCullough, J.B. Jordon, P.G. Allison, T. Rushing, L. Garcia, Fatigue crack nucleation and small crack growth in an extruded 6061 aluminum alloy, Int. J. Fatig. 119 (2019) 52–61.
[315] A.A. Luo, R.C. Kubic, J.M. Tartaglia, Microstructure and fatigue properties of hydroformed aluminum alloys 6063 and 5754, Metall. Mater. Trans. 34 (11) (2003) 2549–2557.
[316] C. Shen, Z. Pan, Y. Ma, D. Cuiuri, H. Li, Fabrication of iron-rich Fe–Al intermetallics using the wire-arc additive manufacturing process, Addit. Manuf. 7 (2015) 20–26.
[317] D. Xu, C. Zhu, C. Xu, K. Chen, Microstructures and tensile fracture behavior of 2219 wrought Al–Cu alloys with different impurity of Fe, Metals 11 (1) (2021) 174.
[318] M. Li, A. Seyeux, F. Wiame, P. Marcus, J. Światowska, Insights on the Al-Cu-Fe-Mn intermetallic particles induced pitting corrosion of Al-Cu-Li alloy, Corros. Sci. 176 (2020) 109040.
[319] R. Ambat, A.J. Davenport, G.M. Scamans, A. Afseth, Effect of iron-containing intermetallic particles on the corrosion behaviour of aluminium, Corros. Sci. 48 (11) (2006) 3455–3471.
[320] X.-M. Chen, Q.-P. Dong, Z.-G. Liu, X.-N. Wang, Q.-Y. Zhang, Z.-R. Hu, H. Nagaumi, Fe-bearing intermetallics transformation and its influence on the corrosion resistance of Al–Mg–Si alloy weld joints, J. Mater. Res. Technol. 9 (6) (2020) 16116–16125.
[321] J.I. Ahuir-Torres, G.J. Gibbons, G. West, A. Das, H.R. Kotadia, Understanding the corrosion behaviour of Al-Mg alloy fabricated using a laser powder bed fusion (L-PBF) additive manufacturing (AM) process, J. Alloys Compd. 969 (2023) 172300.

[322] A. Chemin, D. Marques, L. Bisanha, A.d.J. Motheo, W.W. Bose Filho, C.O. F. Ruchert, Influence of Al7Cu2Fe intermetallic particles on the localized corrosion of high strength aluminum alloys, Mater. Des. 53 (2014) 118–123.
[323] C. Berlanga-Labari, M.V. Biezma-Moraleda, P.J. Rivero, Corrosion of cast aluminum alloys: a review, Metals 10 (10) (2020) 1384.
[324] J.O. Park, C.H. Paik, Y.H. Huang, R.C. Alkire, Influence of Fe-rich intermetallic inclusions on pit initiation on aluminum alloys in aerated NaCl, J. Electrochem. Soc. 146 (2) (1999) 517.
[325] J.I. Ahuir-Torres, H.R. Kotadia, T.T. Öpoz, M.C. Sharp, A study on the corrosion behaviour of laser textured pure aluminium in saltwater, Processes (2023).
[326] The Aluminum Can Advantage: Sustainability Key Performance Indicators, The Aluminum Association, 2024.
[327] H. Kaufmann, W. Fragner, H. Suppan, A.B. Spierings, P.J. Uggowitzer, A. Schubert, M. Hummel, Starting Material, Use Thereof, and Additive Manufacturing Process Using Said Starting Material, Google Patents, 2023.
[328] T. Haga, S. Imamura, H. Fuse, H. Watari, S. Nishida, Roll casting and die casting of Si-added Al-Mg alloy. Materials Science Forum, Trans Tech Publ, 2020, pp. 12–17.